Theoretical and Phenomenological Study of G_2 Compactifications of M Theory

by

Ran Lu

A dissertation submitted in partial fulfillment
of the requirements for the degree of
Doctor of Philosophy
(Physics)
in the University of Michigan
2013

Doctoral Committee:

Professor Gordon L. Kane, Chair
Professor Lizhen Ji
Professor Finn Larsen
Associate Professor Aaron T. Pierce
Professor Bing Zhou

2013

A C K N O W L E D G M E N T S

This thesis would have been impossible without the excellent support of my advisor, Gordon Kane. I am very lucky to have the opportunity to work with you and I sincerely grateful for all that you have done for me.

I would also like to thank my collaborators: Bobby Acharya, Daniel Feldman, Eric Kuflik, Piyush Kumar, Brent Nelson, LianTao Wang, Scott Watson and Bob Zheng. It has been a great pleasure to work with all of you and I learned so much during our collaborations.

I have had helpful discussions with many other people, including (non-exhaustively): Michele Cicoli, Jim Halverson, Jack Kearney, Ian-Woo Kim, Finn Larsen, Jim Liu, Sam McDermott, Malcolm Perry, Aaron Pierce, Stuart Raby, Saúl Ramos-Sánchez, and Haibo Yu.

TABLE OF CONTENTS

LIST OF FIGURES

LIST OF TABLES

ABSTRACT

Theoretical and Phenomenological Study of G_2 Compactifications of M Theory

by

Ran Lu

Chair: Gordon Kane

This thesis focuses on the study of G_2 compactification of M theory. With the assumption that the low energy effective theory is the minimal supersymmetric standard model (MSSM), these kinds of compactifications produce an interesting model called G_2-MSSM with distinctive particle spectrum. An approximate discrete symmetry on the G_2 manifold combined with symmetry breaking Wilson lines provide a solution to the doublet-triplet splitting problem and generate a suppressed μ term. This small μ term is consistent with electroweak symmetry breaking and the so called "little hierarchy" problem is alleviated in G_2-MSSM. The phenomenology of G_2-MSSM is also studied. The lightest supersymmetric particle (LSP), which is almost always a wino, is stable because of the R-parity of the theory, and has the right relic abundance when non-thermally produced by the moduli decay. And due to its large annihilation cross section, it might provide a partial explanation of the signals observed by indirect detection experiments. Because of the suppressed μ term, the mass of the lightest Higgs particle in G_2-MSSM is about 125 GeV when the scalars are O(50 TeV). The gauginos are much lighter than the scalars in G_2-MSSM. The gluino and chargino have interesting collider signals at the LHC.

CHAPTER 1

Introduction

1.1 Introduction

String/M theory is a framework that may help to formulate a underlying theory to understand the world better, If so, it will be essential to "compactify" the 10 dimensional string theories or the 11 dimensional M theory to four dimensions. We concentrate on the best motivated case where the small dimensions are Planck scale size (but still large enough so the supergravity calculations are reliable). Even though the energy scale of the extra dimensions is assumed to be much above the center-of-mass energy of collisions at the Large Hadron Collider (LHC), the extra dimensions still manifest themselves at lower energies through the presence of moduli fields. These are modes of the extra dimensional graviton whose vacuum-expectation-values (*vev*'s) determine the shapes and sizes that the extra dimensions take. Being modes of the extra dimensional graviton, the moduli couple to matter with Planck suppressed interactions universally. The moduli have to be stabilized since all couplings and masses are determined from their *vev*'s. Although understanding phenomenologically relevant supersymmetry breaking in string theory is a challenging task, many results, including those needed to calculate the Higgs boson mass, can be obtained with rather mild, well motivated assumptions.

G_2 compactification of M theory (i.e. compactification on a manifold with G_2 honolomy) has made a lot progress in the recent years. Due to the mathematical difficulties associated with constructing G_2 manifolds, studying string compactifications on Calabi-Yau manifolds was and still is more popular than studying G_2 compactifications. Calabi-Yau 3-folds and 4-folds are understood much better than G_2 manifolds, mainly because algebraic geometry is very powerful on complex manifolds. Using Yau's theorem[7] one only need to calculate the first chern class to check the existence of Calabi-Yau structure. On the other hand, the only way to verify a manifold admits a G_2 structure is to show that there is actually a G_2 invariant metric. However, moduli stabilization, which requires great effort in Calabi-Yau compactification, is simplified in the G_2 case. On a Calabi-Yau manifold, one needs to stabilize complex structure moduli and Kähler moduli sep-

arately, usually with different mechanisms. Because G_2 manifolds only have geometric moduli, all of them can be stabilized using QCD like interactions. When there are gaugino condensations as well as meson fields from quark condensations, it is possible to stabilize moduli to a de Sitter vacuum with small cosmological constant. In the scenario studied in [8, 9], the F-terms of the moduli are much smaller than the F-term of the meson field.

In the simplest case, the low energy spectrum only contains the MSSM, and the effective theory is called G_2-MSSM. But due to the unification of the gauge couplings, one naturally expects the field theory after compactification is a grand unification theory (GUT) like $SU(5)$. Doublet-triplet splitting must be implemented to maintain the gauge coupling unification. This is also related to the so-called "μ problem" which is one of the most fundamental issues in making a systematic theory of the physical world. It is a large hierarchy problem, with μ naturally being of the order the unification scale, but only make sense if it were at the TeV scale. It will be shown in the following chapters that there is an elegant solution using an approximate discrete symmetry on the G_2 manifold, first studied by Witten. We extended the idea to embed μ in the theory with stabilized moduli and estimate its size, thus proposing a solution to this fundamental problem.

This also provides a new approach to the little hierarchy problem. Even though there are still unsolved problems in G_2 compactifications, it is possible to study the phenomenology with some mild assumptions about the spectrum. In this thesis I will mainly consider the G_2-MSSM. Once the spectrum is fixed, it is straightforward to calculate the mass of the lightest Higgs particle, study new physics signals at the LHC, and explore the implications for cosmology and dark matter.

The Standard Model suffers from "naturalness" or "hierarchy" problem(s). In addition to the well-known technical naturalness problem of the Higgs, there is the basic question of the origin of the electroweak scale. In the context considered here: the embedding of the (supersymmetric) Standard Model in a UV complete microscopic theory like string/M theory has to explain why the electroweak scale is so much smaller than the natural scale in string theory, the string scale, which is usually assumed to be many of orders of magnitude above the TeV scale. The μ parameter (which sets the masses of Higgsinos and contributes to the masses of Higgs bosons) must also be around TeV scale. The models we describe here, with softly broken supersymmetry, include solutions for all of these problems.

The organization of this thesis is the following. In Chapter 2 we briefly review the theoretical setup of M theory compactified on G_2-manifolds. Following this, in Chapter 3 we study the low energy effective theory G_2-MSSM. We show the discrete symmetry provides a satisfying solution to the doublet-triplet splitting problem. The discrete symmetry must be anomaly free, which puts non-trivial constraints on the discrete symmetry itself as well as the eigenvalues of the Yukawa coupling matrices. We then show the small μ term is compatible with electroweak symmetry breaking condition and the G_2-MSSM serves as an example of a new approach to solve the little

hierarchy problem. In Chapter 4 we obtain a lower bound of the gravitino mass from cosmology, and show the dark matter candidates in G_2-MSSM are consistent with the non-thermal history of the universe and current results from direct and indirect dark matter experiments. The Higgs mass is calculated in Chapter 5. For the general heavy scalar MSSM scenario, the Higgs mass has a large uncertainty due to $\tan\beta$, for G_2-MSSM however, the requirement of consistent electroweak symmetry breaking (EWSB) fixes $\tan\beta$ to a relatively small range. For $O(50\,\mathrm{TeV})$ scalars, the Higgs mass is very nearly 125 GeV, consistent with the current observations[10, 11]. In Chapter 6 we study the LHC phenomenology of G_2-MSSM, mainly focusing on the gluino and chargino signals.

CHAPTER 2

M theory compactification on G_2 manifolds

2.1 G_2 manifolds

G_2 manifolds are 7 dimensional manifolds with holonomy group G_2. Holonomy group describes the behavior of vectors and spinors under parallel transportation on general manifolds. The G_2 manifolds play a similar in M theory as Calabi-Yau 3-folds do in string theory and 4-folds do in F-theory. Because of the special holonomy, a global spinor field can be defined on the manifold. Thus when compactified on a G_2 manifold, M theory gives a low energy effective $N = 1$ supersymmetric theory in the uncompactified 4D spacetime. Unlike the more familiar Calabi-Yau case, there is nothing similar to the Yau's theorem for G_2 manifold. So in order to show a manifold is really a G_2 manifold, one needs to show explicitly the metric is G_2 invariant.This is much harder than proving a manifold is Calabi-Yau where one just need to calculate the first Chern class. Because of this, only a few examples of the G_2 manifolds are known, and the general properties of the G_2 manifolds are much less well-understood. Joyce [12, 13] constructed examples of smooth compactified G_2 manifolds as resolutions of $T7/\Gamma$ orbifolds, here Γ is a discrete group. And non-compact G_2 manifolds with conical singularities are studied in [14]. Recently Corti et al.[15] has constructed coassociative $K3$ fibred compact G_2 manifolds using the so-called twisted connected sum construction starting with $K3$ fibred (semi-)Fano 3-folds. The $K3$ fibres in the construction are generally smooth, with a finite number of singular fibres. However, in order for the low energy effective theory to be phenomenologically relevant, the G_2 manifolds must have $K3$ fibration with generic singular fibres, and isolated conical singularities. It is still an open problem if one can construct this kind of manifold by generalizing the constructions mentioned above.

2.2 Matter and Gauge Theory

Gauge interactions are the most important building blocks of new physics models. In M theory compactified on a G_2 manifold, gauge symmetry is usually realized by requiring the existence of

a $K3$-fibration with singular fibres. ADE-type gauge symmetries ($SU(n)$, $SO(2n)$ and E_6, E_7, E_8) are localized along three dimensional submanifolds of orbifold singularities [16, 17]. Chiral matter, charged under the ADE gauge theory, is localized at conical singularities in the seven dimensional G_2 manifold, at points where the ADE singularity is enhanced [18, 19, 20]. Matter will additionally be charged under the $U(1)$ symmetries, corresponding to the vanishing 2-cycles that enhances the singularity. Hence, all chiral matter will charged under at least one $U(1)$ symmetry. Bi-fundamental matter, charged under two non-Abelian gauge groups, is also possible, and potentially will play an important role in explaining the $O(1)$ top Yukawa coupling [14, 21].

As argued by Pantev and Wijnholt [22], the additional $U(1)$ symmetries are never anomalous. Therefore, there is no Green-Schwarz mechanism [23] needed for anomaly cancellation, and GUT-scale FI D-terms are not present in the theory. This will be important later, since it removes a possibility for generating large scalar vacuum expectation values (vevs) for charged matter fields.

Two gauge theories will generically only have precisely the same size gauge coupling if they arise from the same orbifold singularities. Therefore, if gauge coupling unification is to be motivated theoretically, and not an approximation or accident, the gauge group of the ADE singularity should be a simple group containing the Standard Model gauge group, which we will take (for simplicity) to be $SU(5)$. Any larger group containing $SU(5)$ will give results similar to those we find below. To obtain the Standard Model gauge group, $SU(5)$ needs to be broken. Perhaps the 4D gauge symmetry can be broken spontaneously, but at this moment only representations smaller than the adjoint are realizable in M theory–the $\mathbf{10}$ and $\mathbf{5}$ representations (and their conjugates) in $SU(5)$. This leaves only "flipped $SU(5)$" [24, 25, 26] as a possible mechanism to break the GUT group and solve doublet-triplet splitting. Given the difficulty in constructing a realistic flipped $SU(5)$ model [27], it will not be considered here. The remaining possibility is to break the higher dimensional gauge theory by Wilson lines and will be discussed below.

2.3 Moduli Stabilization

In the mid-80's it was realized that, classically, string vacua contain a plethora of moduli fields. The standard lore was that, after supersymmetry(SUSY) breaking, the moduli fields would obtain masses and appropriate vacuum expectation values. Part of this lore was also the idea that strong dynamics in a hidden sector would be responsible for breaking supersymmetry in the visible sector at, or around, the TeV scale. Though some progress was made, it was not until recently that it has been clearly demonstrated that these ideas can be completely realized in string/M theory: in M theory compactified on a G_2-manifold (without fluxes) strong gauge dynamics can generate a potential which stabilizes all moduli and breaks supersymmetry at a hierarchically small scale [28, 29]. These vacua will be the starting point for our considerations.

The G_2 structure of a manifold X is determined by the unique G_2 invariant 3-form φ. φ can be written as

$$\varphi = \sum_i s^i \beta_i \tag{2.1}$$

where β_i are a basis of 3rd cohomology group $H^3(X, \mathrm{R})$, and s^i are the moduli fields. The Kähler potential of the moduli fields is chosen to be [30]

$$K_0 = -3 \log\left(4\pi^{1/3} V_X\right) \tag{2.2}$$

where V_X is the volume of the G_2 manifold. The only requirement for V_X is that it is a homegeneous polynomial of s^i of degree $7/3$, for example

$$V_X = \prod_i \left(s^i\right)^{a_i}, \tag{2.3}$$

and a_i satisfies $\sum_i a_i = 7/3$.

The moduli stabilization is achieved by introducing at least 2 hidden sectors with QCD-like interactions. The 3D submanifolds supporting the two ADE sigularities must have similar form, and for the simplicity of the discussion we assume they are the same 3-cycle in X with the volume

$$V_Q^R = \sum_i N_i s^i. \tag{2.4}$$

There is also a 3-form C in the 11D supergravity interaction. When compactified on the 3-cycles it gives axions a^i (not to be confused with a_i in (2.3)) in the low energy theory, which pair with the moduli fields and become chiral multiplets in the $N = 1$ supersymmetric effective theory (The fermionic partners arise from the gravitino fields). So we can define the complexified 3-form volume as

$$V_Q = \sum_i N_i z^i \qquad \text{where} \qquad z^i = s^i + i a^i. \tag{2.5}$$

With 2 hidden sectors a non-perturbative superpotential is generated from gaugino condensation

$$W_0 = A_1 e^{b1 V_Q} + A_2 e^{b2 V_Q}. \tag{2.6}$$

To obtain a de Sitter vacuum with almost zero cosmological constant, it is necessary to include extra matter content like the chiral fermions as well as gaugino fields in at least one hidden sector [31], which will generate a meson field ϕ when the interaction becomes strong. The Kähler

potential for the meson field is

$$K_C = \frac{k\left(s^i\right)}{V_X}\bar{\phi}\phi. \tag{2.7}$$

For simplicity we will take $k\left(s^i\right) = 1$. And the superpotential follows the standard super-QCD results:

$$W_C = A_1\phi^a e^{b1V_Q} + A_2 e^{b2V_Q}. \tag{2.8}$$

From the interaction K_0, K_C, W_C defined above, we can calculate the scalar potential

$$V = e^{K_0+K_C}\left(K^{ij}D_iW_CD_jW_C - 3|W_C|^2\right) \quad \text{where} \quad D_iW_C = \partial_iW_C + \partial_iK_CW_C \tag{2.9}$$

and show there is a local minimum corresponding to a metastable dS vacuum with broken SUSY. Details of the calculation can be find in [28, 29]. Intuitively, in the large volume limit, without considering the meson field ϕ, all the moduli can be stablized in an AdS vacuum, and the vacuum expectation value(vev) of the moduli at this point can be formally expressed as:

$$s^i = -a_i\frac{W_0}{\partial_iW_0} \tag{2.10}$$

Here we use (2.3) as the Kähler potential of the theory. For more general scenarios we can still define a_i as a function of s_i and its numerical value can be calculated directly (without knowing the vev of the moduli) at the vacuum.

After including the meson, using the obvious ansatz for moduli fields

$$s^i = -a_i\frac{W_C}{\partial_iW_C}L \tag{2.11}$$

L is a constant, and after minimizing the scalar potential

$$L = 1 + O\left(\frac{1}{P_{eff}}\right) \tag{2.12}$$

P_{eff} is some large constant. When considering two gauge group $SU(P)$ and $SU(Q)$

$$P_{eff} = P\log\left(\frac{QA_1\phi^a}{PA_2}\right) \tag{2.13}$$

Because SUSY is restored when $L = 1$, the SUSY breaking F-term of the moduli fields are suppressed by P_{eff}. On the other hand, the meson fields are in some sense unconstrained by the approximate supersymmetric AdS vacuum, and its F-term has to be large in order to achieve vanishing cosmological constant.

In these vacua, the gravitino mass (and therefore also the moduli masses [32]) $m_{3/2} \sim \frac{\Lambda^3}{m_{pl}^2}$, where Λ is the strong coupling scale of the hidden sector gauge interaction. This is parametrically of order $\Lambda \sim e^{-2\pi/(\alpha_h b)} m_{pl}$, where α_h is the coupling constant of the hidden sector and b is a beta-function coefficient. The vacuum expectation values of the moduli fields are also determined in terms of α_h: Roughly speaking, one has:

$$\langle s^i \rangle \sim 1/\alpha_h \tag{2.14}$$

where the modulus here is dimensionless and not yet canonically normalized. The physical meaning of the vevs of s^A is that it characterizes the volumes in eleven dimensional units of 3-cycles in the extra dimensions, e.g., the 3-cycle that supports the hidden sector gauge group. Thus, self-consistently when the hidden sector is weakly coupled in the UV, the moduli are stabilized at large enough volumes in order to trust the supergravity potential which only makes sense in this regime. In general, the rough formula exhibits the scaling with α_h and, numerically the moduli vevs in the vacua considered thus far range from about $1 \leq s^A \leq 5/\alpha_h$.

In order to incorporate the moduli vevs into the effective field theory in an M theory vacuum, we have to consider the normalized dimensionful vevs which appear in the Einstein frame supergravity Lagrangian. For obtaining the normalization it suffices to consider the moduli kinetic terms alone:

$$\mathcal{L} \supset m_{pl}^2 \frac{1}{2} g_{AB} \partial_\mu s^A \partial^\mu s^B \tag{2.15}$$

where s^A are the dimensionless moduli described above and g_{AB} is the (Kahler) metric on the moduli space. From the fact that the extra dimensions have holonomy G_2, it follows that each component of g_{AB} is homogeneous of degree *minus* two in the moduli fields

$$g_{AB} = \partial_A \partial_B K = \partial_A \partial_B \left(-3 \ln V_7 + \dots \right) \tag{2.16}$$

because the volume of X, V_7, is homogeneous of degree $7/3$.

For isotropic G_2-manifolds, i.e. those which receive similar order contributions to their volume from each of the N moduli, studying examples shows that, not only is the metric of order $\frac{1}{s^2}$, but also of order $1/N$:

$$g \sim \frac{1}{N} \frac{1}{(s^A)^2} \tag{2.17}$$

Therefore in a given vacuum the order of magnitude of the entries of g_{AB} are

$$g \sim \frac{\alpha_h^2}{N} \tag{2.18}$$

Therefore, a dimensionless modulus vev of order $1/\alpha_h$ translates into a properly normalized

dimensionful vev

$$\langle \hat{s^A} \rangle \sim \frac{1}{\sqrt{N}} \sim 0.1 m_{pl} \tag{2.19}$$

for $N \sim 100$, which is a typical expectation for the number of moduli [12, 13][1].

2.4 Geometric Symmetries and Moduli Transformations

Compact, Ricci-flat manifolds with finite fundamental groups, such as manifolds with holonomy G_2 or $SU(3)$ cannot have continuous symmetries. They can, however, have *discrete* symmetries. Witten [33] was considering just such a discrete symmetry (G) of a G_2-manifold when he proposed the symmetry which prevents μ. More discussion about the implementation can be found in the next chapter, here we focus on the more general picture. Below we will focus on an abelian symmetry Z_N in order to be concrete, but the general conclusion does not depend on this assumption.

The fact that the particular G_2-manifold, characterized by the particular point in moduli space s_0^A, is $\mathbf{Z_N}$-invariant is simply the statement that, in some properly chosen basis, s_0^A is invariant under the discrete symmetry:

$$s_0^B M_A^B = s_0^A \tag{2.20}$$

Here M_A^B are some representation of the discrete symmetry. Clearly, this will not be true for a generic vector s^A; hence, for a generic point in the moduli space, the entire $\mathbf{Z_N}$ symmetry will be broken. Since the representation of $\mathbf{Z_N}$ defined by the matrix M is real, it must be the sum of a complex representation plus its conjugate. Thus, the basis β_B can be chosen such that the complex representation is spanned by *complex* linear combinations of moduli fields. For instance, there might be a linear combination

$$S = \hat{s}^1 + i\hat{s}^2 \tag{2.21}$$

which we choose to write in-terms of the dimensionful fields ($\hat{s}$), that transforms as

$$S \to e^{2\pi i/N} S. \tag{2.22}$$

Since we usually consider complex representations of discrete symmetries acting on the matter fields in effective field theories, it will be precisely the linear combinations of moduli (those in the form (2.21)) which span $\mathbf{r_C}$ which will appear in the "symmetry breaking sector" of the effective Lagrangian. In other words, the moduli will appear in complex linear combinations such as (2.21) in the Kähler potential operators containing other fields that transform under the $\mathbf{Z_N}$. Note that in (2.21) we are abusing notation in the sense that the "i" which appears is in general an N-by-N

[1] Presumably, N is of the same order as the number of renormalizable coupling constants of the effective low energy theory.

matrix whose square is minus the identity.

2.5 Discrete symmetries and Moduli Stabilization

The discrete symmetries of the G_2 manifolds have important phenomenological applications. In the next chapter we will show the matter(R) parity can be realized by discrete symmetry on G_2 manifold. And an approximate discrete symmetry can be used to suppress the μ term. It is important to understand how the moduli stabilization mechanism interacts with the discrete symmetry. Unfortunately we do not have an explicit example of a G_2 manifold with the required QCD like hidden sector. So there is no concrete demonstration it is indeed possible to stabilize to a G_2 manifold with the preferred exact and approximate symmetry.

Discrete symmetries are much better understood in Calabi-Yau manifolds. Witten has constructed families of Calabi-Yau 3-folds that always have a Z_2 symmetry, no matter what values the moduli vevs are. It is possible similar constructions can be found for the G_2 manifolds.

For the approximate discrete symmetries, it is important to estimate the size of the symmetry breaking. In principle one can use the distance on the moduli space between the manifold picked by the moduli stabilization mechanism and the manifold on which the said symmetries are exact. This kind of calculation is possible for some simple Calabi-Yau manifolds but still unfeasible for G_2 manifold. One still can make some educated guesses. In the well-understood quintic Calabi-Yau varieties, complex structure moduli are just coefficients of the 5th order monomial in the defining homogeneous polynomial of the quintic Calabi-Yau. And when their values are properly chosen, the variety can have various kinds of discrete symmetries. For example, the Fermat quintic

$$Q_0(x) = Z_1 \sum_i x_i^5 + Z_2 x_1 x_2 x_3 x_4 x_5 \tag{2.23}$$

has a large discrete symmetry $S_5 \times (Z_5)^3$. Moduli stabilization, if possible, will produce some different configuration

$$Q_1(x) = \sum_{abcde} f_{abcde} x^a x^b x^c x^d x^e. \tag{2.24}$$

Suppose some physical quantities we are interested are protected by the $(Z_5)^3$ symmetry. This symmetry is broken by those non-zero f_{abcde} which does not respect this symmetry on Q_1. So we will assume for the G_2 case, the vevs of the moduli (at least in some well-chosen basis) can be used to estimate the size of the symmetry breaking. Furthermore, in order for the above argument to make sense, it is necessary to assume Q_1 or its G_2 counterpart is close to Q_0 or its G_2 counterpart. So the symmetry breaking moduli vevs can be treated as a perturbation. These perturbations can be expanded using functions defined on Q_0 and respecting the discrete symmetry. Thus the symmetry

breaking vevs furnish some linear representation of the discrete symmetry, to the leading order.

CHAPTER 3

G_2-MSSM

3.1 The spectrum

As mentioned in the previous chapter, the gauge groups correspond to the 3-cycles in the G_2 manifold, and the gauge couplings are proportional to the volume of the 3-cycles. Because of the evidence of gauge coupling unification in MSSM, it is reasonable to assume all the gauge interactions are coming from a single 3-cycle. So the theory at compactification scale is a grand unification theory(GUT). We will focus on $SU\,(5)$ GUT with the doublet triplet problem solved by the forementioned discrete symmetry. The triplets in general receive masses of unification scale. So the TeV scale spectrum is just MSSM. We call this effective theory G_2-MSSM.Once we fix the low energy spectrum to be MSSM, it is straightforward to apply the standard supergravity formalism [34] to calculate the particle masses and couplings [8, 9]. Figure 3.1 shows a typical spectrum of G_2-MSSM. The prominent feature of the spectrum is that the gaugino mass is much suppressed compared to the masses of the scalar superpartners. This can be traced back to the moduli stabilization mechanism. Classically, it is well known that string/M theory has no vacuum with a positive cosmological constant (de Sitter minimum). From the effective field theory point of view, this is the statement that moduli fields tend to have potentials which, in the classical limit have no de Sitter minimum. If we now consider quantum corrections to the moduli potential, which *only* involve the moduli fields – if they are computed in a perturbative regime – they tend to be small and hence are unlikely to generate de Sitter vacua. Positive, larger sources of vacuum energy must therefore arise from other, non-moduli fields. This is indeed the case in the M theory vacua described in the previous chapter. Here the dominant contribution to the vacuum energy arises from a *matter* field in the hidden sector (where it can be shown that, without the matter field, no de Sitter vacuum exists).

Adopting supersymmetric terminology, this suggests that the fields with the dominant F-terms are not moduli. Hence, the moduli F-terms are suppressed relative to the dominant contribution (in fact, in M theory the suppression is of order α_h). This affects the spectrum of new particles.

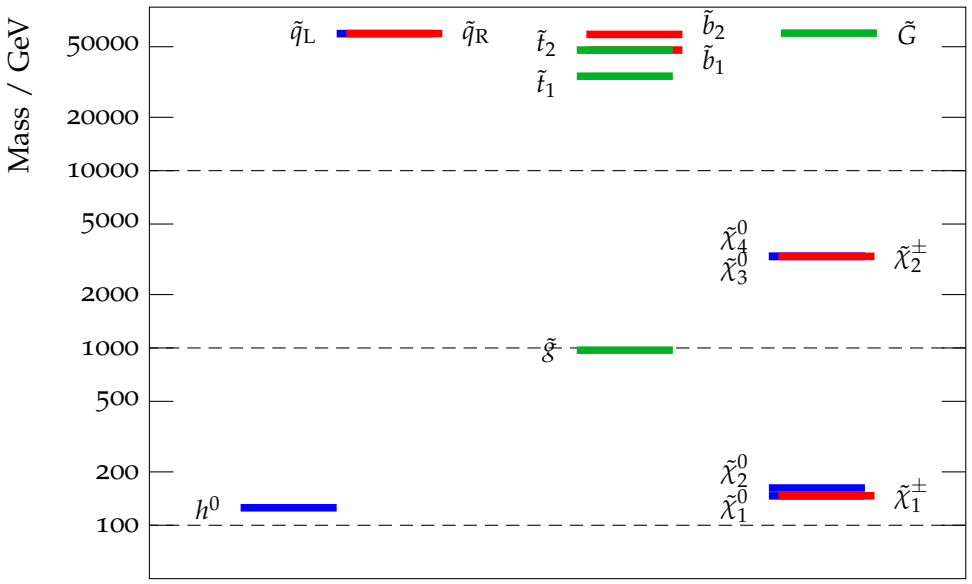

Figure 3.1: One typical spectrum of G_2-MSSM, All the scalars are $O(50)$ TeV, with the third family squarks slightly lighter because of the large Yukawa coupling and the renormalization group running. The lightest neutralino $\tilde{\chi}_1^0$ is mostly wino because of the anomaly mediation contribution at the unification scale. μ is suppressed relative to $m_{3/2}$, so the higgsinos are only a few TeV. The gluino is relatively sensitive to the unification scale threshold corrections, assuming these threshold correction are not larger than the tree level contribution, the gluino cannot be heavier than a few TeV

In string/M theory, gaugino masses are generated through F-terms of moduli vevs (because the gauge coupling function is a superfield containing volume moduli). Hence, at leading order these will be suppressed relative to, say, scalar masses which receive order $m_{3/2}$ contributions from all F-terms in the absence of accidental symmetries. Therefore, in the G_2-MSSM (and presumably other classes of string vacua) the scalar superpartners and moduli fields will have masses of order $m_{3/2}$ whereas the gaugino's will have masses which are suppressed; in fact in the G_2-MSSM the gaugino masses at the GUT scale are at least two orders of magnitude below $m_{3/2}$. This is what makes the anomaly mediated contributions to gaugino masses relevant to the G_2-MSSM and also why the models often contain a Wino LSP [8, 35]. For the phenomenology considered in the following chapters, it is also important that the suppression of the gaugino masses is greater than the suppression of moduli vevs discussed above by one order of magnitude (at the GUT scale), at least for G_2-manifolds with less than O(10^4) moduli.

3.2 Doublet-triplet splitting and μ

As the first step of constructing G_2-MSSM, we need to decouple the triplet in the $\mathbf{5}$ and $\bar{\mathbf{5}}$ in the Higgs multiplets, while keep the coupling between the doublet, the μ term small. This is the well known doublet-triplet splitting problem. In Heterotic string theory, doublet-triplet splitting is often solved by orbifold compactifications[1]. Non-trivial Wilson lines in an orbifold compactification break the GUT symmetry, and at the same time the orbifold is so chosen such that the zero modes of the Higgs triplets are projected out (since they transform non-trivially under the orbifold symmetry) leaving zero modes of only the Higgs doublets[2]. In M theory in contrast, although gauge fields propagate in extra (seven) dimensions, matter fields only live in four dimensions, hence they are *not* zero modes of a Kaluza-Klein (KK) tower of fields. So, the above mechanism of splitting will not work in M-theory. Furthermore, proposals based on symmetries that forbid μ either by a $U(1)$ or stringy selection rules, will also forbid the triplet mass M_T; these will not work as well.

An elegant solution was proposed by Witten [33] using the discrete symmetry of the G_2 manifolds. This geometric discrete symmetry can be combined with a discrete Wilson line that breaks $SU(5)$, so that the resulting symmetry (call it $F \cong Z_N$) does not commute with $SU(5)$. This allows the different components of an $SU(5)$ multiplet, which are assumed to be localized on the fixed points set of F, to have different Z_N charges [40]. Therefore, this has the potential to solve the doublet-triplet splitting problem. It is important to note that this discrete symmetry owes its origin to *local* symmetries, arising from the Lorentz group and gauge group in higher dimensions.

[1] Field theoretic constructions with similar features involving an extra orbifold dimension are given in [36, 37, 38, 39].

[2] A similar mechanism can be employed in Type II intersecting brane models with a GUT gauge group.

As such, this symmetry cannot be violated by quantum gravity effects, provided it is anomaly-free[41]. We extended this idea and made the discrete symmetry only an approximate symmetry after moduli stabilization. This provided a concrete estimation of the μ term. When we have $O(100)$ moduli fields, the μ term is about $O(0.1)\, m_{3/2}$. In the next two Chapters we will show that this result has strong implication for the dark matter detection and calculating the Higgs boson mass.

3.2.1 Review of Witten's Proposal

Here we review the geometric origin of the Z_N symmetry constructed in [40], which splits the $SU(5)$ Higgs multiplets and solves the doublet-triplet splitting problem. In M-theory compactified on a manifold X of G_2 holonomy, gauge fields are localized on a three-dimensional subspace Q of the internal G_2 manifold (in addition to that in the usual Minkowski spacetime). On the other hand, as mentioned above chiral superfields are localized on points in Q where X develops conical singularities. Thus, they only live in Minkowski spacetime.

Now, in order to break the GUT gauge symmetry ($SU(5)$ here) on Q by Wilson lines, Q must not be simply connected. In the simplest example, Q is the quotient of a three-sphere by a discrete Z_N symmetry group L, $Q \cong \mathbf{S^3}/L$. If we describe the coordinates on $\mathbf{S^3}$ by two complex numbers z_1 and z_2 with $|z_1|^2 + |z_2|^2 = 1$, then the action of L on $\mathbf{S^3}$ is given by:

$$L : z_i \to e^{2\pi i/N} z_i, \quad i = 1, 2 \tag{3.1}$$

As Q has a non-vanishing fundamental group $\pi_1(Q)$, it admits a flat $SU(5)$ vacuum gauge field configuration with non-trivial holonomy [42, 43], i.e. a Wilson line. This Wilson line takes the form

$$W = Diag\left(e^{2i\rho}, e^{2i\rho}, e^{2i\rho}, e^{-3i\rho}, e^{-3i\rho}\right), \tag{3.2}$$

where $e^{i\rho}$ is some N-th root of unity. Now, we have all the ingredients to construct the desired discrete symmetry F. We consider (or assume) X with a discrete symmetry $F \cong Z_N$, and which acts on Q as follows:

$$F : z_1 \to z_1, \;\; z_2 \to e^{2\pi i/N} z_2. \tag{3.3}$$

The fixed points of Q under F can be described by two circles S_1 and S_2, where S_1 is defined by $|z_1| = 1, z_2 = 0$ and S_2 is defined by $z_1 = 0, |z_2| = 1$. S_1 is trivially left fixed by F, while S_2 is left fixed by F modulo the equivalence relation (1) generated by L. The resulting unbroken discrete symmetry acts as F on S_1, but acts as $F \times W$ on S_2.

Now, we assume that all chiral superfields ($SU(5)$ multiplets here) are localized on $S_1 \cup S_2$.

Then, all components of a given $SU(5)$ multiplet localized on S_1 will transform with the same Z_N charge due to the action of F, but the Z_N charges of the $SU(5)$ multiplets localized on S_2 will be split by the action of the Wilson line W defined by (3.2). By localizing the Higgs $\mathbf{5_H}$ on S_1 and $\overline{\mathbf{5}}_\mathbf{H}$ on S_2 or vice versa, doublet-triplet splitting can be readily achieved by appropriately adjusting ρ and their charges under F, $q_{\mathbf{5}}$ and $q_{\overline{\mathbf{5}}}$.

However, the freedom we have in splitting the charges within the $SU(5)$ multiplets is significantly constrained. It is well-known that the Wilson line W which breaks $SU(5)$ to the SM gauge group commutes with the hypercharge $U(1)_Y$; *hence an important consequence of such Wilson line breaking is that the splitting of charges (under F) within an $SU(5)$ multiplet will be proportional to some integer times $U(1)_Y$ hypercharge*. In particular, for a $\mathbf{10_M}$ $SU(5)$ multiplet,

$$\begin{aligned} q_Q &= q_{10_M} + \rho \cdot \delta_{10} \\ q_U^c &= q_{10_M} - 4\rho \cdot \delta_{10} \\ q_E^c &= q_{10_M} + 6\rho \cdot \delta_{10} \end{aligned} \tag{3.4}$$

where q_{10} is the global charge of the $SU(5)$ multiplet under F, and $\delta_{10} = 1(0)$ if the $\mathbf{10_M}$ is localized on $S_2(S_1)$. We have normalized ρ so that it is an integer between 0 and $N-1$. Similarly, for a $\overline{\mathbf{5}}_\mathbf{M}$ multiplet,

$$\begin{aligned} q_L &= q_{\bar{5}_M} - 3\rho \cdot \delta_{\bar{5}_M} \\ q_D^c &= q_{\bar{5}_M} + 2\rho \cdot \delta_{\bar{5}_M} \end{aligned} \tag{3.5}$$

where again $\delta_{\bar{5}_M} = 1(0)$ if $\overline{\mathbf{5}}_\mathbf{M}$ is localized on $S_2(S_1)$. Triplet-doublet splitting requires the Higgs triplets to be vectorlike under the Z_N symmetry, $q_{T_u} + q_{T_d} = 0$. Since $q_{T_u/T_d} = q_{5_H/\bar{5}_H} \mp 2\rho \cdot \delta_{5_H/\bar{5}_H}$ and $q_{H_u/H_d} = q_{5_H/\bar{5}_H} \pm 3\rho \cdot \delta_{5_H/\bar{5}_H}$, requiring $q_{T_u} + q_{T_d} = 0$ leads to:

$$q_{H_u} + q_{H_d} = 5\rho \left(\delta_{5_H} - \delta_{\bar{5}_H}\right) \quad Mod\ N \tag{3.6}$$

with $\delta_{5_H}, \delta_{\bar{5}_H}$ similarly defined such that $\delta = 1(0)$ if the given multiplet is localized on $S_2(S_1)$. Therefore in order for doublet-triplet splitting to occur, one of the Higgs multiplets must be localized on S_1 and the other on S_2, giving rise to $q_{H_u} + q_{H_d} = \pm 5\rho$. Since the Z_N symmetry solves the doublet-triplet splitting problem by forbidding the μ term, Z_N must be broken in some way to generate a non-zero μ term. In section 2.3, we discuss how moduli stabilization can break this discrete symmetry and generate a non-zero μ of the correct size.

3.2.2 An Aside: R versus Non-R Discrete Symmetry

It is important to realize that the discrete symmetry F discussed in the previous subsection can in principle be of two types - R and non-R. Usually, one thinks of the discrete symmetries as non-R, i.e. in which all θ components of a given chiral superfield transform in the same manner. However, discrete symmetries can also be an R-symmetry. In the context of M theory, this happens when the G_2-invariant three-form Φ in an M-theory compactification on a G_2 manifold is not strictly invariant under the discrete symmetry F, but transforms by a phase. Since the three-form Φ is *real*[3], the only possibility is[4] :

$$\Phi \to \pm\Phi \tag{3.7}$$

Now, Φ can be written in components as :

$$\Phi_{abc} = \eta^T \, \Gamma_{abc} \, \eta, \tag{3.8}$$

where η is the covariantly constant spinor on the G_2 manifold, and Γ_{abc} is the 7 dimensional gamma matrix. Therefore, we see that when Φ transforms non-trivially ($\Phi \to -\Phi$), η transforms under F as :

$$\eta \to \pm i \, \eta. \tag{3.9}$$

Since η transforms non-trivially, the discrete symmetry F in this case is an R-symmetry.

For concreteness, the analysis in later sections is done for case when F corresponds to a discrete non-R symmetry. It is straightforward to modify the analysis for a discrete R-symmetry.

3.2.3 Generating μ via Moduli Stabilization

As discussed in above, the $\mathbf{Z_N}$ symmetry is a geometric symmetry of the internal G_2 manifold, under which the moduli are charged. The G_2 moduli [28] reside in chiral supermultiplets whose complex scalar components,

$$z^j = t^j + i s^j, \tag{3.10}$$

are formed from the geometric moduli of the manifold[5], s_i, and axionic components of the three-from C-field, t_i. We expect the moduli to break the discrete symmetry just below Planck scale

[3] This is because the G_2 manifold is a real manifold, unlike a Calabi-Yau manifold.

[4] In contrast, the holomorphic three-form in a Calabi-Yau manifold can transform by an arbitrary phase under F.

[5] Note section 2. The "i"'s are not the same in S and z.

when their vevs are stabilized [29, 8] (see Section (2.2)),

$$\langle \hat{s}_i \rangle \sim 0.1 m_p. \tag{3.11}$$

Likewise, the moduli F terms are expected to give gaugino masses in the usual way, so that

$$\langle F_{z^i} \rangle \simeq m_{1/2}\, m_p. \tag{3.12}$$

where $m_{1/2}$ is the tree level gaugino mass at the GUT scale. The axion shift symmetries $t_i \to t_i + a_i$ require that only imaginary parts of the moduli appear in perturbative interactions. The superpotential, being holomorphic in the fields, will not contain polynomial terms that explicitly depend on the moduli. The μ-term can then only be generated via Kähler interactions when supersymmetry is broken via a Guidice-Massiero like mechanism [44], i.e., from Kähler potential couplings quadratic in the Higgs fields.

To understand the size of μ (and $B\mu$) we we first find a combination of moduli fields (or product of moduli fields), invariant under the axion symmetries, that transform under (a complex representation of) $\mathbf{Z_N}$ with charge $q_{H_u} + q_{H_d}$

$$S^1 = \hat{a}^i + i\hat{s}^j \tag{3.13}$$

and another with charge $-q_{H_u} - q_{H_d}$

$$S^2 = \hat{a}^m + i\hat{s}^n. \tag{3.14}$$

These fields have the correct charge to break the symmetry and generate the μ-term which has total $\mathbf{Z_N}$ charge $-q_{H_u} - q_{H_d}$.

In a general supergravity theory [45, 34] the fermion mass matrix is

$$m^{\psi}_{ij} = m^3_{pl} e^{G/2} \left(\nabla_i G_j + G_i G_j \right) \tag{3.15}$$

and the holomorphic components of the scalar mass matrix are

$$m^{\phi\ 2}_{ij} = m^4_{pl} e^{G} \left(\nabla_i G_j + G^k \nabla_i \nabla_j G_k \right) \tag{3.16}$$

where $G = m_{pl}^{-2} K + \ln(m_{pl}^{-6} |W|^2)$ and subscripts on G denote derivatives with respect to the scalar fields ϕ_i or their conjugates $\phi^*_{\bar{i}}$. Respectively, (3.15) and (3.16) can be used to find μ

$$\mu = \langle m_{3/2} K_{H_u H_d} - F^{\bar{k}} K_{H_u H_d \bar{k}} \rangle \tag{3.17}$$

and $B\mu$

$$\begin{aligned} B\mu &= \langle 2m_{3/2}^2 K_{_{H_u H_d}} - m_{3/2} F^{\bar{k}} K_{_{H_u H_d \bar{k}}} + m_{3/2} F^m K_{_{H_u H_d m}} \\ &- \left(m_{3/2} F^m K^{n\bar{l}} K_{\bar{l} m H_u} K_{n H_d} + \left({}_{H_d} \leftrightarrow {}_{H_u} \right) \right) \\ &- F^n F^{\bar{m}} \left(\tfrac{1}{2} K_{_{H_u H_d n \bar{m}}} - K^{j\bar{l}} K_{\bar{l} n H_u} K_{j \bar{m} H_d} + \left({}_{H_d} \leftrightarrow {}_{H_u} \right) \right) \rangle \end{aligned} \tag{3.18}$$

where the indices run over the moduli fields and we have used that the superpotential does not contribute to either mass. Leading contributions come from Kahler potential terms

$$K \supset \alpha \frac{(S^1)^\dagger}{m_{pl}} H_u H_d + \beta \frac{(S^2)}{m_{pl}} H_u H_d + h.c. \tag{3.19}$$

where the coefficients α, β are expected to be $\mathcal{O}(1)$. Plugging the Kahler potential (3.19) into the formulas for μ and $B\mu$ gives

$$\begin{aligned} \mu &= \alpha \tfrac{\langle S^1 \rangle}{m_{pl}} m_{3/2} + \alpha \tfrac{\langle F^{S^1} \rangle}{m_{pl}} \\ B\mu &= 2\alpha \tfrac{\langle S^1 \rangle}{m_{pl}} m_{3/2}^2 + \alpha \tfrac{\langle F^{S^1} \rangle}{m_{pl}} m_{3/2} + \beta \tfrac{\langle F^{S^2} \rangle}{m_{pl}} m_{3/2}. \end{aligned} \tag{3.20}$$

However, as a result of (3.11), (3.12) and the suppression of $m_{1/2}$ by order two orders of magnitude in the G_2-MSSM, $\langle S^i \rangle m_{3/2} \simeq 10 \;\; \langle F^{S^i} \rangle$, the contribution to μ and $B\mu$ coming from F-terms are sub-dominant, at least if we assume that $N \ll 10^4$. Therefore, to a good approximation

$$B\mu \simeq 2\, \mu m_{3/2} \tag{3.21}$$

a fact which will have significant phenomenological consequences[6] .

The coefficients of the operators in (3.19) are in principle determined from M theory, but is not yet known how to calculate them. It is natural to assume that the coupling coefficients are of $\mathcal{O}(1)$. When combined with a model of moduli stabilization, such as in the G_2-MSSM described in [28, 29, 8] and briefly reviewed section (2.2), μ and $B\mu$ can be approximately determined. Since the real and imaginary components of the complex fields, S^1 (3.13) and S^2 (3.14), are expected to have similar, but not necessarily identical vevs, μ will generically have a phase that will be unrelated to the phases that enter the gaugino masses. But, $B\mu$ and μ will have the same phase since both are proportional to S^1 and the same coupling constant.

Before moving on to the next section we discuss the possibility that other matter fields may be charged under the $\mathbf{Z_N}$ symmetry, spontaneously break the $\mathbf{Z_N}$ symmetry, and generate μ. Consider an $SU(5)$-singlet matter field X that generates the μ-term via the superpotential coupling $X H_u H_d$. Since X is a matter field, M theory requires that it is charged under least one $U(1)$ symmetry. Then $H_u H_d$ is not invariant under the $U(1)$, and consequently, the triplet mass term $T_d T_u$ is not invariant,

[6] We leave the case of $N \geq 10^4$ for further study.

spoiling doublet-triplet splitting. Thus, such contributions should not occur.

Alternatively, the μ-term may be generated by a $U(1)$ invariant combination of two fields, for example by the operator

$$\frac{X_1 X_2}{\Lambda} H_u H_d. \tag{3.22}$$

Requiring $\mu \gtrsim 10^3$ GeV, and taking $\Lambda \sim M_{GUT}$ this would require $\sqrt{\langle X_1 X_2 \rangle} \gtrsim 10^{10}$ GeV. Radiative symmetry breaking will generally give a vev $\sim m_{3/2}$– usually large vevs are associated with FI D-terms. But since FI D-terms are absent in M theory, it may be difficult for such large vevs to arise from here. The recent results of [46] do suggest that the F-term potential can generate large matter field vevs, however in that case the vevs are too large to be relevant for the μ problem. Therefore, we very tentatively conclude that a matter field spurion is not responsible for breaking the $\mathbf{Z_N}$ symmetry and giving a physically relevant μ-term.

Finally, we comment on a potential domain wall problem. The moduli are stabilized away from a $\mathbf{Z_N}$ point, which implies that the $\mathbf{Z_N}$ symmetry was really only an approximate symmetry of the G_2-manifold. The moduli stabilization serves to parameterize the amount that the G_2-manifold differs from a $\mathbf{Z_N}$ symmetric manifold. Therefore, since the $\mathbf{Z_N}$ symmetry is not an exact symmetry of the G_2 manifold, the Lagrangian will explicitly break the $\mathbf{Z_N}$ symmetry, and domains walls would not have formed in the early universe.

3.2.4 Non-Perturbative Contributions to μ

A few points are worth mentioning regarding the arguments in the previous subsections. First, since F owes its origin to gauge or Lorentz symmetry in higher dimensions, any potential anomalies must cancel, either manifestly or by employing the Green-Schwarz mechanism in which an axion shifts in an appropriate way to cancel any apparent anomalies[47, 48]. We will discuss the constraints on low-energy physics arising from anomaly cancellation in section A.1.1.

In the arguments above, we have implicitly assumed that the discrete symmetry $F \cong Z_N$ is *manifestly* non-anomalous. If the discrete symmetry F (whether non-R or R) were anomalous with respect to any of the SM gauge symmetries, this means that at least one combination of axions must shift to cancel the corresponding anomaly. In that case, it is possible in principle to have a non-perturbative instanton term in the superpotential of the following form

$$W \supset \lambda\, e^{-b\, z}\, m_{pl}\, H_u\, H_d, \tag{3.23}$$

which is invariant under F. Here z is a holomorphic modulus with the appropriate shift under F to make $e^{-b\, z}\, H_u\, H_d$ invariant under F[7], and λ is a numerical coefficient. Note that this is true

[7]Of course, whether such a term is *really* present in a given model depends on the charge assignments of $H_u H_d$

for both anomalous discrete non-R and R symmetries; the difference between the two cases only lies in the charge assignments of $H_u H_d$ and z under F which allows the $e^{-b\,z}\,H_u\,H_d$ operator in the superpotential. In this case it is still possible to have the Kähler potential operator (3.19) in addition, if there exists a modulus S with the appropriate F charge.

Thus, if the discrete symmetry F is anomaly-free only after taking the Green-Schwarz mechanism into account, then there are two potential contributions to the μ parameter - one from a non-perturbative superpotential term (3.23), and one from a Kähler potential term. In particular, the contribution from the superpotential operator is rather uncertain, because the exponential prefactor in (3.23) is model-dependent[8]. Furthermore, for a given axionic shift Δz, the contribution to μ from (14) is exponentially sensitive to the charge of $H_u\,H_d$, as $b\,\Delta z = i\ (q_{H_u} + q_{H_d}\ \ Mod\,2\pi)$ and the contribution to the μ term is proportional to $e^{-b\langle z\rangle}$.

For the particular case in which $H_u\,H_d$ has charge 0 under a discrete R-symmetry, the non-perturbative contribution to μ can be related to the vev of non-perturbative hidden sector superpotential W_0 responsible for low scale supersymmetry for a vanishingly small cosmological constant [50]. Now, it is known that in $\mathcal{N}=1$ SUGRA, the gravitino mass is :

$$m_{3/2} = e^{K/2}\,\langle W\rangle \simeq \frac{W_0}{\mathcal{V}^p} \tag{3.24}$$

where $\mathcal{V}$ is the volume of the internal manifold in string units, and p is a rational number depending on the type of string/M theory in question ($p=1$ for Heterotic, while $p=3/2$ for M-theory).

Therefore, even after assuming $\lambda = \mathcal{O}(1)$, the contribution to μ from (3.23) can only be related to $m_{3/2}$ up to a volume factor which is very model and moduli-stabilization dependent. In contrast, for a discrete symmetry which is manifestly non-anomalous, the only possible contribution to μ arises from the Kähler potential operator (3.19) and is determined much more precisely. In the rest of the paper, to be precise, we will only consider a discrete non-R symmetry for which the dominant comtribution to μ comes from Giudice-Masiero operators (3.19), which is natural to expect in the case of a manifestly anomaly free discrete symmetry.

On the other hand, we will show that as far as the implications for Yukawa couplings and RPV operators are concerned, our results are independent of whether F is manifestly anomaly-free or not.

---

and z under F.

[8]For a discussion of this in an F-theory context, see [49]

3.2.5 Constraints on the (approximate) Z_N Symmetry

3.2.5.1 Theoretical Constraints from Anomaly Cancellation

Having discussed the origin of the Z_N symmetry which potentially solves the μ problem, we now discuss theoretical constraints on this discrete symmetry. As mentioned earlier, if the Z_N is consistently embedded within a UV complete theory, the gauge-gauge-Z_N anomaly coefficients in the low energy theory should vanish. For instance, if the discrete symmetry is consistently embedded within a gauge symmetry broken at some higher scale[41], gauge invariance implies that anomaly cancellation constraints on Z_N must be satisfied [51, 52]. In addition, arguments from t'Hooft anomaly matching conditions imply that if the discrete Z_N symmetry results from a geometric symmetry in higher dimensions, the linear Gauge-Gauge-Z_N anomaly cancellation constraints should hold [53, 54, 55]. We will not consider Z_N-Gravity anomalies below, in general one can always add hidden sectors to balance the anomaly coefficients.

The $SU(3)-SU(3)-Z_N, SU(2)-SU(2)-Z_N$ and $U(1)_Y-U(1)_Y-Z_N$ anomaly coefficients A_3, A_2, A_1 are provided in Appendix A.1.1 for a non-R Z_N symmetry. Anomaly universality (which must occur for $SU(5)$ unification [48]) requires[9]:

$$\begin{aligned} A_3 &= \sigma_A \bmod \eta \\ A_2 &= \sigma_A \bmod \eta \\ 5A_1 &= 5\sigma_A \bmod \eta \end{aligned} \tag{3.25}$$

where $\eta = N$ for odd N and $\eta = N/2$ for even N. For non-zero σ_A mod η, anomaly cancellation requires that a Green-Schwarz axion be present with a discrete shift symmetry which cancels the anomaly in order to make anomaly freedom manifest.

Ibanez and Ross were the first to systematically discuss these anomaly constraints and categorize anomaly free abelian Z_N symmetries which forbid dangerous proton-decay inducing operators [51], with an extended analysis performed by Dreiner et. al in [57]. Motivated by this work, many authors have constructed anomaly free Z_N R-symmetries [58, 47, 59, 60, 61, 56, 62] which address the μ problem while forbidding dangerous B-L violating operators. In particular, [59] demonstrated that requiring a Z_N which solves the μ problem, commutes with $SO(10)$ and allows the Weinberg LH_uLH_u neutrino mass operator leads to a unique Z_4^R symmetry, which can be obtained as a remenant of an internal symmetry in heterotic orbifold compactifications [63, 56].

In contrast to the case of a Z_N^R symmetry, anomaly cancellation constraints are more difficult to

[9] Because of the normalization of the hypercharge used in the definition of A_1, A_1 is only defined $\bmod \frac{\eta}{5}$. See for example Appendix B of [56]

satisfy for non-R Z_N symmetries which solve the doublet-triplet splitting problem. This was first pointed out in [59], where it was shown that if a non-R Z_N symmetry commutes with $SU(5)$ in the matter sector, it can not simaltaneously satisfy anomaly cancellation and doublet-triplet splitting. Indeed if $q_{Q^i} = q_{U^i}$ and $q_{D^i} = q_{L^i}$, the anomaly constraint $A_3 = A_2 \bmod \eta$ is equivalent to:

$$(q_{T_u} + q_{T_d}) = (q_{H_u} + q_{H_d}) \bmod N \tag{3.26}$$

completing the aforementioned proof. However, assuming that the $\mathbf{10}$ and $\overline{\mathbf{5}}$ matter multiplets are not split by the Z_N symmetry is in a sense ad-hoc. With the doublet-triplet splitting mechanism discussed in Section 2, the same mechanism that splits the Higgs $SU(5)$ multiplets can also split matter sector $SU(5)$ multiplets. Using the language of Section 2, the no-go theorem of [59] is not applicable if some of the $\mathbf{10_M}, \overline{\mathbf{5}}_\mathbf{M}$ matter fields are localized on S_2 such that their Z_N charges are split by the action of the Wilson line (3.2).

Combining the Wilson line contraints with the requirements of anomaly cancellation and doublet-triplet splitting significantly limits the possible Z_N charge assignments for the MSSM fields. The consequences of combining these constraints are discussed in detail in Appendix A.1. An interesting result which arises is that at least one of the mass eigenvalues in the down quark or lepton sector will be forbidden by the Z_N symmetry. The derivation of this result is provided in Appendix A.1.2. Thus in order for this solution to the μ problem to give realistic physics, at least one of the fermion masses must be generated in some manner once the Z_N symmetry is broken by moduli stabilization. Therefore this $SU(5)$ Wilson line solution to the doublet-triplet splitting problem implies a direct connection between the μ term and textures in the fermion Yukawa couplings. The only phenomenological input required to derive this result is the requirement of doublet-triplet splitting; the anomaly and $SU(5)$ Wilson line constraints are purely theoretical and arise from consistently embedding the Z_N symmetry in a UV completion, such as the M-theory compactifications discussed in [40].

3.2.5.2 Phenomenological Constraints from Proton Decay

In addition to anomaly constraints, there are also phenomenological constraints on the nature of the Z_N symmetry. As already discussed, the Z_N symmetry must forbid the μ term and allow the triplet mass term $T_u T_d$. Additional constraints arise from considering the proton decay rate induced by R-parity violating operators if they are not forbidden by the Z_N. The possible R-parity violating superpotential operators in the MSSM are given by:

$$W_{RPV} \supset \mu_i L_i H_u + \lambda'_{ijk} L_i L_j {E^c}_k + \lambda''_{ijk} Q_i L_j D^c_k + \lambda'''_{ijk} D^c_i D^c_j U^c_k, \tag{3.27}$$

where gauge invariance requires antisymmetry of λ' and λ''' under interchange of the first two indices. All three bilinear $\mu_i L_i H_u$ terms must be forbidden by the Z_N symmetry in order to not destabilize the weak scale. The trilinear QLD^c and $U^cU^cD^c$ terms induce proton decay; constraints on the proton lifetime result in (see for example section 5 of [64]):

$$\lambda''\lambda''' \lesssim 10^{-24}, \tag{3.28}$$

where λ'' and λ''' in the preceding expression are taken to be the dominant RPV couplings in $\lambda''_{ijk}, \lambda'''_{ijk}$. Thus, in order to satisfy proton decay constraints, at least one of the QLD^c, $U^cD^cD^c$ operators must be forbidden by Z_N. Since LLE^c does not induce proton decay, constraints on this coupling are not as strong, although the presence or absence of this coupling will significantly impact LSP phenomenology.

In addition to dimension 4 RPV operators, it is well known that dimension 5 RPV superpotential operators $QQQL$ and $U^cD^cU^cE^c$ can also induce proton decay rates which contradict current experimental bounds, despite being suppressed by the heavy Higgs triplet mass scale[65]. In order to avoid proton decay constraints, these dimension 5 operators must also be forbidden by Z_N[10]. Combining these constraints, we consider only Z_N symmetries which satisfy the following criteria[11]:

1. The Z_N charge of $T_u\, T_d = 0 \bmod N$. This can always be satisfied by imposing (3.6) and appropriately choosing $q_{\mathbf{5_H}}$ and $q_{\bar{\mathbf{5}}_{\mathbf{H}}}$.
2. The Z_N charge of $H_u\, H_d \neq 0 \bmod N$. This can always be satisfied by imposing (3.6) and the requirement $5\rho \neq 0 \bmod N$.
3. The Z_N charge of $L_i\, H_u \neq 0 \bmod N$ for all three generations.
4. The Z_N charge of either $Q\, L\, D^c$, $U^c\, D^c\, D^c$, or both $\neq 0 \bmod N$ for all generation indices.
5. The Z_N charge of both $QQQL$ and $U^cD^cU^cE^c \neq 0 \bmod N$ for all generation indices.

These conditions are necessary but not sufficient for a fully realistic theory. This is because generating a nonzero μ term will break the Z_N symmetry; this can potentially regenerate the dangerous RPV terms in (3.27), resulting in unacceptable proton decay rates and/or experimentally excluded neutrino masses. As we will discuss in the following section, there must be some left-over Z_M symmetry which remains when Z_N is broken to generate the μ term in order to satisfy

[10] If forbidden by the Z_N symmetry, such couplings can still be induced once the Z_N symmetry is broken and the μ term is generated. However the coefficients of these couplings will be suppressed by a factor of μ/m_{pl} in addition to the triplet mass scale, avoiding proton decay constraints by several orders of magnitude.

[11] We assume a cosmological history in which baryogenesis is achieved via an Affleck-Dine type mechanism [66], so that the presence of RPV terms will not wash-out any baryon asymmetry.

experimental constraints. The embedding of the exact Z_M symmetry within the Z_N symmetry will determine the resulting R-Parity violating or R-parity conserving structure of the low energy theory.

3.2.6 The Necessity of Another Exact Symmetry

As discussed in section 3.2.3, the discrete Z_N symmetry must be broken by moduli stabilization in order to generate the μ term. In addition to the μ term, the RPV operators in (3.27) can potentially be regenerated with coefficients $\mu_i \sim \mu$, $\lambda, \lambda'\lambda'' \sim \mathcal{O}(\mu/m_{pl})$. Alternatively, there may be a leftover discrete symmetry that remains exact once the μ term is generated, such that some or all of these RPV operators are still forbidden when moduli stabilization breaks Z_N. This is equivalent to saying that there is some Z_N symmetry in moduli space, which breaks to an exact $Z_M \subset Z_N$ subgroup upon moduli stabilization.

If the Z_N symmetry forbids all RPV operators in (3.27), but moduli stabilization completely breaks the Z_N symmetry (i.e. Z_M is trivial), we expect the RPV superpotential to be generated as discussed in [64]:

$$W_{RPV} \sim \epsilon\mu L_i H_u + \mathcal{O}\left(\frac{\mu}{m_{pl}}\right) LLE^c + \mathcal{O}\left(\frac{\mu}{m_{pl}}\right) QLD^c + \mathcal{O}\left(\frac{\mu}{m_{pl}}\right) D^c D^c U^c \tag{3.29}$$

Making the field redefinition

$$H_d' = \frac{(\mu H_d + \epsilon\mu L_i)}{\sqrt{\mu^2 + \epsilon\mu^2}} \tag{3.30}$$

$$L_i' = \frac{(\epsilon\mu L + \mu H_d)}{\sqrt{\mu^2 + \epsilon\mu^2}} \tag{3.31}$$

absorbs the LH_u term into the μ term, but due to the Yukawa couplings this field redefinition will also generate superpotential couplings such that:

$$W_{RPV} \sim \epsilon\left(y_\ell LLE^c + y_d QLD^c\right) + \mathcal{O}\left(\frac{\mu}{m_{pl}}\right) D^c D^c U^c \tag{3.32}$$

where we have assumed $\epsilon \lesssim \mathcal{O}(1)$.

Applying the proton decay constraint (3.28) with $\lambda' \sim \epsilon y_d$ and $\lambda'' \sim \mu/m_{pl}$, we see that the superpotential in (3.29) is excluded by several orders of magnitude unless $\epsilon \lesssim 10^{-5}$. A similar constraint on ϵ arises from neutrino mass constraints. This corresponds to a fine-tuning of the coefficient in the Kähler potential which gives the LH_u term as we naturally expect $\epsilon \lesssim \mathcal{O}(1)$. Thus in order for the Z_N symmetry to be phenomenologically viable, it can not be broken such

that all RPV couplings are regenerated with naturally expected coefficients[12].

Even if moduli stabilization results in a "nearby" manifold in moduli space, such that the breaking of this Z_N can be parameterized by non-renormalizable operators proportional to some modulus *vev* as in (3.32), small breaking effects can still violate the numerous experimental constraints discussed in this paper. For the Z_4^R symmetry from the heterotic orbifold considered in [59], it is assumed that instantons break this symmetry to an exact Z_2 which acts as R-parity. Since this Z_4^R is the remnant of a geometric symmetry on the orbifold, one must check that moduli stabilization does not stabilize moduli far away from the orbifold point, or else the Z_2 symmetry will be badly broken and operators similar to (3.32) will be generated[13].

3.2.7 Embedding Z_M within Z_N

In principle the exact symmetry and the approximate symmetry are unrelated to each other, after all they correspond to two different manifolds. In order to be explicit in the following discussion however, we adopt the simplest possibility: We assume the exact symmetry Z_M is a subgroup of the approximate symmetry Z_N, with compatible charge assignment of the matter and moduli fields. In other words Z_N is not completely broken by moduli stabilization and generation of the μ term. To achieve this we must impose the additional constraint that the Z_N charges of some RPV superpotential terms in (3.27) are such that they are not necessarily generated upon moduli stabilization. If we denote S as the "effective modulus field" which transforms in a complex representation of Z_N and generates the μ term as in equation (3.19), then an RPV superpotential operator forbidden by Z_N will be generated once the μ term is generated if the Kähler potential terms

$$K \supset \frac{S^n}{(m_{pl})^{n+1}}\mathcal{O}^{D3}_{RPV} + \frac{S^n}{(m_{pl})^{n}}\mathcal{O}^{D2}_{RPV} \tag{3.33}$$

are uncharged under Z_N, where $\mathcal{O}^{D3}_{RPV}$ and $\mathcal{O}^{D2}_{RPV}$ represent dimension 3 and dimension 2 RPV superpotential operators forbidden by the Z_N symmetry. Stated in terms of Z_N charges, if S has Z_N charge q_S and the operator $\mathcal{O}$ has charge $q_{\mathcal{O}}$, $\mathcal{O}$ will be generated when the μ term is generated if:

[12] One could imagine suppressing further suppressing the LH_u operator with a $U(1)_\chi$ gauge symmetry. Any such gauge symmetry must be broken at or above the TeV scale in order to avoid experimental constraints, and doing so requires additional model building. For example, if there are no additional $\mathcal{O}(1)$ Yukawa couplings in the superpotential besides the top yukawa, a significant non-universality in the soft-breaking scalar masses is required to break $U(1)_\chi$ with a right-handed sneutrino VEV[67]. On the other hand, if there are exotics charged under $U(1)_\chi$ with large superpotential couplings, these couplings can drive the breaking of $U(1)_\chi$ without a non-universal soft-mass spectrum [68]. We will not consider such non-minimal further models in this work.

[13] A similar analysis examining instanton effects which generate proton-decay operators forbidden by an anomalous $U(1)$ was performed in the context of intersecting D-brane models [69].

$$n\, q_S + q_{\mathcal{O}} = kN. \tag{3.34}$$

for some integer n and k. Applying Bezout's lemma[14] to (3.34), it is straightforward to show that an operator $\mathcal{O}$ forbidden by Z_N will be generated by moduli stabilization if:

$$Mod\,(q_{\mathcal{O}}, q_{eff}) = 0 \tag{3.35}$$

where q_{eff} is the greatest common divisor of N and q_s. In other words, once the μ term is generated, the Z_N symmetry will be broken to at least a Z_M symmetry, where $M = q_{eff}$. It is possible that the Z_N symmetry will be further broken by some other modulus VEV $\langle S' \rangle$ with some other Z_N charge $q_{S'}$. In this case, q_{eff} in equation (3.35) becomes the greatest common divisor of N, q_S and $q_{S'}$. The generalization to several different charges for moduli VEVs is straightforward, although given a finite integer N the maximum number of different moduli VEVs which still give a nontrivial Z_M symmetry is limited.[15]

In either case, in order to satisfy the experimental constraints mentioned in this section the remaining Z_M symmetry should not be trivial ($M = q_{eff} \neq 1$). From this, we immediately see that N can not be prime, and that N, q_S and q'_S must have some non-trivial common factor. For the simplest case involving only a single modulus VEV with charge q_s, $N = 4$ is the lowest possible order for the Z_N symmetry. If $q_S \neq q_{S'}$, the lowest order symmetry we can obtain which has a non-trivial leftover symmetry is a Z_8 symmetry. Because the μ term is by definition uncharged under Z_M, we can use equation (6) to obtain a relationship between the Wilson line parameter ρ and M:

$$5\rho = 0 \text{ Mod } M. \tag{3.36}$$

This relation will enable us to derive important results in the RPV scenario.

Even if there is a non-trivial exact[16] Z_M symmetry which remains upon moduli stabilization, the possible patterns of RPV operators allowed by the Z_M symmetry are severely restricted by experimental constraints. In addition to proton decay constraints, one must also consider con-

[14] Bezout's lemma states that for integer a, b and d, the equation $x\,a + y\,b = d$ will have solutions for integer x and y if d is a multiple of the greatest common divisor of x and y. Applying this to (3.34) with $a = q_s, b = N$ and $d = q_{\mathcal{O}}$ results in (3.35).

[15] Instead of the operator given in (3.19), it is possible that the dominant contribution to the μ term comes from operators of the form $K \supset (S/m_{pl})^m H_u H_d$, such that $m\, q_S = -q_{Hu} - q_{Hd}\ \ Mod\ N$. In this case, the μ term will be suppressed by additional powers of the modulus VEV. In this scenario, q_{eff} is still the greatest common divisor of N, q_S and q'_S, and thus the results regarding the Z_M symmetry are unchanged.

[16] In this work we assume that the remaining Z_M symmetry is exact. In principal, Z_M could be broken at some scale Λ such by some mechanism; if $\Lambda \ll \mu$ then the regenerated RPV operators might have coefficients small enough to avoid experimental constraints. However, this requires the introduction of a new scale of Z_M breaking Λ, which at this point seems ad hoc.

Z_4 Charge	Q_1	Q_2	Q_3	U_1	U_2	U_3	E_c^1	E_c^2	E_c^3
	3	3	3	3	3	3	3	3	3

Z_4 Charge	D_1	D_2	D_3	L_1	L_2	L_3	H_u	H_d	T_u	T_d
	3	1	1	1	1	1	2	0	0	0

Table 3.1: Non anomalous Z_4 symmetry which satisfies Wilson line and phenomenological constraints. This symmetry is manifestly anomaly free and does not require any GS mechanism for anomaly cancellation. One of the down quark masses is forbidden by this Z_4, and therefore must be radiatively generated once the symmetry is broken, for example by non-holomorphic Higgs coupling between the $\bar{H}_u$ and the down-type quarks/leptons. If all moduli fields have even charge under this Z_4, this Z_4 symmetry can be broken to an exact Z_2 R-parity upon moduli stabilization.

straints on neutrino masses from bilinear $\mu_i L H_u$ operators and astrophysical constraints on the LSP lifetime.

Despite the numerous theoretical and phenomenological constraints on Z_N/Z_M symmetries discussed in this work, it is not difficult to find examples of Z_N symmetries which satisfy all specified constraints. The lowest order symmetry with all the desired properties is a Z_4 symmetry; an example is given in Table 3.1. This symmetry can be broken to an exact Z_2 R-Parity once moduli stabilization generates the μ term. A key point is that for any leftover symmetry to remain upon moduli stabilization, the moduli fields must be uncharged under a subgroup of Z_N. For the example in Table 3.1, the moduli fields must have even charge under Z_4 so that a leftover Z_2 symmetry remains upon moduli stabilization.

3.3 Electroweak Symmetry Breaking and Little Hierarchy Problem

The main result of the previous section is the prediction of a suppressed μ term.

$$\mu \sim \frac{\langle \mathrm{S} \rangle}{m_{pl}} m_{3/2} \tag{3.37}$$

This result by itself is a top-down prediction. One still need to check whether the electroweak symmetry breaking (EWSB) condition is compatible with this result. In fact, this is deeply related to the little hierarchy problem. Most of the new physics models introduces new particles and interactions that are constrained by experimental results. The easiest solution to avoid the experimental bounds is to make new particles heavy. Then one needs to explain the hierarchy between the electroweak scale and the new physics scale. In the G_2-MSSM case, there are two scales: The scalars

are typically $O(50\,\mathrm{TeV})$, and the μ term is $O(5\,\mathrm{TeV})$. One of the EWSB conditions is:

$$M_Z^2 = -2|\mu|^2 + 2\frac{m_{H_d}^2 - m_{H_u}^2 \tan^2\beta}{\tan^2\beta - 1} \tag{3.38}$$

It is not obvious the equation can be satisfied with μ so much smaller than the scalar masses. However as we are going to show in the following subsections, cancellation naturally occurs in G_2-MSSM, and EWSB is perfectly consistent with a suppressed μ term.

3.3.1 Electroweak Symmetry Breaking

The first and foremost phenomenological constraint is that the theory accurately produce electroweak symmetry breaking. That is, the theory must give a stable potential (bounded from below), break the electroweak symmetry and allow for the correct Z-boson mass. Respectively, these three conditions can be quantified by the following tree level constraints at the EWSB scale

$$\begin{aligned} |B\mu| &\leq \tfrac{1}{2}(m_{H_u}^2 + m_{H_d}^2) + |\mu|^2 \\ |B\mu|^2 &\geq (m_{H_u}^2 + |\mu|^2)(m_{H_d}^2 + |\mu|^2) \\ M_Z^2 &= -2|\mu|^2 + 2\frac{m_{H_d}^2 - m_{H_u}^2 \tan^2\beta}{\tan^2\beta - 1} \end{aligned} \tag{3.39}$$

where $\tan\beta$ is not an independent parameter, but is determined by

$$\sin 2\beta = \frac{-2B\mu}{m_A^2}. \tag{3.40}$$

and

$$m_A^2 = m_{H_u}^2 + m_{H_d}^2 + 2|\mu|^2. \tag{3.41}$$

where A is the pseudoscalar Higgs boson.

To get a feeling for $\tan\beta$, we plug in the expected values (at the unification scale and with degenerate scalars) of $B\mu \simeq 0.2 m_{3/2}^2$ and $m_A^2 \simeq 2m_{3/2}^2$, into (3.40) which gives $\tan\beta \simeq 10$. On the other hand, RGE flow will lower the values of both $B\mu$ and m_A^2, resulting in variations around $\tan\beta \simeq 10$. When $\tan\beta$ is not small, it can be approximated as

$$\tan\beta = \frac{m_{H_d}^2}{B\mu}. \tag{3.42}$$

Inserting (3.42) to (3.39) and solve for μ while assuming μ is small, we obtain

$$\mu^2 = \frac{m_{H_d}^2}{B^2 - m_{H_d}^2} m_{H_u}^2. \tag{3.43}$$

It is obvious the solution is self-consistent when B and m_{H_d} are not very close and m_{H_u} is small. In the next section we will show these conditions are satisfied by the RGEs solutions.

3.3.2 Renormalization Group Equations of MSSM

The masses and couplings we calculated from the supergravity formalism are the values at the unification scale. In order to study EWSB, it is necessary to calculate their values at the electroweak scale using the RGEs. When $\tan\beta$ is not very large, the relevant RGEs at 1-loop are the RGEs of the gauge couplings, the top Yukawa coupling, the soft masses of H_u, H_d, Q_3 and T_3, the trilinear coupling A_t, and $B\mu$.

First we consider the one-loop RGEs for the gauge couplings:

$$16\pi^2 \frac{dg_1}{dt} = \frac{33}{5} g_1^3, \tag{3.44}$$

$$16\pi^2 \frac{dg_2}{dt} = g_2^3, \tag{3.45}$$

$$16\pi^2 \frac{dg_3}{dt} = -3g_3^3, \tag{3.46}$$

where $t = \log(\mu/M_{GUT})$. Applying the boundary condition that all the gauge coupling unify at the unification scale, we can solve for $\alpha_i = g_i^2/4\pi$:

$$\frac{1}{\alpha_1} = \frac{1}{\alpha_0} - \frac{33}{10\pi} t, \tag{3.47}$$

$$\frac{1}{\alpha_2} = \frac{1}{\alpha_0} - \frac{1}{2\pi} t, \tag{3.48}$$

$$\frac{1}{\alpha_3} = \frac{1}{\alpha_0} + \frac{3}{2\pi} t. \tag{3.49}$$

$t = 0$ corresponds to the unification scale and α_0 is the unified gauge coupling.

After solving the RGEs for the gauge coupling, we can consider the top Yukawa coupling

$$16\pi^2 \frac{dy_t}{dt} = y_t \left(6|y_t|^2 - \frac{16}{3} g_3^2 - 3g_2^2 - \frac{13}{15} g_1^2 \right). \tag{3.50}$$

The solution can be written as

$$\alpha_t(t) \equiv \frac{y_t^2}{16\pi^2} = \frac{\alpha_t(0)E(t)}{1-12\alpha_t(0)F(t)}. \tag{3.51}$$

Here as usual $\alpha_t = y_t^2/4\pi$, and the function $E\,(t)$ and $F\,(t)$ are defined as

$$E(t) = \left(1+6\frac{\alpha_0}{4\pi}t\right)^{-\frac{16}{9}} \left(1-2\frac{\alpha_0}{4\pi}t\right)^3 \left(1-\frac{66}{5}\frac{\alpha_0}{4\pi}t\right)^{\frac{13}{99}}, \tag{3.52}$$

$$F(t) = \int_0^t E(t')dt'. \tag{3.53}$$

$F(t)$ has to be evaluated numerically, if we assume $\alpha_0 = \frac{1}{25}$, the unification scale is $2.88 \times 10^{16}\,\mathrm{GeV}$, SUSY breaking scale is $6.96 \times 10^3\,\mathrm{GeV}$, $t = -29$, then $E(t) = 8.26$ and $F(t) = -92.57$. Because $y_t(M_{\mathrm{SUSY}}) = 0.8$, we can calculate $y_t(0) = 0.41$, ($6\alpha_t(0)F(M_{\mathrm{SUSY}}) \approx$-0.6).

Finally it is easy to solve the RGEs of the trilinear coupling and the soft masses.

$$\frac{dA_t}{dt} = 12\alpha_t(t)A_t, \tag{3.54}$$

$$\frac{dB}{dt} = 6\alpha_t(t)A_t, \tag{3.55}$$

$$\frac{dm_{H_u}^2}{dt} = 6\alpha_t(t)(m_{Q_3}^2 + m_{U_3}^2 + m_{H_u}^2 + |A_t|^2), \tag{3.56}$$

$$\frac{dm_{U_3}^2}{dt} = 4\alpha_t(t)(m_{Q_3}^2 + m_{U_3}^2 + m_{H_u}^2 + |A_t|^2), \tag{3.57}$$

$$\frac{dm_{Q_3}^2}{dt} = 2\alpha_t(t)(m_{Q_3}^2 + m_{U_3}^2 + m_{H_u}^2 + |A_t|^2). \tag{3.58}$$

The solutions are

$$B(t) = B(0) + \frac{6\alpha_t(0)F(t)}{1-12\alpha_t(0)F(t)}A_t(0) \approx 2m_0 - 0.3A_0, \tag{3.59}$$

$$A_t(t) = \frac{A_t(0)}{1-12\alpha_t(0)F(t)} \approx 0.45A_0, \tag{3.60}$$

$$m_{H_U}^2 = \frac{1}{2}\left(m_{H_U}^2(0) - m_{U_3}^2(0) - m_{Q_3}^2(0) + G\,(t)\right) \approx 0.18m_0^2 - 0.12A_0^2, \tag{3.61}$$

$$m_{U_3}^2 = \frac{1}{3}\left(-m_{H_U}^2(0) + 2m_{U_3}^2(0) - m_{Q_3}^2(0) + G\,(t)\right) \approx 0.45m_0^2 - 0.08A_0^2, \tag{3.62}$$

$$m_Q^2 = \frac{1}{6}\left(-m_{H_U}^2(0) - m_{U_3}^2(0) + 5m_{Q_3}^2(0) + G\,(t)\right) \approx m_0^2 - 0.04.A_0^2 \tag{3.63}$$

For the numerical result, we assume the scalar masses are unified to m_0 at the unification scale,

and $B_0 = 2m_0$. We also define $G(t)$ as:

$$G(t) = \frac{m_{H_U}^2(0) + m_{U_3}^2(0) + m_{Q_3}^2(0)}{1 - 12\alpha_t(0)F(t)} + \frac{12\alpha_t(0)F(t)A_t^2(0)}{(1 - 12\alpha_t(0)F(t))^2} \tag{3.64}$$

3.3.3 General Mechanism and Numerical Results

As shown in the previous subsection, the RG equations for the Higgs mass-squared parameters $m_{H_u}^2(t)$ and $m_{H_d}^2(t)$–which will feed directly into the calculation of the Higgs vev (see Eq.(3.39))–shows that $m_{H_d}^2$ essentially does not run, while $m_{H_u}^2$ does, so that one has that $m_{H_d}^2(t) \simeq M_0^2$ and

$$m_{H_u}^2(t) \simeq f_{M_0}(t)M_0^2 - f_{A_0}(t)A_0^2 + R(t)\ , \tag{3.65}$$

where $t = ln(Q/M_{GUT})$, M_{GUT} being the unification scale. The functions f_{M_0}, f_{A_0} are, to leading order, determined by Standard Model quantities (gauge couplings and Yukawa couplings) and the unification scale. Analytical formulas for f_{M_0}, f_{A_0} are given in the Appendices for one-loop running, while the numerical calculations are performed using the full two-loop RG equations. $R(t) = f_3(t)A_0M_3(0) + f_4(t)M_3^2(0) + \ldots$ are corrections that are smaller or the same size as the sum of the first two terms in Eq. (3.65). One finds that f_{M_0} and f_{A_0} at the EWSB scale have a value of

$$f_{M_0} \simeq f_{A_0} \simeq 0.1\ . \tag{3.66}$$

Thus $m_{H_u}^2$ is suppressed by the values of f_{M_0}, f_{A_0}. To illustrate this effect, we plot f_{M_0} vs. f_{A_0} in Fig. (3.2) which shows the dependence of $m_{H_u}^2(Q_{\rm EWSB})$ on the soft masses is reduced, as is the size of $m_{H_u}^2(Q_{\rm EWSB})$ relative to $M_{3/2}$.

At first it may seem that results in Eq.(3.66) are independent of the scale of the soft masses, but in-fact large scalar masses, of order 10 TeV and larger, are necessary for this effect. This scale already arises as a bound from BBN on moduli-masses, which in turn gives a similar bound on the soft-breaking scalar superpartner masses [32]. As discussed in the previous subsection, the values of f_{M_0} and f_{A_0} are mostly sensitive to the top Yukawa coupling. The top mass receives large $(10 - 15)\%$ corrections from squark/gluino loops [70] in the models we discuss, resulting in a lower top Yukawa coupling required to produce the correct top-quark mass. In other types of models which are not the type studied here, loop corrections from lighter squarks below about 5 TeV do not provide sufficient suppression, and the large Yukawa coupling would drive $m_{H_u}^2$ negative.

G_2-MSSM predicts an additional cancellation in $m_{H_u}^2(Q_{\rm EWSB})$, since the supergravity Lagrangian generically predicts that

$$M_0 \simeq A_0 \simeq M_{3/2}\ . \tag{3.67}$$

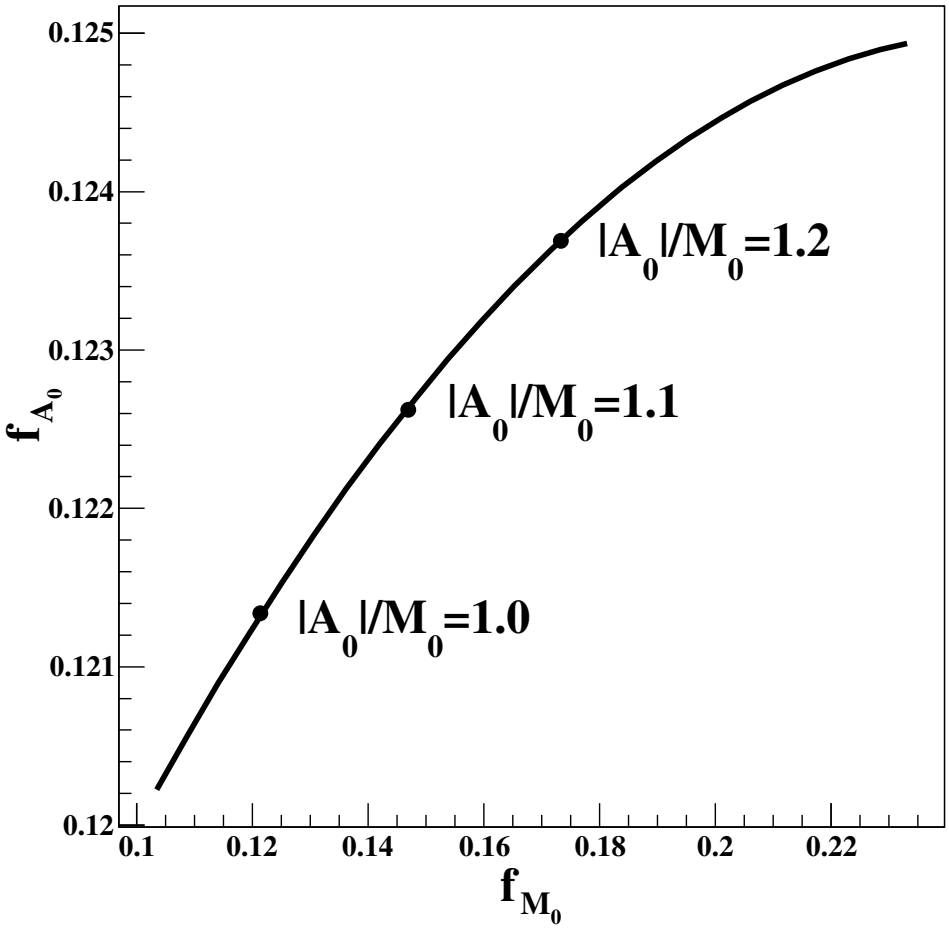

Figure 3.2: The 1 loop RGE coefficients f_{M_0} and f_{A_0} at $Q_{\rm EWSB}$ as given in Eq.(3.65). The amount of cancellation in the Eq.(3.65) for $m^2_{H_u}(Q_{\rm EWSB})$ depends on $|A_0|/M_0$, and we show the values that minimize $m^2_{H_u}$ at one-loop. In this figure, M_0 runs from 10 TeV at the lower end of the curve to 50 TeV at the top of the curve. (See Fig. (3.4) for the full analysis with with 2 loop running and the threshold/radiative corrections.)

Since the values of f_{M_0}, f_{A_0} are naturally each order 0.1 and their difference leads to another suppression of order 0.1, the natural scale of $m^2_{H_u}(Q_{\rm EWSB})$ is

$$m^2_{H_u} \sim 10^{-2} M^2_{3/2} \sim \mathcal{O}({\rm TeV}^2) \ . \tag{3.68}$$

Thus, the effects of the large M_0^2 and A_0^2 in the determination of $m^2_{H_u}(Q_{\rm EWSB})$ are absent, and the naive fine-tuning is significantly reduced.

As a result of this cancellation the corrections of the size R in Eq.(3.65) are smaller or the same size as the term that cancels: $f_{M_0}(t)M_0^2 - f_{A_0}(t)A_0^2$. This allows for a value μ (and M_3) at

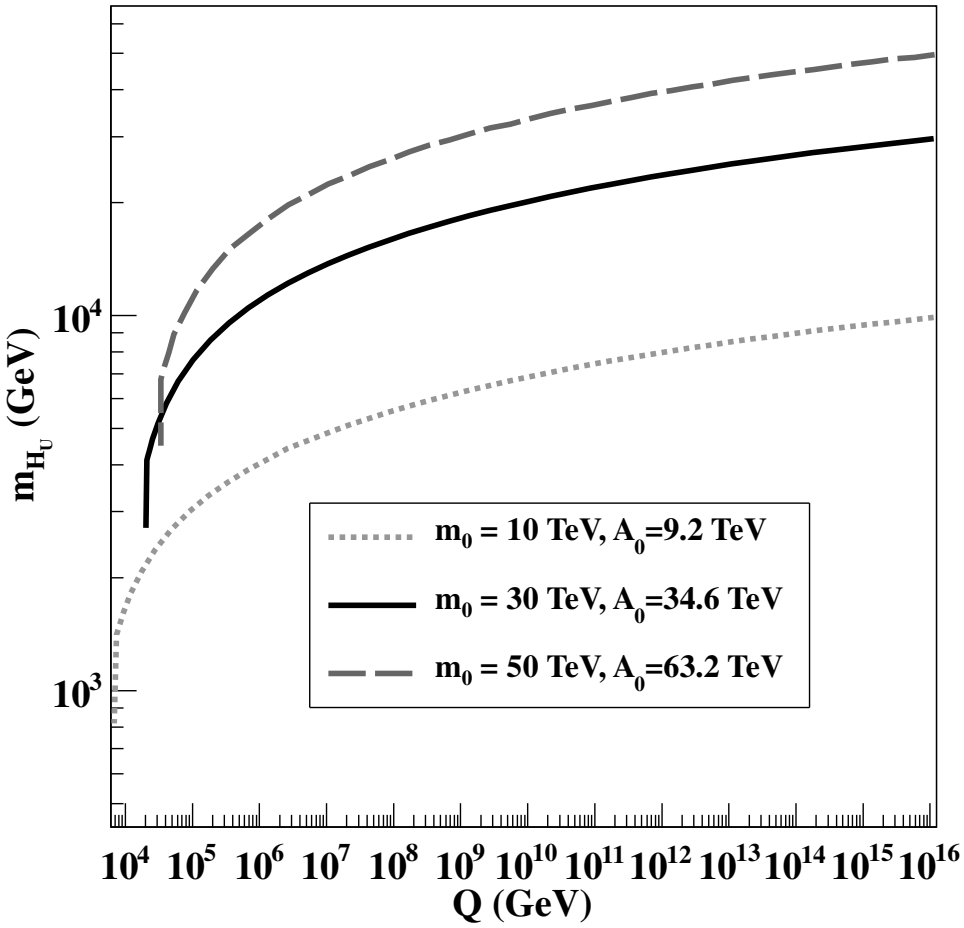

Figure 3.3: Two-loop renormalization group running of m_{H_u} for 3 models for the cases $M_0 = (10, 30, 50)$ TeV. The tadpole corrections are shown, and appear as a vertical drop at $Q_{\rm EWSB} = \sqrt{m_{\tilde{t}_1} m_{\tilde{t}_2}}$ as is appropriate. The numerical value of $\bar{m}_{H_u}$, which is the tree + tadpole value, continue to take the same value at scales Q below the point $Q_{\rm EWSB}$ as is theoretically expected. The values of μ are $\mu = (500\ {\rm GeV},\ 1.0\ {\rm TeV},\ 1.8\ {\rm TeV})$. This can be seen for example for the $M_0 = 30$ TeV in figure 3.4 using Eq. (3.43).

the electroweak symmetry breaking scale that is of order a TeV or smaller when the soft scalars masses and trilinear couplings are large, in the range (10-50) TeV or larger.

The cancellation in Eqs. (3.65,3.66,3.68) coupled with equation, Eq. (3.43), can be taken as our basic result. Eqs.(3.65,3.66,3.68,3.43) shows that with inputs having all the soft-breaking parameters of order 30 TeV one finds the conditions for EWSB are always satisfied for reasonable ranges of the parameters, and the values of μ can be at (or below) the TeV scale consistent with EWSB and the measured value of M_Z.

Equation (3.43), with the important numerical values, is realized naturally with heavy scalars

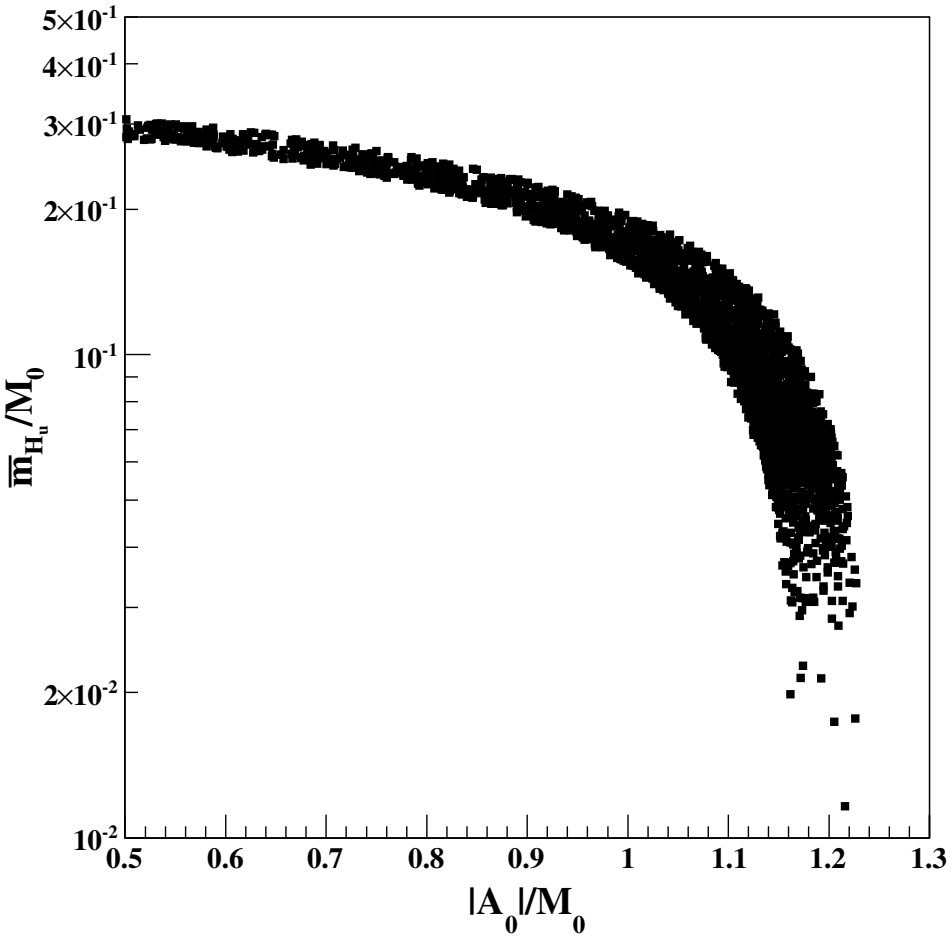

Figure 3.4: A large parameter space sweep using the full numerical analysis discussed in the text for $M_0 = 30$ TeV, with $\mu \in [0.9, 2]$ TeV, with $\tan\beta \in [3, 15]$ showing a robust region where $\bar{m}_{H_u}$, the loop corrected value at the EWSB scale, is reduced significantly relative to $M_0 = 30$ TeV, with the greatest suppression occurring for trilinear of about the same magnitude.

M_0 and large bilinear B_0 and trilinear A_0 couplings of comparable size. We add that Eq. (3.43) is a derived result and not assumed; we interpret this as then a true prediction of string models with the breaking of superysmmetry through gravitationally coupled moduli. We note that the result $\mu^2 \sim \bar{m}^2_{H_u}$ can be obtained in gauge mediation (where $\mu^2 \ll B\mu$) in models for which $B\mu \ll \bar{m}^2_{H_d}$ is assumed [71] (see also [72]).

In our numerical analysis we employ the 2-loop renormalization group equations (RGEs) for the soft supersymmetry breaking masses and couplings [73] with radiative corrections to the gauge and Yukawa couplings as computed in [70]. Radiative electroweak symmetry breaking is carried out with SOFTSUSY [74]. In the Higgs sector, we include all the 2-loop corrections [75, 76].

Explicitly we find Eq. (3.43) is a consistent representation of μ for

$$M_{3/2} = M_0 = 30 \text{ TeV with } \mu \in [0.9, 2] \text{ TeV} . \tag{3.69}$$

For $M_{3/2} = M_0 = 10$ TeV we find μ as low 300 GeV, though about (500-600) GeV appears more 'natural' as a lower limit from our scan of the parameter space. In the numerical analysis we increase the maximum trials in obtaining the solution of the RGEs relative to the default number in SOFTSUSY which serves, in part, to optimize our focussed scan. This is described in more detail in Ref. [74]. Our analysis is focussed on $M_0 \in [10, 30]$ TeV, with $M_0 \simeq |A_0|$. We do not perform an extensive study of solutions with $M_{3/2} \gtrsim 50$ TeV because the programs may not be reliable there with the desired accuracy.

Figure (3.3) shows m_{H_u} for appropriate A_0, M_0, and how it runs down to values of order $M_{3/2}/10$ from the RGE effects alone, where in the last step the Coleman-Weinberg corrections to the potential brings down the size of the up type Higgs mass^2 soft term by additional factors. It is the very fact that string models tell us $B_0 \sim M_{3/2}, A_0 \simeq M_{3/2}, M_0 \simeq M_{3/2}$ that leads to this solution. If one put the trilinear coupling to zero, this solution to a very large reduction of μ would be missed. The result we propose here is very different from the focus point solution where $m^2_{H_u}$ runs to a common invariant value and turns tachyonic [77, 78, 79], and for which scalar masses and trilinear couplings order 30 TeV were not discussed. We elaborate further on this in the Appendices.

In contrast we discuss here a new phenomenon where there is a cancellation of the coefficients of A_0^2 and M_0^2 which are of comparable size but with opposite sign and thus results in a suppression of $m^2_{H_u}$ relative to the very heavy gravitino mass of order $(10 - 50)$ TeV. The solution for μ in the models we discuss is naturally in the range $\mu \lesssim (0.5 - 3)$ TeV for $M_0 = (10 - 50)$ TeV when $|A_0| \simeq M_0$. Differently, in our case one can think in terms of a cancellation of the two contributions to Eq.(3.65), but it is natural and not tuned. The top Yukawa runs significantly from the GUT scale and drives the soft up type scalar higgs mass parameter to be small relative to the gravitino mass and it is positive and not tachyonic, and in addition, the large trilinear also leads to a faster running of $m^2_{H_u}$.

As mentioned above, Fig. (3.3) shows the the running of the up type Higgs soft mass for 3 sample models with values of μ at EWSB scale, $\mu = (500 \text{ GeV}, \ 1.0 \text{ TeV}, \ 1.8 \text{ TeV})$, for the three cases $M_0 = (10 \text{ TeV}, 30 \text{ TeV}, 50 \text{ TeV})$ and with the other soft breaking parameters of comparable size, and with the $SU(2), U(1)$ gaugino masses well below 1 TeV; the gluino masses are the heaviest and range from 400 GeV to 1 TeV. In Figure (3.4) we show a robust and large parameter space, for the case $M_0 = 30$ TeV where the largest suppression of the loop corrected value, $\bar{m}_{H_u}$, occurs for a trilinear coupling of size M_0 which in turn suppresses μ at the EWSB scale. For the

case of $M_0 = 30$ TeV, one sees the largest suppression of $\bar{m}_{H_u}$ occurs at $|A_0|/M_0 \simeq 1.2$. For the case of $M_0 = 10$ TeV we find a similar analysis shows the point of maximal suppression occurs closer to $|A_0|/M_0 \simeq 0.9$.

CHAPTER 4

Cosmology and Dark Matter

In Chapter 2 and Chapter 3 we have studied the theoretical aspects of the G_2 compactification of M theory and introduced a low energy effective model G_2-MSSM. It features heavy scalars, large trilinear couplings, suppressed μ term and relatively light gauginos. In the following chapter we are going to study the phenomenological predictions of G_2-MSSM. Each of these results are also true for a wider range of models, and we extend the results to other models whenever possible.

4.1 Cosmological Moduli/Gravitino Problem

In the previous chapter we used $m_{3/2} = O(50\,\mathrm{TeV})$ to motivate features of G_2-MSSM. But we have not yet explained why we want gravitino to be so heavy. This requirement mainly comes from the constraint of the moduli masses. The fact that, generically, the lightest modulus mass is of the same order as the gravitino mass has significant implications for the phenomena described by a typical string/M theory vacuum, with some rather mild assumptions, which we now enumerate. In addition to the requirement of stabilizing all moduli in a vacuum with TeV-scale supersymmetry (as described in the Chapter 2) which picks the set of string compactifications we choose to study, the assumptions are essentially that the supergravity approximation is valid and that the Hubble scale during inflation is larger than $m_{3/2}$.

The above implies that the light moduli fields (of order $m_{3/2}$) are generically displaced during inflation, causing the Universe to become moduli-dominated shortly after the end of inflation due to coherent oscillations of the moduli. Requiring that these decay before big-bang nucleosynthesis (BBN) so as to not ruin its predictions, puts a lower bound on $m_{3/2}$ of about 25 TeV or so. Thus, the cosmological moduli problem [80, 81] generically requires that $m_{3/2} > 25$ TeV. Since $m_{3/2} \simeq \frac{F}{M_{pl}}$ for vacua with a vanishingly small cosmological constant, this further implies that the supersymmetry breaking scale $\sqrt{F}$ has to be "high", as is natural in gravity mediation models. Low-scale supersymmetry breaking scenarios like gauge mediation do not seem to be compatible with these cosmological constraints.

Generically, within high scale supersymmetry breaking mechanisms such as gravity mediation, the squark, slepton and heavy Higgs masses are also of order $m_{3/2}$. It has been argued that in special cases, squarks and sleptons may be "sequestered" from supersymmetry breaking, giving rise to a suppression in their masses relative to $m_{3/2}$. However, it was shown in [82] that in string/M theory compactifications with moduli stabilization, the squark and slepton masses are generically not sequestered from supersymmetry breaking once all relevant effects are taken into account. This has important implications for collider physics, implying in particular that squarks and sleptons should *not* be directly observed at the LHC [32, 83].

4.2 Dark Matter Candidates in G_2-MSSM

There are two dark matter candidates in G_2-MSSM. The first is the lightest supersymmetric particle (LSP) that may be protected by the R-parity. Dark matter composed of the LSP has been a very well motivated candidate for all or part of the dark matter of the universe for nearly three decades. The dark matter annihilation cross section is of order $\sigma \sim \alpha_2/M_\chi^2$, where α_2 is the weak coupling. In the past decade the particular possibility where the dark matter is mainly the partner of the W boson, the wino, has been very well motivated in any theory where supersymmetry is broken by the anomaly mediation mechanism [84], or more generally where the anomaly mediation contribution to gaugino masses is comparable with other sources of gaugino masses (as in the G_2 construction), and in other approaches such as U(1) mediation [85]. In a universe where the relic density emerged in thermal equilibrium the wino mass had to be of order 2 TeV to get the right relic density. But in the non-thermal universes where the dark matter mainly arose from decay of additional particles, such as the moduli generically present in any string theory, the correct temperature at which to evaluate the Hubble parameter was the moduli decay or reheating temperature. This is quite different from the freeze-out temperature [86, 35, 87]. Then the correct relic density emerged for wino masses of order 150 GeV, for which $\langle \sigma v \rangle \simeq 3 \times 10^{-24}\,\mathrm{cm}^3\mathrm{s}^{-1}$. Although the winos arise continuously as the moduli decay, rather than the superpartners being mainly present at the big bang, a "non-thermal wimp miracle" still occurs when the scaling of the Hubble parameter and cross section with temperature and mass are taken into account [86, 35, 87].

The other candidate of the dark matter is axions. The requirement of stabilizing a large number of moduli in a realistic compactification with a simple mechanism naturally picks mechanisms in which many axions[1] are exponentially lighter than $m_{3/2}$, one of which can naturally be the QCD axion [88, 89]. Hence, this provides a string theory solution of the strong-CP problem with stabilized moduli and axions, and also naturally predicts an $\mathcal{O}(1)$ fraction of Dark Matter in the form of axions, the abundance of which must now be computed with a non-thermal cosmological

[1] the imaginary parts of the complex moduli

history [88].

4.3 The non-thermal WIMP 'Miracle'

Compactified string/M theory generically gives rise to moduli fields in the effective low energy description of physics. These are the low energy manifestations of the extra dimensions present in string/M theory and are necessarily present as long as the supergravity approximation is valid. Moduli fields couple gravitationally universally to matter with interactions suppressed by a large scale, such as the GUT or Planck scale. They generically will dominate the energy density of the Universe after inflation but must decay before big-bang nucleosynthesis (BBN). When they decay, they not only dilute the density of any thermal relics by many orders of magnitude, but they also produce WIMPs as decay products.

This gives rise to a WIMP number density of order :

$$n_\chi \sim \frac{\Gamma_X}{\langle \sigma\, v \rangle^{tot}_{\chi\chi}} \sim \frac{H(T_R)}{\langle \sigma\, v \rangle^{tot}_{\chi\chi}} \tag{4.1}$$

where T_R is the reheat temperature generated when the modulus X decays, Γ_X the modulus decay width and $H(T)$ the Hubble scale at temperature T. By contrast, in the thermal case, $n_\chi^{thermal} \sim \frac{H(T_F)}{\langle \sigma\, v \rangle^{tot}_{\chi\chi}}$, where T_F is the WIMP freezeout temperature. This implies that to obtain a roughly correct abundance in the non-thermal case, $\langle \sigma\, v \rangle^{tot}_{\chi\chi}$ has to be larger compared to that for the thermal case by a factor of $\frac{T_F}{T_R}$. Finally, within the framework of supersymmetry there naturally exist WIMP LSP candidates like the Wino or the Higgsino with annihilation cross-sections precisely in the required range. Since Winos have a larger annihilation cross-section than Higgsinos for the same mass, a Wino-like LSP with a small Higgsino component is favored[2].

In the next section, we describe an approach which satisfies all the conditions required for the "non-thermal WIMP miracle" to work, and which also gives rise to Wino-like LSPs in a large region of parameter space. Henceforth, we will study this case in detail.

4.4 Indirect Detection

Indirect Detection experiments are designed to search for particles that are potentially produced by the annihilation/decay of the dark matter in our galaxy. How does one learn what physics interpretation to give to tentative signals of antimatter and gammas in the galaxy? Could it be due to annihilating dark matter? Answering this is not straightforward – it strongly depends on

[2]For simplicity, we do not consider models beyond the MSSM.

assumptions that are not always made explicit, and the answer is also very sensitive to assumptions about propagation in the galaxy, and to parameters used to describe the propagation. Perhaps surprisingly, assumptions about cosmological history are crucial. It also depends on whether more than one mechanism is providing the signals.

As the recent PAMELA [1], Fermi [5] and then AMS-02 satellite data [2] appeared, essentially everyone who studied it assumed that the universe cooled in thermal equilibrium after the big bang (dark matter particles χ annihilated into Standard Model particles, which could annihilate back into dark matter particles if they had enough energy, until the cooling led to freeze-out of the dark matter at some relic density). Then the relic density is $\rho \approx H/\langle\sigma v\rangle$, where the Hubble parameter H is evaluated at the freeze-out temperature (about $M_\chi/25$). This remarkable formula, with the relic density depending only on the cosmological Hubble parameter and on the weak scale annihilation rate, has been called the "wimp miracle". Getting the correct relic density implied that $\langle\sigma v\rangle \approx 3 \times 10^{-26}\,\mathrm{cm}^3\mathrm{s}^{-1}$, so any candidate with a larger annihilation cross section was excluded. In recent years, however, it has become increasingly clear that comprehensive underlying theories which explain more than one thing at a time generically have additional sources of dark matter, such as decaying particles, and therefore that assuming thermal equilibrium as the universe cools is oversimplified and misleading. This was noticed in [90, 91, 92], emphasized a decade ago by Moroi and Randall[86], and more recently documented in detail in a model based on a string theory construction with M theory compactified on a manifold with G_2 holonomy[35]. See also [87].

Further, the standard assumption of most studies was that a single candidate had to describe the data for electrons, positrons, antiprotons, and gammas at all energies. It's not clear why one would assume that, since in the presence of dark matter there will in general be contributions from the annihilating dark matter, and also from several astrophysical sources such as interstellar medium accelerated by supernova remnant shock waves, pulsars, and perhaps more. In some theories the dark matter is metastable, its decay induced by much higher dimension operators, and contributes *both* via annihilation and via decay (work in progress)

Remarkably, this 150 GeV mass scale is just the one that is right for the PAMELA data. In a universe where the relic density arises non-thermally, as generically in string theories, a wino LSP with relic density normalized to the observed local relic density ($0.3\,\mathrm{GeV/cm}^3$) gives about the amount of positrons and antiprotons (and their distributions) reported in the PAMELA experiment! No "boost factor" is needed.

Positrons and antiprotons have long resident times in the galaxy, millions of years. In order to compute the number of events as functions of energy that PAMELA and Fermi should observe one needs to include all the effects of propagation in the galaxy. There are two main programs to facilitate that, GALPROP[93] and DarkSUSY[94, 95], each valuable for somewhat different calculations. Here we use GALPROP since we need to have one program that treats the signal

and background particles in a self-consistent manner as they are affected by the galactic magnetic fields, lose energy by synchrotron radiation, inverse Compton scattering, collisions, escape the galactic disk, etc. As we will explain, this is crucial for understanding the antiprotons, where we argue that use of parameterized backgrounds has led people incorrectly to assume that PAMELA was not seeing an annihilation signal in antiprotons.

We find that in the PAMELA region the results can depend significantly on a number of astrophysical parameters (see Table 4.1), and that there are many degeneracies and flat directions among the parameters. The GALPROP running time is long, of order several hours, so we have not yet been able to do full parameter scanning. Improved computing, and additional constraints from satellite data that should be reported in the next few months, should improve this situation significantly. It should be emphasized that the positrons and antiprotons "injected" into the galaxy by pure wino annihilation have no parameters apart from the mass scale, which can only vary at the 5-10% level. All the issues about describing the data arise from the propagation.

If annihilation of LSP dark matter is the origin of the excess positrons, it obviously must give excess antiprotons since all MSSM states will include quarks and antiquarks in their annihilation products, and the antiquarks fragment into antiprotons. In particular, for the wino LSP the annihilation of winos is to $W^+ + W^-$, and the W-bosons have known branching ratios to leptonic and quark final states, and the probability they will give antiprotons was measured at LEP. The relevant processes are incorporated into PYTHIA and we use them. There is no freedom. This has led to many statements in literature that the apparent absence of an antiproton excess excludes MSSM LSP models, and in particular excludes wino annihilation as the explanation of the positron excess, and forces one to approaches that only give leptons. It turns out that these conclusions are wrong, for three interesting reasons. First, the antiproton spectrum from quark fragmentation is significant down to quite soft antiprotons, and it gives a significant number of antiprotons in the $1 - 10\,\mathrm{GeV}$ region and even below. The positron spectrum from W's has many energetic positrons at higher energies, and is peaked at higher energies than the antiproton spectrum. Second, the antiprotons do not lose much energy as they propagate compared to the positrons, so the GeV antiprotons are detected by PAMELA, while the positrons lose energy readily and the soft ones do not make it to the detector. This can be seen from the figures below, where the signal from antiprotons is above the background down to the lowest energies, while the positron signal is at the background level below about $5\,\mathrm{GeV}$, and essentially gone below $10\,\mathrm{GeV}$. Thus the positron spectra for signal and background have different shapes, while the antiproton spectra have essentially the same shape and mainly differ in normalization.

The third issue concerns how the background is defined. The "background" can only be defined if one either has data in a region where there is known to be no signal, or if one has a theory of the background. There are two points. Some time ago reference [96] showed that solving the

propagation equations allowed a rather large variation in the antiproton background normalization, about a factor of five for parameters that were consistent with other constraints such as the Boron/Carbon ratio. This has also been emphasized by [96, 97]. Low energy data for antiprotons has existed for over a decade[98, 99, 100]. People proceeded by fitting the antiproton data and defining the fit as the background. Then they compared the PAMELA data with such backgrounds, and of course concluded there was no signal, because the signal had already been included in the background! If a dark matter annihilation contribution was included, it was double counted! As we show below, for entirely reasonable GALPROP parameters one can self-consistently compute the antiproton background, and with a wino annihilation signal it gives a good description of the data. Consequently the early experiments such as BESS and HEAT *did* detect dark matter via antiprotons.

There is another effect that has been neglected so far in most interpretations of the PAMELA and Fermi data. Dark matter annihilation is proportional to the square of the relic density. Because galaxies are built from smaller galaxies, and also because of normal random density fluctuations, the relic density throughout the relevant parts of the galaxy for a given observable will not be a flat $0.3\,\mathrm{GeV/cm^3}$, but will vary. Since $\langle\rho^2\rangle - \langle\rho\rangle^2 \neq 0$, density fluctuation effects must occur. Initial studies have been done by several authors[101, 102], who have established that the effects differ for positrons and for antiprotons, and are energy dependent, because the energy loss mechanisms are significantly different for positrons and antiprotons. While it is not clear yet how to calculate accurately the sizes and energy dependences of these effects, it is likely that assuming no effect is a less good approximation than initial approximate calculations of the effects. We include small effects we estimate semi-analytically and show results with and without them. Ultimately it will be very important to learn how to calculate these effects well and include them.

The positron data below $10 - 15\,\mathrm{GeV}$ is not consistent among experiments, and is not well described by models. This is assumed to be due to charge-dependent solar modulation effects and is being actively studied by experts in that area, and by the experimenters [103]. We do not attempt to put in detailed corrections for this, but we do include the (non-charge-dependent) effects in the simulation. Results in general also depend on the profile of the dark matter in the galaxy, most importantly for gammas from the galactic center. We do not study this dependence much here since it does not much affect the positron and antiproton results, and we are computer-limited. We remark on it in context below.

The PAMELA experiment has reported deviations from expected astrophysics for positrons, and as we explained above, for antiprotons, below about $100\,\mathrm{GeV}$. In this paper our goal is to demonstrate that a wino LSP is a strong candidate for explaining these deviations. We assume that possible astrophysical sources can be added to give a complete description of the data including Fermi (which light wino annihilation obviously cannot explain). We only parameterize the higher

energy astrophysical part, and assume it can be accommodated by some combination of acceleration of the interstellar medium electrons by supernova remnant shock waves, pulsars, etc with a net e^+/e^- ratio of 1/3. Once we do that we make a number of predictions for the positron ratio and antiprotons at energies above those already reported, for diffuse gammas and gammas from the galactic center, and for gamma fluxes from dwarf galaxies in our galactic halo. We check constraints from synchrotron radiation and "WMAP" haze. Our prediction for gammas assumes the source of higher energy $e^+ + e^-$ does not also produce a significant flux of high energy gammas. So corrections may be needed here, but the gammas from wino annihilation will be an irreducible source.

We also do not criticize any other attempt to describe the data – in nearly all cases forthcoming PAMELA and Fermi data will favor one or another approach. Many are based on interesting ideas and models. While some predictions are very sensitive to propagation effects, others such as whether the positron ratio rises or falls above $100\,\mathrm{GeV}$ is not very sensitive to propagation and different models have very different predictions. We predict a fall or flattening (depending somewhat on the high energy astrophysical component), while most models predict a strong rise. While propagation uncertainties do not modify our qualitative predictions, it is clear that the presence of the rather hard contribution to the $e^+ + e^-$ flux introduces uncertainty in our predictions, since it could affect the positron ratio at lower energies, and it might or might not contribute to antiproton and gamma fluxes. As described below, we simply parameterize it and we assume it only contributes to the electrons and positrons, and that it contains mostly electrons ($e^+/e^- = 1/3$). This limits the quality of our predictions.

In the following we first describe our use of GALPROP in some detail, including some effects or constraints we incorporate. Then we show the data and a description of the data based on annihilation of $180\,\mathrm{GeV}$ dark matter winos plus cosmic ray backgrounds, with signal and backgrounds computed in a consistent manner. What we show is not a fit to data but merely educated guesses since the computing time for a full parameter scan is still prohibitive for us. As shown in Table 4.1 below, we vary eight GALPROP parameters and some others, and all of them affect the interpretation. We have established that comparable descriptions of the data can be obtained for different GALPROP parameters from those we show since there are degeneracies. We emphasize that our goal is to show that the wino LSP in the mass range of order $200\,\mathrm{GeV}$ is a good candidate for the dark matter of the universe, including theoretical and experimental information as well as it is possible today. Even though much is not known about the propagation of the electrons, positrons, antiprotons and gammas, quite a lot *is* known. Then we describe the contribution we arbitrarily assume for the higher energy electrons and positrons. We will report on studies of the GALPROP parameter degeneracies and the wino mass later, assuming our predictions for the positron and antiproton higher energy data are correct.

After that we turn to presenting the data and the descriptions. We do that for one mass and one set of propagation parameters, and one dark matter profile (NFW). Descriptions and predictions for higher energies are shown for the PAMELA positron excess, the PAMELA antiproton excess, the $e^+ + e^-$ sum, the diffuse gammas, the gammas from the galactic center, dwarf galaxies, and checks such as the Boron/Carbon ratio.

4.4.1 GALPROP Parameters

We use GALPROP v50.1p[93] to simulate the propagation of both cosmic rays and dark matter annihilation products in the galaxy in a consistent way. The rates and spectrum for both will change if the propagation parameters change. The propagation process is described by the propagation equation for the particle density ψ:

$$\frac{\partial \psi}{\partial t} = q\left(\vec{r}, p\right) + \vec{\nabla} \cdot \left(D_{xx}\vec{\nabla}\psi - \vec{V}\psi\right) + \frac{\partial}{\partial p}p^2 D_{pp}\frac{\partial}{\partial p}\frac{1}{p^2}\psi - \frac{\partial}{\partial p}\left[\dot{p}\psi - \frac{p}{3}\left(\vec{\nabla}\cdot\vec{V}\right)\psi\right] - \frac{1}{\tau_f}\psi - \frac{1}{\tau_r}\psi, \tag{4.2}$$

where D_{xx} is the diffusion constant which is determined by:

$$D_{xx} = \beta D_{0xx}\left(\frac{\mathcal{R}}{\mathcal{R}_0}\right)^{\delta}, \tag{4.3}$$

where β is the velocity of the particle, $\mathcal{R}$ is the particle rigidity, and $\mathcal{R}_0$ is the reference rigidity which is taken to be $4\,\mathrm{GV}$ in all the simulations. In order to consider the propagation of the dark matter signals in the same framework, the official GALPROP code is modified to accept the dark matter injection spectrum calculated using PYTHIA via DarkSUSY 5.0.4[94]. The parameters used in this paper are based on the conventional model with constant Xco-factor provide in GALPROP source code (galdef_50p_599278). In general we vary the parameters D_{xx}, δ , the half height of the diffusion zone z_h, the primary electron injection index γ_0, the normalization of the primary electron flux N_{e^-}, the scaling factor for inverse Compton scattering, the convection velocity V_c, and the Alfvén velocity V_a. We survey ranges of these parameters (but do not fit data or scan parameters because of computing limitations) in order to learn if a combination of conventional cosmic ray physics plus dark matter annihilation can give a reasonable description of the PAMELA and Fermi data within certain constraints such as the B/C ratio described further below.

We find a set of parameters that give a good description of the data, and those are used in the figures below except when stated otherwise.The half height of the diffusion zone $z_h = 2\,\mathrm{kpc}$. The diffusion coefficient is $D_{0xx} = 2.5 \times 10^{28}\,\mathrm{cm^2 s^{-1}}$, $\delta = 0.5$. We also assume a softer

GALPROP Parameters	
$D_{xx0}\,(\mathrm{cm^2 s^{-1}})$	2.5×10^{28}
δ	0.5
$\mathcal{R}_0\,(\mathrm{GV})$	4
$z_h\,(\mathrm{kpc})$	2
γ_0	2.6
$N_{e^-}\,(\mathrm{cm^{-2} s^{-1} sr^{-1} MeV^{-1}})$	2.88×10^{-10}
$V_c\,(\mathrm{kms^{-1} kpc^{-1}})$	5
$V_a\,(\mathrm{kms^{-1}})$	31
ISRF factors (optical, FIR, CMB)	$0.5, 0.5, 0.5$
Solar Modulation Parameters	
$\phi\,(\mathrm{MV})$	500
$p_c\,(\mathrm{GeV})$	1
Astrophysical Flux Parameters	
a	1.0
b	1.8
$z_0\,(\mathrm{kpc})$	0.2
γ	1.5
$M\,(\mathrm{GeV})$	950
Density Fluctuation Factor Parameters	
B_c	2.5
f	0.5

Table 4.1: The parameters used for simulation. The physical meaning of these parameters is described in the text.

primary electron injection spectrum by setting the injection index γ_0 for primary electrons between $4\,\mathrm{GeV}$ to $10^6\,\mathrm{GeV}$ to 2.6. Also the primary electron flux is normalized to $N_{e^-} = 2.88 \times 10^{-10}\,\mathrm{cm^{-2} sr^{-1} s^{-1} MeV^{-1}}$ at $34.5\,\mathrm{GeV}$. The scaling factors for inverse Compton (ISRF factor) are adjusted to 0.5, which is approximately equivalent to setting $\tau = 2 \times 10^{16}\,\mathrm{s}$ in the energy loss rate formula for electron $b\,(\varepsilon)_{e^\pm} = \frac{1}{\tau}\varepsilon^2$. The convection velocity is $V_c = 5\,\mathrm{km\,s^{-1} kpc^{-1}}$, and the Alfvén speed which determines the reacceleration process is $V_a = 31\,\mathrm{km\,s^{-1}}$. The summary of the parameters we are using can be found in Table 4.1. Other parameters not mentioned here are the same as galdef_50p_599278.

As described in the introduction, the dark matter we focus on is the theoretically well-motivated case of a pure wino LSP, which annihilates to W's: $\widetilde{W} + \widetilde{W} \to W^+ + W^-$. The dark matter injection parameters are then completely determined by the wino mass and $W^\pm$ decays.

4.4.2 Solar Modulation

The effect of solar modulation is estimated by the Force-Field approximation [104], The flux observed at Earth's orbit $J_E(\varepsilon)$ is related to the flux in the interstellar flux by the following relation:

$$J_E(\varepsilon) = \frac{\varepsilon^2 - m^2}{\varepsilon_\infty^2 - m^2} J_\infty(\varepsilon_\infty) \tag{4.4}$$

where ε_∞ is the energy of the corresponding interstellar flux, which is determined by:

$$\varepsilon_\infty = \begin{cases} p \log\left(\frac{p_c+\varepsilon_c}{p+\varepsilon}\right) + \varepsilon + \Phi & \varepsilon < \varepsilon_c \\ \varepsilon + \Phi & \varepsilon \geq \varepsilon_c \end{cases} \tag{4.5}$$

Φ is the modulation energy shift which can be calculated from the modulation potential $\Phi = |Z|\, e\phi$, In our simulation the modulation potential ϕ is $500\,\mathrm{MV}$, the reference momentum p_c is $1\,\mathrm{GeV}$. Only the solar modulation effect for electron/positron and antiproton/proton is considered in this work. These effects do not include charge dependent solar modulation, which is under study [103]

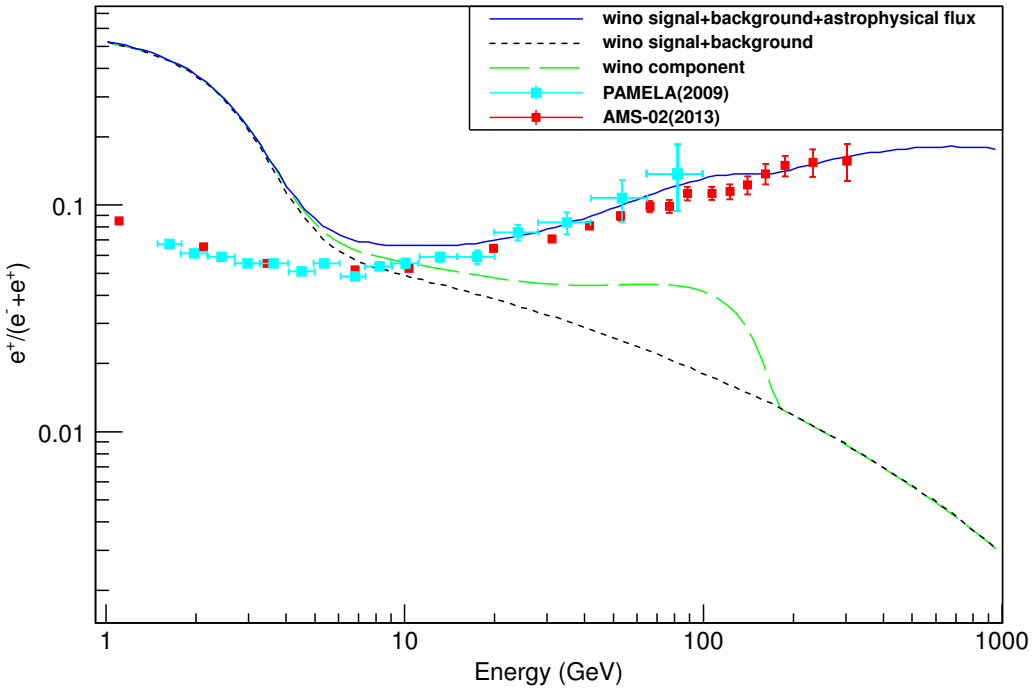

Figure 4.1: The positron flux ratio, generated with the parameters described in the text and Table 4.1 with a $M_{\widetilde{W}} = 180\,\mathrm{GeV}$ wino. The solid line is the ratio of the total positron flux, which includes the positrons from the wino annihilation, the astrophysical flux and the conventional astrophysics background to positrons plus electrons. The long dash line contains just the wino annihilation and the conventional astrophysics background, and the short dash line is the ratio of the secondary positrons only.The data are from [1] and [2], Our analysis assumes the reported normalization of the PAMELA and AMS-02 data. If those change it will affect the higher energy extrapolation here.

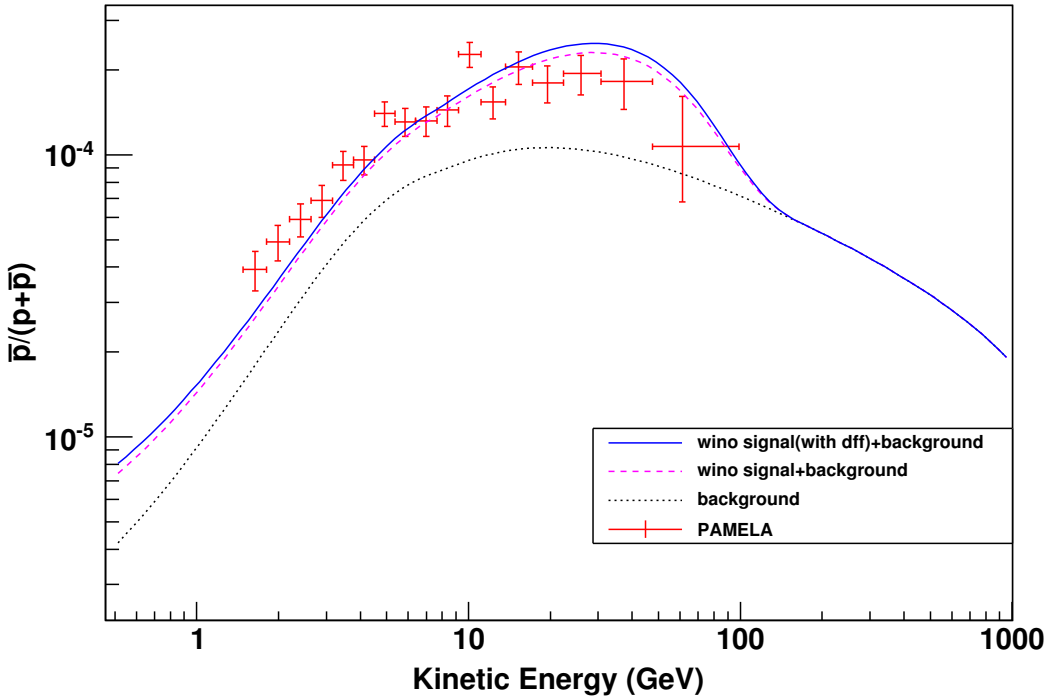

Figure 4.2: The antiproton flux ratio. The solid line is the ratio of the total antiproton flux, which include the antiproton from wino annihilation, and conventional astrophysics background, the dash line has the same components but without the density fluctuation factor, the dot line is astrophysics background only. The data are from PAMELA [3]. Note the signal is larger than the background down to very low energies.

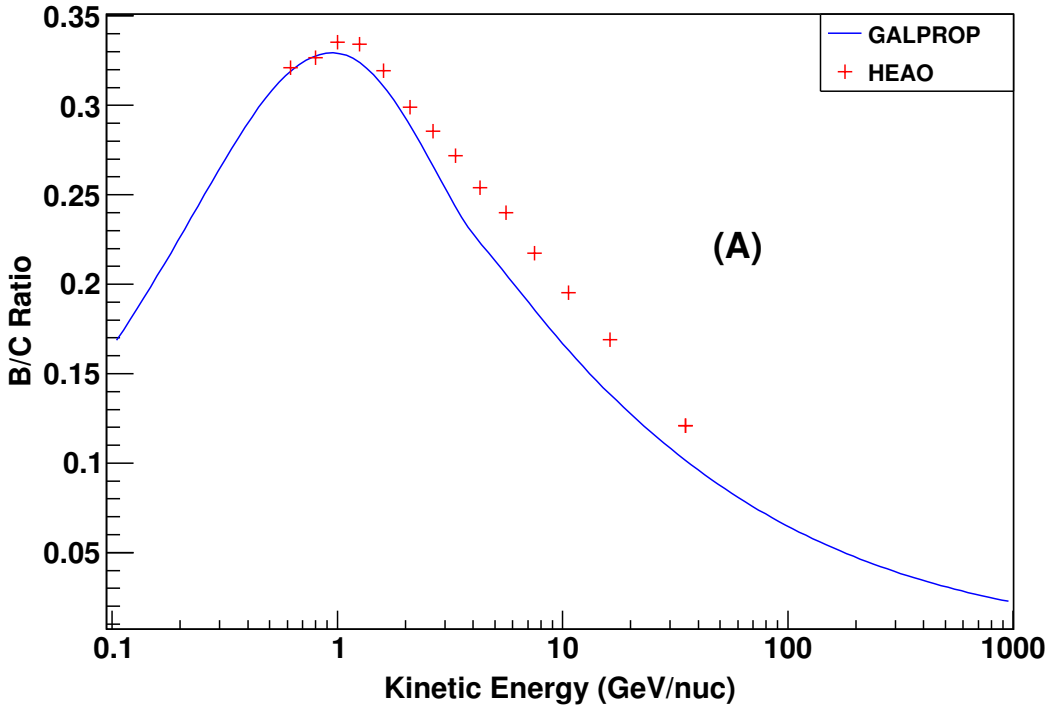

Figure 4.3: The Boron to Carbon ratio with our standard parameters, solar modulation effect is not included, The data are from [4].

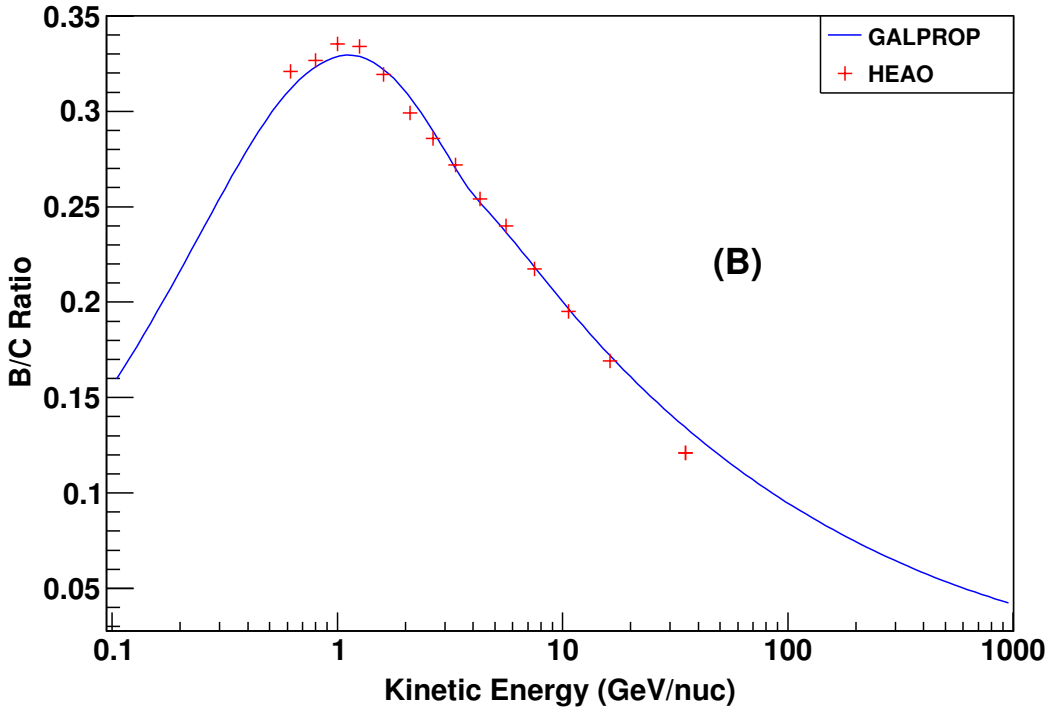

Figure 4.3: The Boron to Carbon ratio with one parameter different (δ changes from 0.5 to 0.4). This illustrates that the Boron to Carbon ratio is very sensitive the diffusion parameters. The data are from [4].

4.4.3 Astrophysical Flux

It is obvious that a $180\,\mathrm{GeV}$ wino alone cannot explain Fermi date and PAMELA data at the same time. There must be some extra flux responsible for the high energy signals. In order to estimate the high energy ($> 200\,\mathrm{GeV}$) electrons/positrons flux, we consider a simple model for extra flux which is suggested by interstellar medium electrons accelerated by supernova remnants and shock waves, or by pulsar spectra models. The basic setup we use is similar to Zhang and Cheng[105]. For a recent review of pulsar models, see Profumo[106]. The spatial distribution of the sources is:

$$\rho\left(r\right) = N\left(\frac{r}{r_{\odot}}\right)^{a} e^{-\frac{b\left(r-r_{\odot}\right)}{r_{\odot}}} e^{-\frac{z}{z_{0}}} \tag{4.6}$$

where N is the overall normalization constant, $z_0 = 0.2\mathrm{kpc}$, $r_{\odot} = 8.5\mathrm{kpc}$, $a = 1.0$ and $b = 1.8$.

The energy dependence of the injection spectrum is:

$$\frac{dN_{e^{\pm}}}{dE} = N' E^{-\gamma} e^{-\frac{E}{M}} \tag{4.7}$$

where N' is another normalization constant, which can be absorbed into N, $\gamma = 1.5$ and $M = 950\,\mathrm{GeV}$. In order to fit PAMELA and Fermi data, we made an ad hoc assumption that the ratio of positron and electron in the unknown extra flux is $1 : 6$. The high energy positrons/electrons are then propagated by GALPROP, and the resulting flux is normalized to fit the Fermi data by requiring the extra electron flux at $275.5\,\mathrm{GeV}$ to be $3.0 \times 10^{-13}\,\mathrm{cm^{-2}sr^{-1}s^{-1}MeV^{-1}}$

4.4.4 Density Fluctuation Factor

The results from N-body simulations [107], and an understanding of how galaxies formed, indicate that it is inevitable for the dark matter halo of our galaxy to have substructures. The existence of these substructures would change the predictions of the cosmic ray fluxes, particularly for dark matter annihilation. Even without substructures, it is clear that the density of dark matter will not be absolutely flat, but will fluctuate around an average value. Both of these effects require the flux from dark matter annihilation, which is sensitive to the square of the dark matter density, to show density fluctuation effects. As emphasized by Lavalle and collaborators[101, 102], the effects of these substructures are different for positrons and antiproton, and must also be energy dependent. The details of these effects depend on the spatial and mass distribution of these substructures. Here we use a very simple model to estimate the effects: Assuming all the substructures share the same mass and density, and the spatial number density of the substructures is proportional to the density profile of the smooth distribution of dark matter halo.

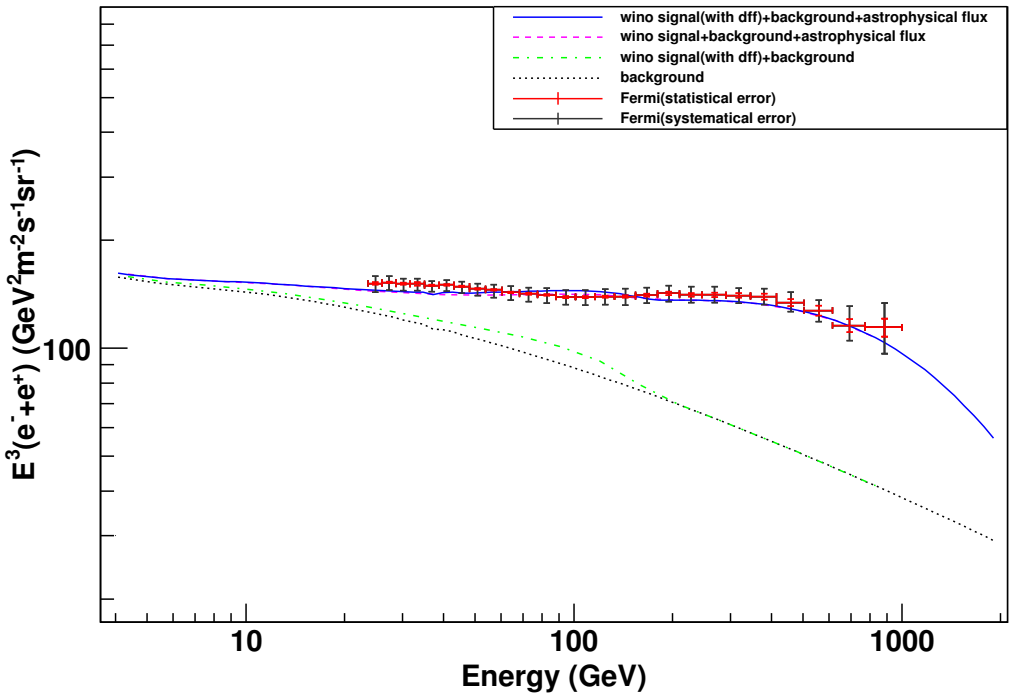

Figure 4.4: The absolute flux of $e^+ + e^-$, The solid line is the sum of electron and positron from the wino annihilation, the density fluctuation factor, our assumed extra flux, and conventional astrophysics background, the dash line has the same components but without the density fluctuation factor. The dash-dot line contains wino annihilation and astrophysics background, and the dot line is the conventional astrophysics background only. See comments in Figure 4.1. The data are from [5].

With these assumptions, the density fluctuation factor can be calculated with:

$$D(E) = (1-f)^2 + fB_c \frac{\mathcal{I}_1}{\mathcal{I}_2} \tag{4.8}$$

where f is the mass fraction of the substructures in the dark matter halo, B_c is the intrinsic density increase of the substructures or fluctuations, and $\mathcal{I}_n$ is determined by

$$\mathcal{I}_n = \int_{\text{DM halo}} G(x,E) \left\{ \frac{\rho_s(x)}{\rho_0} \right\}^n d^3x \tag{4.9}$$

where $G(x,E)$ is the Green's function of the propagating particle.

We assume $f = 0.5$ and $B_c = 2.5$. Only the density fluctuations of positron and antiproton are considered. The electron/positron Green's function from Baltz and Edsjö[108] and the fast formulae for antiproton Green's function from Maurin, Taillet and Combet[109] are used to evaluate the integral. With these assumptions we find the effects of the density fluctuations are small. We included them for completeness. Theory curves including them are labeled "dff" (for "density fluctuation factors") in the figures.

4.5 Direct Detection

Direct detection experiments of dark matter are based on the detection of collisions between the dark matter particle and the nuclei. In contrast to the large annihilation cross section, a pure wino has a very small direct detection cross section, which makes the direct detection searches for wino LSP dark matter extremely challenging.

In the decoupling limit, defined when the pseudoscalar mass is much larger that the Z-boson mass, $m_{A^0} \gg M_Z$, the charged and heavy CP-even Higgses are also heavy, $m_{H^\pm} \simeq m_{H^0} \simeq m_{A^0}$. The other Higgs boson h^0 remains light and behaves in the same way as the SM Higgs boson. Here we will assume its mass is 125 GeV. Since the squarks are also heavy in G_2-MSSM, the light Higgs boson exchange will give the only substantial contribution to the spin-independent scattering cross sections. The scattering of the LSP off nuclei is via the Higgsino and gaugino component. While the LSP will be mostly Wino-like, the prediction that μ is of order the TeV scale implies that the LSP wavefunction can have non-trivial Higgsino mixing.

Following [110] we estimate the size of the direct detection cross section in the decoupling

limit to be

$$\sigma_{\rm SI}\left(\chi N \to \chi N\right) \approx 3.6 \times 10^{-45}{\rm cm}^2 \left(\frac{125\,{\rm GeV}}{m_h}\right)^4 \left(\frac{Z_{H_u}\sin\beta - Z_{H_d}\cos\beta}{0.1}\right)^2 \times \left(Z_W - \tan\theta_W Z_B\right)^2 \tag{4.10}$$

where the Z's give the composition of the LSP

$$\chi \equiv Z_B\,\tilde{B} + Z_W\,\tilde{W} + Z_{H_d}\,\tilde{H}_d + Z_{H_u}\,\tilde{H}_u. \tag{4.11}$$

This gives us an estimate of the largest direct detection scattering cross sections, which naively may seem that for $Z_{H_u} \sim 0.1$ can be very close to the reach of XENON. Eq. (4.10) can further be simplified, with the aid of analytical expressions for the neutralino mass matrix eigenvalues and eigenvectors [111, 112, 113]. Taking the limit $M_1 = M_2$, which maximizes the scattering cross section for fixed μ and $\tan\beta$, (4.10) becomes

$$\sigma_{\rm SI}^{\rm MSSM}\left(\chi N \to \chi N\right) \approx 4.3 \times 10^{-45}{\rm cm}^2 \left(\frac{125\,{\rm GeV}}{m_h}\right)^4 \left(\frac{1\,{\rm TeV}}{\mu}\right)^2 \left(\frac{\sin 2\beta + M_2/\mu}{1-(M_2/\mu)^2}\right)^2 \tag{4.12}$$

which falls off both with $\tan\beta$ and μ. Allowing for the variation in M_1 and M_2 in the G_2-MSSM will only decrease this fraction. The value M_2/μ is typically around $.1 \sim .2$. For general MSSM, $\sin 2\beta$ can be almost 1, corresponding to a very small $\tan\beta$. For G_2-MSSM, as mentioned in the previous chapter, $\tan\beta \sim 10$, which makes $\sin 2\beta \sim 0.1$. So the upper limit of the direct detection cross section for G_2-MSSM is about $10^{-47}{\rm cm}^2$

CHAPTER 5

The Mass of the Lightest Higgs Particle

5.1 Higgs Mass Calculation

Most physicists agree that understanding the origin of electroweak symmetry breaking is essential for progress in going beyond the Standard Model. We will demonstrate that, with some broad and mild assumptions motivated by cosmological constraints, generic compactified string/M-theories with stabilized moduli and low-scale supersymmetry imply a Standard Model-like single Higgs boson with a mass $105\,\mathrm{GeV} \lesssim M_h \lesssim 129\,\mathrm{GeV}$ if the matter and gauge spectrum surviving below the compactification scale is that of the MSSM, as seen from Figure 5.1. For an extended gauge and/or matter spectrum, there can be additional contributions to M_h. Furthermore, in G_2-MSSM models we find that the range of possible Higgs masses is apparently much smaller, For $30\,\mathrm{TeV} \lesssim m_{3/2} \lesssim 100\,\mathrm{TeV}$, which is consistent with cosmology and dark matter observations, $122\,\mathrm{GeV} \lesssim M_h \lesssim 129\,\mathrm{GeV}$. When we choose $m_{3/2} = 50\,\mathrm{TeV}$, the mass is $126 \pm 1.5\,\mathrm{GeV}$.

In connecting string/M theory to low-energy particle physics, one has to compactify the extra dimensions. Motivated by grand unification and its successful embedding into string/M theory we assume that the string/M theory scale, the Kaluza-Klein scale and the unification scale are all within an order of magnitude of 10^{16} GeV. Within the theoretical precision desired, numerical results for M_h are not sensitive to variations of an order of magnitude or so in these scales.

We will be interested in models with supersymmetry breaking mechanisms which give rise to TeV-scale supersymmetry, and hence solve the naturalness problems in the Standard Model. The basic mechanisms were described in [28, 29] for M-theory and in [114, 115, 89] for Type IIB compactifications, where it was shown that all moduli can be stabilized and supersymmetry can be broken with $\sim$ TeV-scale superpartners with a natural choice of parameters - in which the only dimensionful scale is M_{pl}! In a vacuum with broken supersymmetry and vanishing cosmological constant, the mass of the gravitino ($m_{3/2}$), which is the superpartner of the massless graviton, is the order-parameter of supersymmetry breaking and sets the mass scale for all superpartners and also indirectly the Higgs mass.

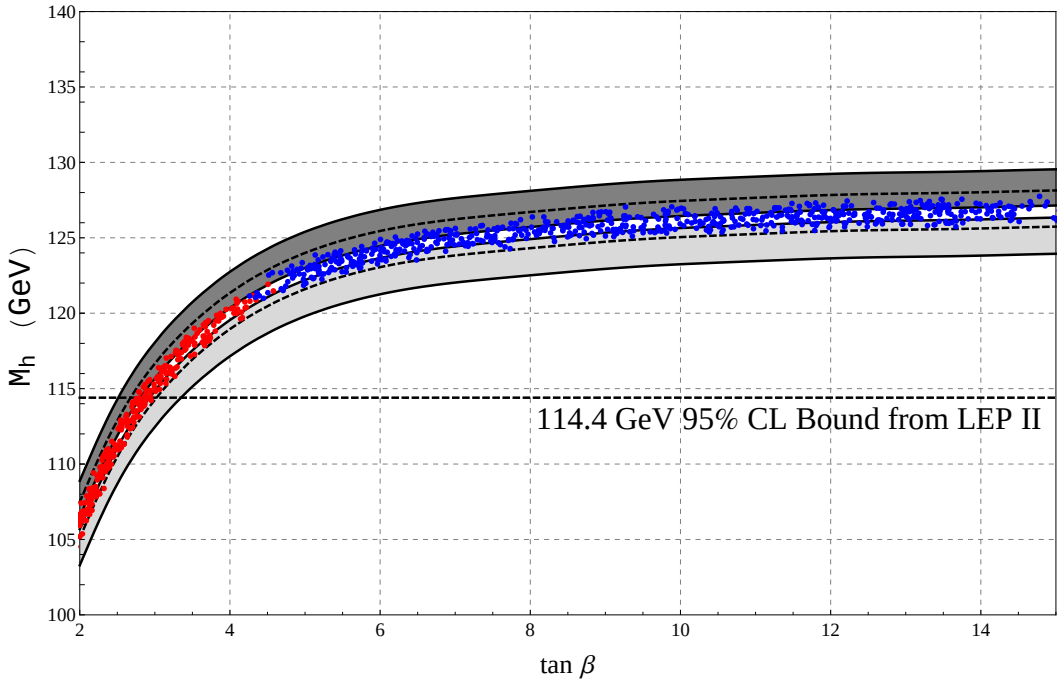

Figure 5.1: The prediction for the Higgs mass at two-loops for realistic string/M theory vacua defined in the text, as a function of $\tan\beta$ for three different values of the gravitino mass $m_{3/2}$, and varying the theoretical and experimental inputs as described below. For precise numbers and more details, see section 5.4. The central band within the dashed curves for which scatter points are plotted corresponds to $m_{3/2} = 50$ TeV. This band includes the total uncertainty in the Higgs mass arising from the variation of three theoretical inputs at the unification scale, and from those in the top mass m_t and the $SU(3)$ gauge coupling α_s within the allowed uncertainties. The innermost (white) band bounded by solid curves includes the uncertainty in the Higgs mass for $m_{3/2} = 50$ TeV only from theoretical inputs. The upper (dark gray) band bounded by solid curves corresponds to the total uncertainty in the Higgs mass for $m_{3/2} = 100$ TeV while the lower (light gray) band bounded by solid curves corresponds to that for $m_{3/2} = 25$ TeV. For $m_{3/2} = 50$ TeV, the red scatter points (with $\tan\beta$ less than about 4.5) and blue scatter points (with $\tan\beta$ greater than about 4.5) correspond to "Large" μ and "Small" μ respectively, as described in section 5.2 and section 5.4.

A natural prediction of such compactifications is that the mass of the lightest modulus is close to $m_{3/2}$. In fact, this is a generic result for compactified string/M-theories with stabilized moduli within the supergravity approximation. In vacua in which the superpotential W is not tuned, it essentially arises from the fact that there is a relationship between the dynamics stabilizing the moduli and the dynamics breaking supersymmetry due to the extremely tiny value of the cosmological constant. Thus, the modulus mass becomes related to the gravitino mass. For more details, see [116, 117, 118, 119, 120, 121]. For the generic case with many moduli, at least some of the moduli are stabilized by perturbative effects in the Kähler potential [29, 89]. Then, it can be shown that the lightest modulus[1] has a mass of the same order as $m_{3/2}$ [122, 32].

5.2 The Higgs and BSM Physics

We are interested in calculating the Higgs mass arising from realistic compactifications satisfying the conditions above. In a supersymmetric theory, two Higgs doublets are required for anomaly cancellation; so by the "Higgs mass" we mean the mass of the lightest CP-even neutral scalar in the Higgs sector. A remarkable fact about the Higgs mass in general supersymmetric theories is that an upper limit on M_h of order $2\,M_Z$ exists just from the requirement of validity of perturbation theory up to the high scale of order 10^{16} GeV [123, 124]. This is due to the fact that the Higgs mass at tree-level only depends on SM gauge couplings (which have been measured), and possibly other Yukawa or gauge couplings (which are bounded from above by perturbativity). However, in addition to the gauge and matter spectrum, the precise value of the Higgs mass depends crucially on radiative effects, which in turn depend on all the soft parameters including the μ and $B\mu$ parameters.

In this work we assume that the visible sector consists of the SM gauge group with the MSSM matter content below the unification scale, as suggested by gauge coupling unification and radiative EWSB in the MSSM. In addition, we consider compactifications in which the gravitino mass $m_{3/2}$ is not too far above the lower bound of ~ 25 TeV from the moduli decay constraint, and the gaugino masses are suppressed by one-to-two orders of magnitude relative to $m_{3/2}$. For μ we study two cases, one in which μ is suppressed by one-to-two orders of magnitude relative to $m_{3/2}$ as predicted in [125], and the other in which μ is of the same order as $m_{3/2}$ [56, 126, 127, 128, 129]. We denote these two cases as "Small" μ and "Large" μ respectively. The two cases are studied as they pick out different regions of $\tan\beta$ and hence give different predictions for the Higgs mass as seen from Figure 1. For more discussion, see section 5.4.

Note that only one of the five scalars in the Higgs sector of the MSSM is light, the rest are all of order $m_{3/2}$. Hence, we are in the "decoupling limit" of the MSSM where the lightest CP-even

[1] more precisely, the real part of the chiral superfield making up the complex modulus in the 4D theory.

Higgs scalar has precisely the same properties as the SM Higgs[2]. The low-energy theory arising from M-theory studied in [8] naturally gives rise to these features, but the results apply to all compactifications with scalars heavier than about 25 TeV and $\lesssim$ TeV gauginos. The Higgs mass can then be reliably computed with a small and controlled theoretical uncertainty. This will be the subject of the following sections.

From a bottom up point of view some authors have noted that heavy scalars have some attractive features [131, 132, 133] and related phenomenology has been studied in [134, 135]. Their conclusions are consistent with ours where they overlap. The framework considered here is quite different from split supersymmetry [136, 137] and high-scale supersymmetry [138, 139] which have much heavier scalars. In split supersymmetry *both* gaugino masses and trilinears are suppressed relative to scalars by a symmetry – in this case an R-symmetry, together with supersymmetry breaking of the D-type as described in [136, 137]. In contrast, in the class of compactifications considered here, the gaugino masses are suppressed by dynamics, since the F-term for the modulus determining the gaugino masses is suppressed relative to the dominant F-term. Hence, gaugino masses can only be suppressed by one-to-two orders of magnitude, not arbitrarily as in split-supersymmetry. For the same reason, the gluinos are not "long-lived" in the realistic string/M theory vacua under consideration here. Also, the trilinears are not suppressed at all. With large trilinears, one has to be careful about charge and color breaking (CCB) minima, and we have confirmed the absence of these in models of interest. Another notable difference from split-supersymmetry and high-scale supersymmetry is that, in those models, (radiative) electroweak symmetry breaking is not implemented when computing the Higgs mass since a huge fine-tuning is present *by assumption*. In contrast, in the string/M theory models considered in this work, (radiative) electroweak symmetry breaking occurs naturally in a large subset of the parameter space. However, the ease in obtaining the correct value of the Higgs vev (or Z-boson mass) depends on the value of μ. For "Small" μ, it can be shown that the fine-tuning involved in obtaining the correct Higgs vev is significantly reduced compared to the naive expectation for heavy scalars due to an "automatic" cancellation between scalar masses and trilinears which are both close to $m_{3/2}$ in this setup; for details see [135]. This can naturally give rise to $\mu \lesssim$ TeV, even when the scalar mass parameters are $\gtrsim 30$ TeV. For "Large" μ, the fine-tuning is quite severe as one would expect. We include both cases here.

[2]In the decoupling limit, the Higgs mixing angle denoted by α in [130] is given by $\alpha = \beta - \frac{\pi}{2}$, where $\beta \equiv \tan^{-1}(\frac{v_u}{v_d})$. v_u and v_d are the vacuum-expectation-values (*vevs*) of the two neutral Higgs fields H_u^0 and H_d^0 in the MSSM.

5.3 Computation of the Higgs Mass

Computing the Higgs mass in the MSSM with scalar masses and trilinears at $M_{susy} \gtrsim 25$ TeV, and gauginos and μ suppressed by one-to-two orders of magnitude relative to the scalar masses, is non-trivial. Although conceptually quite different, some of the technical issues involved have an overlap with split-supersymmetry and high-scale supersymmetry.

Since the scalar masses are much larger than a TeV, they could lead to non-trivial quantum corrections in the gaugino-higgsino and Higgs sectors enhanced by "large logarithms" of the ratio between the electroweak scale and the scalar mass scale. Many numerical codes tend to become less reliable for scalar masses larger than a few TeV for the above reason. However, in contrast to split supersymmetry and high-scale supersymmetry models, the scalar masses here are 25-100 TeV which is not that "large", since $\log(\frac{M_{susy}}{M_{EW}})$ is not large. So, numerical codes should still provide a reasonable estimate. The ratio of the two Higgs fields vevs, $\tan\beta$ cannot yet be calculated accurately, and significantly affects the value of M_h if $\tan\beta \lesssim 10$, so we include the variation from $\tan\beta$. This dependence actually allows an approximate measurement or useful limit on $\tan\beta$ which is otherwise very difficult to do.

In light of the above, we adopt the following procedure. At the unification scale around 10^{16} GeV, in accord with theoretical expectations we fix the soft parameters - the scalar masses equal to $m_{3/2}$, the trilinears A close to $m_{3/2}$, and the gaugino masses suppressed by one-to-two orders of magnitude relative to the scalar masses as described in [8]. Then, for a given value of $\tan\beta$, the numerical codes SOFTSUSY [74] and SPHENO [140] are used to renormalize these quantities down to $M_{susy} \approx m_{3/2}$, where electroweak symmetry breaking is implemented. This determines μ and $B\mu$. The quantities are chosen such that the values of μ and $B\mu$ are consistent with the theoretical expectations. One consequence of this is that $\tan\beta$ is not expected to span the fully phenomenologically allowed range from ~ 2 to ~ 60, but only a restricted range from ~ 2 to ~ 15 [32]. In any case, from Figure 1, since the Higgs mass saturates for $\tan\beta \gtrsim 12$, plotting higher values of $\tan\beta$ will not provide new information.

Then, we compute the Higgs mass in the "match-and-run" approach using values of gaugino masses, μ and $B\mu$ at M_{susy} determined from above. We follow a procedure similar to that in [141] except that we only consider those parameters at the unification scale which after RG evolution to M_{susy} give rise to viable electroweak symmetry breaking. We also compute the Higgs mass directly with SOFTSUSY using theoretical inputs at the unification scale, and compare to the results obtained with the "match-and-run" approach, the detailed procedure for which is described below.

5.3.1 Matching at M_{susy}

At the scale M_{susy}, the full supersymmetric theory is matched to a low energy theory with fewer particles, consisting of the SM particles, the gauginos and the higgsinos for the "Small" μ case, and only the SM particles and the gauginos for the "Large" μ case. The matching condition for the quartic coupling of the Higgs in the low-energy theory is given at M_{susy} by:

$$\lambda = \frac{1}{4}\left[g_2^2 + \frac{3}{5}\,g_1^2\right]\,\cos^2\,2\beta + \delta_{th}^{\lambda} \tag{5.1}$$

where $g_1,\ g_2$ are the $U(1)_Y$ and $SU(2)_L$ gauge couplings evaluated at M_{susy}. The threshold corrections to the quartic coupling at one-loop consist of leading log (LL) as well as finite corrections. The above matching condition is strictly valid only in the $\overline{DR}$ scheme, so there is an additional correction if one wants to convert to the $\overline{MS}$ scheme as explained in the appendix of [142]. We use the standard choice $M_{susy} = \sqrt{M_{\tilde{t}_1}\,M_{\tilde{t}_2}}$ where $M_{\tilde{t}_1}, M_{\tilde{t}_2}$ are the masses of the two stop squarks, and include all the relevant LL and finite threshold corrections. The dominant finite threshold effects to the Higgs quartic coupling comes from stop squarks, and is given by:

$$\delta_{th}^{\lambda} \approx \frac{3\,y_t^4}{8\pi^2}\,\left(\frac{A_t^2}{m_{\tilde{t}}^2} - \frac{A_t^4}{12\,m_{\tilde{t}}^4}\right) \tag{5.2}$$

Since the trilinears A are of the same order as scalars, this is a non-trivial correction when the scalars and trilinears are around 25 TeV. Other finite threshold corrections are smaller, and have been neglected as they do not affect the result to within the accuracy desired.

The matching conditions for the gaugino-higgsino-Higgs couplings (denoted by κ in general) at M_{susy} in the $\overline{DR}$ scheme are given by:

$$\begin{aligned}
\kappa_{2u} &= g_2\,\sin\,\beta;\ \kappa_{2d} = g_2\,\cos\,\beta; \\
\kappa_{1u} &= \sqrt{\frac{3}{5}}\,g_1\,\sin\,\beta;\ \kappa_{1d} = \sqrt{\frac{3}{5}}\,g_1\,\cos\,\beta;
\end{aligned} \tag{5.3}$$

where the gauge couplings are to be evaluated at M_{susy}. As for the Higgs quartic coupling, additonal corrections are present in the $\overline{MS}$ scheme, which can be obtained from [142].

5.3.2 Two -loop RGEs and Weak Scale Matching

We use two-loop RGEs computed in [141] for the gauge couplings, third-generation Yukawa couplings $y_t,\ y_b,\ y_\tau$, the Higgs quartic λ, and the gaugino-higgsino-Higgs (κ) couplings (for "Small" μ), to renormalize them down to the weak scale. For "Large" μ, the κ couplings are not present in the low-energy theory, and (5.3) is used to compute the threshold correction from higgsinos at

M_{susy}.

Note that unlike the κ couplings and the quartic coupling, the boundary conditions for which are defined at M_{susy}, the boundary conditions for the gauge and Yukawa couplings y_b, y_τ are defined at M_Z - the Z-pole, while that for the top Yukawa coupling y_t is defined at the top pole mass $m_t = 173.1 \pm 0.9$ GeV [143]. In particular, the boundary values of the running gauge and Yukawa couplings in the $\overline{MS}$ scheme are extracted from experimental observables at the weak scale by including threshold effects, as explained in [142]. For the top Yukawa coupling y_t, non-trivial three-loop QCD corrections, and one-loop electroweak and superpartner threshold corrections are also included as they are non-negligible and play an important role in the precise prediction for the Higgs mass.Since the boundary conditions are given at different scales, an iterative procedure is required to solve the coupled differential RGE equations. We follow a procedure similar to that in [141, 144, 142]. Then, the Higgs mass is given by:

$$M_h = \sqrt{2}\, v \sqrt{\lambda(Q) + \delta_\lambda(Q) + \tilde{\delta}_\lambda(Q)} \tag{5.4}$$

where $v = 174.1$ GeV, δ_λ stands for the corrections from the SM particles, and $\tilde{\delta}_\lambda$ stands for the corrections from the supersymmetric fermions at the weak scale, and all couplings are evaluated at the $\overline{MS}$ scale $Q = m_t$. The expressions are given in [141]. Finally, as mentioned earlier, since numerical codes are expected to give a good estimate of the Higgs mass, we compute the Higgs mass directly with SOFTSUSY. We find very good agreement between the two results, to within 1 GeV.

5.4 Result

Figure 5.1 gives the Higgs mass as a function of $\tan\beta$ by varying the theoretical inputs at the unification scale in ranges predicted by the theory, and m_t and α_s within the allowed uncertainties. The values of the Higgs mass shown are in the "match-and-run" approach. The ranges of the theoretical and experimental inputs, and the resulting uncertainties are discussed in detail below. The μ and $B\mu$ parameters are related by electroweak symmetry breaking to $\tan\beta$, so by varying $\tan\beta$ one is effectively varying μ and $B\mu$. As pointed out in section 5.1, theoretical considerations typically give rise to two different classes of phenomenologically viable predictions for μ – one in which μ is suppressed by one-to-two orders of magnitude relative to $m_{3/2}$, and the other in which μ is comparable to $m_{3/2}$. As seen from Figure 1, the two classes of predictions for μ give rise to different values of $\tan\beta$ because of the EWSB constraints that relates them; hence a measurement of the Higgs mass will not only determine or constrain $\tan\beta$, it will also favor one class of μ-generating mechanisms over the other! For instance, in G_2-MSSM models arising from M theory,

Witten's solution to the doublet-triplet splitting problem [33] results in μ being suppressed by about an order of magnitude. Hence, in these vacua, the Higgs mass sits in the range 122 GeV $\lesssim M_h \lesssim$ 129 GeV.

Case	Variation of Input	ΔM_h
"Small" μ	Theoretical	± 0.5
$0.05\, m_{3/2} \leq \mu \leq 0.15\, m_{3/2}$	Theoretical + Experimental	± 1.1
"Large" μ	Theoretical	± 0.5
$0.5\, m_{3/2} \leq \mu \leq 1.5\, m_{3/2}$	Theoretical + Experimental	± 1.25

Table 5.1: Uncertainties in the calculation of the Higgs mass for a given value of $m_{3/2}$ and $\tan\beta$, as shown in Figure 1. All masses are in GeV.

It is important to understand the origin of the spread in the Higgs mass for a given value of $m_{3/2}$ and $\tan\beta$, seen in Figure 1. This spread arises from theoretical and experimental uncertainties schematically shown in Table I. The two cases in Table I correspond to "Small" μ and "Large" μ as mentioned in section 5.2. As the name suggests, "Theoretical" in the second column corresponds to the variation of input quantities from the theory at the unification scale. For a given $m_{3/2}$, this includes the variation in the trilinears A and those in the gaugino mass parameters M_1, M_2, M_3 consistent with theoretical expectations. "Experimental", on the other hand, stands for the variation of the experimental inputs, the top mass m_t and the $SU(3)$ gauge coupling α_s, within the current uncertainties. The precise variations in the theoretical and experimental inputs are shown in Table II.

Theoretical	Experimental
$600 \leq m_{\tilde{g}} \leq 1200$	$172.2 \leq m_t \leq 174$ [143]
$0.8\, m_{3/2} \leq A_t \leq 1.5\, m_{3/2}$	$0.1177 \leq \alpha_s^{\overline{MS}}(m_Z) \leq 0.1191$ [145]

Table 5.2: Variation of the theoretical and experimental inputs. All masses are in GeV.

The variations in the bino and wino mass parameters M_1 and M_2 have a negligible effect on the Higgs mass, and are not shown above. Although we have not fully estimated uncertainties arising from higher-loop effects in the RGE and threshold effects, the fact that our results agree so well with SOFTSUSY suggests that these are at most of the same order as those listed in Table I. Finally, let us discuss the uncertainty in the gravitino mass scale. Figure 1 shows the Higgs mass for three different values of $m_{3/2}$ - 25 TeV, 50 TeV and 100 TeV. As explained at the end of section 5.1, the lower limit on $m_{3/2}$ of about 25 TeV arises from the general result that the lightest modulus mass is generically of the same order as $m_{3/2}$. The modulus decays with a decay constant which is effectively suppressed by the string scale, and the requirement of generating a sufficiently high reheat temperature so that BBN occurs in the usual manner, puts a lower bound on

$m_{3/2}$. Therefore, the lower limit on $m_{3/2}$ is uncertain only by a small amount. Although the upper limit is less tightly constrained, theoretical expectations constrain it to be not be much above 100 TeV. This is because in the string/M theory vacua considered here, gaugino masses are suppressed only by one-to-two orders of magnitude relative to $m_{3/2}$ in accord with theoretical expectations [146, 147, 148, 149, 150, 151]. Therefore, the requirement of gauginos to be light enough (with masses $\lesssim$ TeV) such that they are part of the low-energy theory at M_{susy} as assumed in section 5.3.1, puts an upper limit on $m_{3/2}$ of about 100 TeV. A similar upper bound also arises in realistic moduli stabilization mechanisms satisfying the supergravity approximation. Improvements in data as well as theory in the future will be extremely helpful in constraining the gravitino mass.

CHAPTER 6

Gluino and Chargino Searches at the LHC

The generic prediction of heavy scalars in G_2-MSSM makes its LHC phenomenology both challenging and interesting. Since we will not be able to produce the scalar particles directly at the LHC, the gauginos will be our main window of new physics: The wino LSP will produce large missing energy. It is possible to study signals rely solely on missing transverse energy(MET) like monojets. Most of the time however, it is much easier to search for other gauginos in G_2-MSSM. The production cross section of gluinos are not small due to the strong coupling. Gluinos decay through the heavy squarks, so the decay channel with the lightest squark is enhanced. In G_2-MSSM this corresponds to the decay channel containing 3rd generation squarks. This enhancement is partially cancelled by the small phase space when top quarks are presented in the decay product. In summary the gluino will decay into all the quarks with similar branching fractions, with the decay channels containing the top and bottom quarks slightly enhanced.

When the LSP is a pure wino like in the G_2-MSSM, the mass of the LSP and the lightest chargino are almost degenerate. The chargino can only decay into soft leptons or pions plus the LSP. This gives the chargino an unusually long lifetime. After being produced in the LHC, it can fly several centimeters, generate signals in the tracking chamber. Then the chargino will decay into the LSP and soft particles, effectively becomes invisible from the detector point of view.Besides being another way to searching for new physics, the chargino tracks also provide unique kinematic information. The 3-momentum of the chargino, which is almost equal to the 3-momentum of the LSP, can be used to estimate the missing energy. With enough chargino tracks and extra information about the mass of the LSP, it might be even possible to reconstruct the entire events.

6.1 General Gluino Search Signatures

In this work we have implemented the complete analytical expressions for soft breaking terms of the G_2-MSSM into SOFTSUSY[74]. The analysis includes the gaugino mass threshold corrections [70] with 2 loop scalar corrections, 2-loop RGEs for the Higgs and gaugino masses, μ, and

Yukawa and gauge couplings [73, 74]. Branching fractions have been computed with SUSY-HIT [152] and production of signal and backgrounds are generated with PYTHIA [153] and PGS4 [154] with the level 1 (L1) triggers designed to efficiently reproduce CMS specifications [155] (for detailed discussions see e.g. [156]). Signal and background have been simulated at $\sqrt{s} = (7, 10, 14)$ TeV in order to generalize our predictions for preliminary LHC runs and future operational center of mass energies. Specifically, SM backgrounds have been generated with QCD multi-jet production due to light quark flavors, heavy flavor jets ($b\bar{b}$, $t\bar{t}$), Drell-Yan, single Z/W production in association with quarks and gluons (Z+ jets / W+ jets), and ZZ, WZ, WW pair production resulting in multi-leptonic backgrounds. Laboriously, samples were generated at $\sqrt{s} = (7, 10, 14)$TeV with up to 5 fb^{-1} of luminosity. In PGS4 jets are defined through a cluster-based algorithm which has a heavy flavor tagging efficiency based on the parametrizations of the CDF Run II tight/loose (secondary) vertex b-tagging algorithm [157]. The standard criteria for the discovery limit of new signals is that the SUSY signals should exceed either $5\sqrt{N_{\rm SM}}$ or 10 whichever is larger, i.e., $N^c_{\rm SUSY} > {\rm Max}\left\{5\sqrt{N^c_{\rm SM}}, 10\right\}$, were c indicates the channel of interest.

The signature space of the models we probe has distinctive dark matter predictions. The models we consider are dominated by dark matter annihilations into W^+W^- and can yield a significant flux of cosmic antimatter in the galactic halo (for early work see [108, 158, 159, 160]). The annihilation cross section receives an enhancement relative to other SUSY modes since it is s-wave and has a relative strength dictated by the SU(2) gauge coupling and the wino component of the LSP. The models are made consistent with the relic density constraints as will be discussed.

6.2 Discovery Prospects and Concrete Signatures

In theories with wino LSPs, the dominant LHC production modes are not strictly those from strongly produced SUSY. The production modes of the wino ($\widetilde{N}_1$) and the lightest chargino ($\widetilde{C}_1$) are competitive with the gluino ($\tilde{g}$) production and sometimes are larger. However due to the small splittings (a fraction of a GeV) between the wino and chargino the decay products here are soft. Except for larger gluino masses, we find that most events that pass the triggers do indeed come from $\tilde{g}\tilde{g}$ production, though as much as 30% of the events come from electroweak production. Thus the dominant production modes are $pp \to [(\tilde{g}\tilde{g}), (\widetilde{N}_1\widetilde{C}_1), (\widetilde{C}_1^{\pm}, \widetilde{C}_1^{\mp})]$. The decays modes lead to rich jet and missing energy signatures with a sizeable number of leptons in the final state. In particular the dominant decays are as follows: $\tilde{g} \to [(\widetilde{N}_2 t\bar{t}), (\widetilde{N}_1 b\bar{b}), (\widetilde{N}_1 q\bar{q}), (\widetilde{C}_1^- \bar{b}t + \text{ h.c.}), (\widetilde{C}_1^- \bar{d}u + \text{ h.c.})]$ with secondary decays $\widetilde{N}_2 \to \widetilde{C}_1 W^* \to (\widetilde{C}_1 l\nu_l), (\widetilde{C}_1 q\bar{q}')$ and $\widetilde{C}_1 \to \widetilde{N}_1 W^* \to (\widetilde{N}_1 l\nu_l), (\widetilde{N}_1 q\bar{q}')$ with tertiary branchings of the produced standard model particles $t \to Wb$ and $W \to [(q\bar{q}'), (l\nu_l)]$.

The models are rather predictive as they typically require no more than 2-3 branchings to complete SUSY cascades resulting in lepton and jet signatures. While this is a typical signature

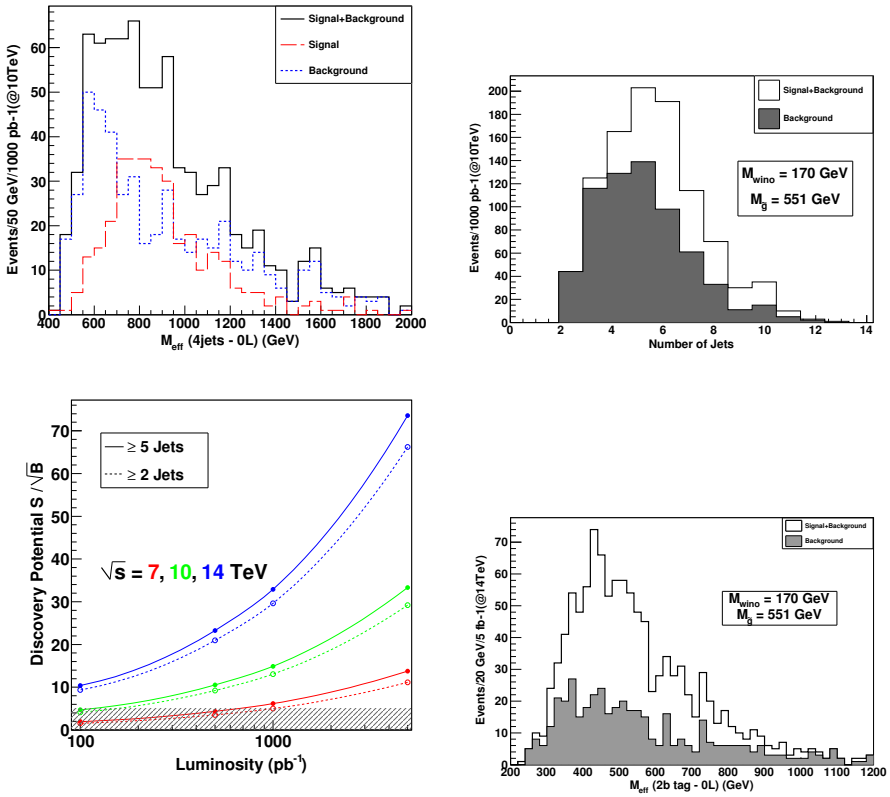

Figure 6.1: Upper left panel: $M_{eff}^{4jets} = \sum_{J=1-4} P_T^J(J) + P_T^{\rm miss}$ at 10 TeV with 1 fb^{-1} for the G_2^1 model benchmark with $S_T \geq 0.25$ (transverse sphericity), $P_T^{\rm miss} \geq 200$ GeV and a lepton veto. The backgrounds mainly comes from dijets, $t\bar{t}$ and W+ jets. Upper right panel: Distribution of jet number showing excesses in events with large jet multiplicities at low luminosity. Lower left panel: Discovery reach for the same model with $\sqrt{s} = (7, 10, 14)$ TeV. Lower right panel: Same model and cuts as the upper panel for 14 TeV with 5 fb^{-1} in the variable $M_{eff}^{2b} = \sum_{J=1-2} P_T^b(J) + P_T^{\rm miss}$.

of SUSY in a generic model, it is actually a prediction of the wino branch of the G_2 model as electroweak symmetry breaking corners the viable parameter space and thus the viable signature space. The decays of $\tilde{C}_1 \to \widetilde{N}_1$ and their jet and lepton by-products will be very soft yet there can be radiation of gluon from the initial or final state partons that can generate a relatively hard jet. Thus one can look for a hard monojet and n-jet events with large missing energy as an early indication of the production of supersymmetric events at the LHC. In Table (6.1) we illustrate some typical spectra found in the G_2 models for $m_{\widetilde{N}_1} \sim (170 - 190)$ GeV (precisely in the mass range pointed to by the recent positron ratio measurements from PAMELA and AMS II [see Chapter 4] along with the dominant branching ratio of the gluino given in Table (6.2).

Table 6.1: Some benchmark models predicting a light gluino and a LSP that is a wino with a degenerate chargino with a light second neutralino (which is mostly bino). The last four columns carry units of GeV.

G_2^m	$m_{3/2}$ (TeV)	δ	V_7	$\tan\beta$	$m_{\tilde{g}}$	$m_{\tilde{W}}$	$m_{\tilde{C}_1^\pm}$	$m_{\tilde{N}_2}$
G_2^1	38.950	-2.9	30.0	1.98	551	170.2	170.4	260
G_2^2	21.186	-10.0	33.0	1.41	717	173.4	174.0	190
G_2^3	20.700	-9.3	36.0	1.57	652	176.0	176.5	185
G_2^4	20.618	-9.1	30.0	1.71	632	180.9	181.3	185
G_2^5	35.492	-5.4	32.0	1.54	761	190.5	190.6	263

For the G_2 models, a central prediction is a relatively light gluino over the range of wino mass that is capable of describing the PAMELA data as is illustrated in Table (6.1). In Figure (6.1) (left upper panel) one observes that the models can produce detectable multi-jet signals even at $\sqrt{s} = 10$ TeV for $\mathcal{L} \sim 1\text{fb}^{-1}$ of integrated luminosity under the standard 5σ discovery reach criteria in the kinematic variable $M_{eff}^{4jets} = \sum_{J=1-4} P_T^J(J) + P_T^{\text{miss}}$. In Figure (6.1) (right upper panel) we show the large number of multijet signals. The analysis shows that the model can produce a large excess in hadronic jets over the backgrounds. The large jet multiplicity arises from the three body decay of the gluinos and from jets arising from initial state radiation. We find the discovery limit is optimal for 4-5 jets with a lepton veto and large missing energy cut. The lower right panel exhibits $M_{eff}^{2b} = \sum_{J=1-2} P_T^b(J) + P_T^{\text{miss}}$ with larger luminosity. The lower left panel shows the discovery reach for the same model with $\sqrt{s} = (7, 10, 14)$ TeV and 5σ can be reached with several hundred inverse picobarns of data.

6.2.1 Global Analysis and Discovery Prospects of SUSY

Having established that the highly constrained, and therefore predictive G_2 model can give rise to testable signals of SUSY with early LHC data, we now extend the analysis to a larger region of the G_2 parameter space rather than focusing on a benchmark model. We have performed a detailed scan of the parameter space of these models over the parameters consistent with radiative

Table 6.2: Dominant branching ratios of the gluinos.

$\mathcal{B}r(\tilde{g} \to X)$	G_2^1	G_2^2	G_2^3	G_2^4	G_2^5
$\tilde{g} \to b\bar{b}\widetilde{N}_1$	14.2	6.4	10.2	11.3	19.5
$\tilde{g} \to q\bar{q}\widetilde{N}_1$	21.0	7.4	12.6	14.6	10.0
$\tilde{g} \to t\bar{t}\widetilde{N}_2$	-	47.6	21.8	14.5	14.6
$\tilde{g} \to t\bar{b}\tilde{C}^- + h.c.$	18.9	16.2	20.8	20.9	24.6
$\tilde{g} \to q_u\bar{q}_d\tilde{C}^- + h.c$	41.5	14.6	25.2	29.0	24.9

Table 6.3: Shown is $\sigma_{\rm SUSY}({\rm fb})$, the theoretical cross section before passing through the detector simulation, $\sigma_{\rm eff}({\rm fb})$, the effective cross section after events have passed the L1 triggers with $\mathcal{L} = 1{\rm fb}^{-1}$ at $\sqrt{s} = 10$ TeV. Observable counts in the number of tagged b-jets and multijets are also shown $N(2b), N(4j)$ along with their signal to square root background ratios. The missing energy cut is ≥ 200 GeV and we have imposed a transverse sphericity cut of $S_T \geq 0.25$.

G_2^m	$\sigma(\tilde{g}\tilde{g})$ (fb)	$\sigma(\widetilde{N}_1\widetilde{C}_1)$ (fb)	$\sigma(\widetilde{C}_1^{\pm}\widetilde{C}_1^{\mp})$ (fb)	$\sigma_{\rm SUSY}$ (fb)	$\sigma_{\rm eff}$ (fb)	$N(4j)$	$\frac{N}{\sqrt{B}}\|_{4j}$	$N(2b)$	$\frac{N}{\sqrt{B}}\|_{2b}$
G_1^1	1613	996	301	2910	1645	416	13.3	37	4.7
G_2^2	236	970	277	1484	353	79	2.5	22	2.8
G_3^2	481	903	280	1665	553	133	4.2	37	4.7
G_4^3	648	877	246	1773	736	217	7.0	32	4.1
G_5^2	182	696	208	1087	250	64	2.0	10	1.2

electroweak symmetry breaking subject to the constraint that the wino mass is in the range (170 - 210) GeV . We uncover a large parameter space where the gluino can be relatively light in the G_2 model. Many of these models have a gluino in the mass range of 500 to 900 GeV (see Fig.(6.2) for the corresponding gaugino mass ratios). LHC predictions with light gluino have been studied recently [32, 6, 161, 162], but without considering the connection to the PAMELA data, which we pursue in the next section.

In Table (6.3) we display the relatively large total theoretical production cross section before cuts ($\sigma_{\rm SUSY}$ from gluino, neutralino, chargino production) and the effective SUSY cross section $\sigma_{\rm eff}$ (cross section after the L1 triggers have been passed). One observes that the L1 triggers are well optimized for these events as a large fraction of the SUSY cross section is maintained. The substantial missing energy arises in many of the models from the prompt branching of the gluino into 2 jets and the LSP wino. Event rates at the LHC are shown in the 4-jet channel and the 2b channel with just 1 fb^{-1} of integrated luminosity at $\sqrt{s} = 10$ TeV along with the ratio of the signal to the square root of the background. These models can be discovered very early with the LHC and can begin to be probed at $\sqrt{s} = 7$ TeV.

Models with wino-like LSPs, and thus nearly degenerate charginos and neutralinos, are well known to be be difficult to study [163]. The chargino lifetime can be of order a centimeter, and the second heavier neutralino can even have order tens of GeV splitting (see Table (6.1) for such theory motivated examples). Once a set of gluino candidates have been identified, an off-line analysis focused towards the study of the chargino and neutralino states in the gluino decay products will

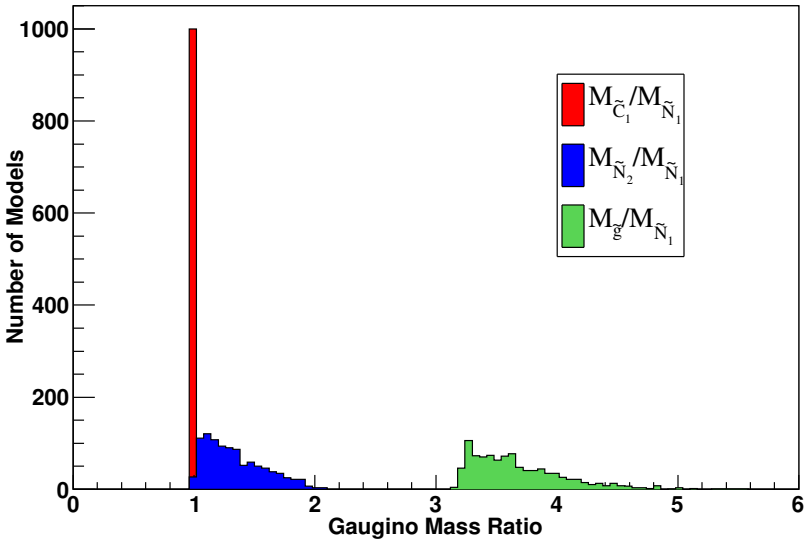

Figure 6.2: Ratio of gaugino masses in the G_2 model. The predicted ratios can be quite different than those that arise in other models of soft SUSY breaking (for a comparison see Ref. [6]). The mass range here for the wino is (170 - 210) GeV and the gluino lies in the range (500-900) GeV.

be necessary.

6.3 Third family enhanced gluino decays

The gluino decays via virtual squarks to $q\bar{q}\chi_1^0$ or $q\bar{q}\chi_1^\pm$. Since the rate for a given diagram scales as the virtual squark mass to the -4 power from the propagator, the lightest squarks dominate. Therefore, we are led to consider decay channels $\tilde{g} \to t\bar{t}\tilde{N}$, $\tilde{g} \to t\bar{b}\tilde{C}^-$, and $\tilde{g} \to b\bar{b}\tilde{N}$. Decays of multiple top quarks lead to b-rich and lepton rich final states, and give excellent potential for early discovery. In fact, we show that significant excesses can be observed at the early LHC-7 TeV. For example, gluino masses larger than 600 GeV can be discovered in the single-lepton plus 4 b-jets channel.

We carry out our study on several benchmark models. To study the reach of gluino pair production, with decays into third generation squarks, a detailed scan of the parameter space involving the gluino mass and LSP mass, for different branching ratios, is performed. We emphasize that the goal of this study is to demonstrate that gluino pair production with decays via third generation squarks provides an ideal channel for early discovery at the LHC, since it leads to lepton and b-quark rich final states.

6.3.1 Benchmark Models

Three benchmark models are considered which will form the basis for the numerical scan discussed below. The model parameters and relevant decay branching ratios are shown in Table 6.4. Model A is a simple example of multi-top physics. The spectrum would have a stop much lighter than the other squarks, and therefore gluino pair production always produces four tops in the final state. Model B is designed to include the decay channel $\tilde{g} \to b\bar{b}\chi_1^0$, which will result if the sbottom is also lighter than the first two generation squarks, and $m_{\tilde{t}} \sim m_{\tilde{b}}$. Model B is observably different than Model A, while somewhat more difficult to discover. These models have a Bino-like LSP. In Model C, the Wino is the LSP, and is approximately degenerate with the lightest chargino, which is also Wino-like. It is designed to further include a chargino in the decay chain, which allows the decay $\tilde{g} \to t\bar{b}\chi_1^+$. Since the charged Wino is approximately degenerate with the wino LSP, it appears only as missing energy; though if one focuses on the signal events the chargino stub [163] can probably be seen in the vertex detector.

	Branching ratios		
	$\tilde{g} \to t\bar{t}\chi_1^0$	$\tilde{g} \to b\bar{b}\chi_1^0$	$\tilde{g} \to t\bar{b}\chi_1^+ + h.c.$
A	1	0	0
B	0.5	0.5	0
C	.08	0.22	0.7

Table 6.4: Relevant branching ratios for the benchmark models considered in this paper. The models A and B have bino LSP. In Model C, the lightest neutralino and lightest chargino are both winos. In all models the first two generation squark masses are taken to be 8 TeV. The third generation is taken to be somewhat lighter and is chosen to generate the required branching ratios of the model.

The three models are taken as a basis for 3 seperate numerical scans, where $m_{\tilde{g}}$ and m_{LSP}, are varied while the branching ratios are fixed, as shown in Table 6.4. In particular, scans in model A and model B varied $m_{\tilde{g}}$ and $m_{\text{LSP}} = m_{\chi_1^0}$. while scan in model C varied $m_{\tilde{g}}$ and $m_{\text{LSP}} = m_{\chi_1^0} \simeq m_{\chi_1^\pm}$.

6.3.2 Signal Isolation and Backgrounds

The relatively large b-jet and lepton multiplicity associated with multiple top production provide for potentially striking signatures that are easily distinguishable above the expected SM background. By requesting multiple b-tagged jets and at least one lepton, it is possible to achieve signal significance $S/\sqrt{B} > 5$ for 1 fb^{-1} of integrated luminosity.

The most significant backgrounds from the SM for final states with many b-jets, several isolated

leptons and missing energy, are from top pair production, $t\bar{t}$. The expected cross-section at the LHC for 7-TeV center-of-mass energy is $\sigma = 164$pb (NLO) [164]. Also included in the analysis are a set of SM backgrounds involving associated production of gauge bosons with third generation quarks. These contribute less significantly to the backgrounds than $t\bar{t}$, but can contribute to signals with high lepton multiplicity. All background sources considered, and their respective cross sections are given in Table 6.5. With the exception of the $t\bar{t}$ cross section, we increased all SM background cross sections by a factor of 2, to account for possible K-factor from NLO corrections. Since the relevant backgrounds for the channels considered end up small (Table 6.5), uncertainties in the cross section are not important.

All background event samples were produced with Madgraph v.4 [165], while the parton shower and hadronization were done by Pythia 6.4 [153]. Additional hard jets (up to three) were generated via Madgraph, while the MLM [166, 167, 168] matching scheme implemented in Madgraph was used to match these jets to the ones produced in the Pythia showers. The events were then passed through the PGS-4 [154] detector simulators with parameters chosen to mimic a generic ATLAS type detector. The b-tagging efficiency was changed to more closely match the expected efficiencies at ATLAS [169, 170]. For b-jets with $50\text{ GeV} \lesssim p_T \lesssim 200\text{ GeV}$, which is typical of the b-jets in the signal, the efficiency is approximately 60% for tagging a b-quark.

Process	σ [fb]	σ_{L1}[fb]	σ_1[fb]	σ_2[fb]
$b\bar{b} + \gamma/Z + \text{jets}$	4.69×10^5	1.41×10^4	34.0	107.8
$b\bar{b} + W^{\pm} + \text{jets}$	2.41×10^4	5.39×10^2	7.71	13.3
$t\bar{t} + \gamma/Z + \text{jets}$	1.54×10^3	7.69×10^2	42.3	95.4
$t\bar{t} + W^{\pm} + \text{jets}$	2.25×10^2	1.31×10^2	14.3	27.6
$t\bar{b} + \gamma/Z + \text{jets} + h.c.$	1.34×10^3	8.09×10^2	7.37	26.6
$b\bar{b} + VV + \text{jets}$	1.14×10^3	2.33×10^2	1.45	3.94
$t\bar{t} + \text{jets}$	1.60×10^5	6.60×10^4	2076.7	5905.6
$VV + \text{jets}$	1.03×10^5	1.03×10^5	108.6	377.7
Model A	1.19×10^3	9.48×10^2	403.8	508.1
Model B	1.19×10^3	1.03×10^3	505.2	703.1
Model C	1.19×10^3	5.80×10^2	300.5	420.5

Table 6.5: Cross sections for production of signal and backgrounds. The first column gives the total production cross section. The second gives the cross section after the L1 triggers defined in PGS-4 (see text). The remaining columns give the cross section after selection cuts in Eq. 6.1 and Eq. 6.2, with an additional missing energy (MET) requirement, $\not{E}_T \geq 100$ GeV. The $b\bar{b} + \text{jets}$ and $b\bar{b}b\bar{b}$-inclusive backgrounds have been considered, and after the applying the selection cuts in Eqs. 6.1-6.2 and requiring at least one lepton, the number of events are negligible in the $\{b, \ell\}$ channels considered here. In this table, we set $m_{\tilde{g}} = 500$ GeV and $m_{LSP} = 100$ GeV.

The signal event samples, for gluino pair production and decay, were produced using Pythia 6.4 and have been passed through the same PGS-4 detector simulation. Basic muon isolation was

applied to all samples. To reduce the number of backgrounds events are required to pass the L1-triggers as defined by PGS. We also display the effect of two possible additional selection cuts, together with the additional requirement $\not{E}_T \geq 100$ GeV,

$$\textit{cut-1} : n_j(p_T \geq 50\,\mathrm{GeV}) \geq 4 \tag{6.1}$$

$$\textit{cut-2} : n_j(p_T \geq 30\,\mathrm{GeV}) \geq 4 \tag{6.2}$$

in the last two columns of Table 6.5. The second cut (weaker than the first) is optimal for discovery signatures, such as the same-sign dilepton signature, that have relatively small SM backgrounds.

Next, the signal is searched for in multi b-jet ($n_b = 2, 3, 4$) and multi lepton channels (1ℓ, SS, OS, 3ℓ). All objects are required to have a minimum p_T of 20 GeV. Same sign (SS) and opposite sign (OS) di-leptons are separated as they can have different origins and sizes. We will use the possible excess in these channels to assess the discovery potential. Table 6.6 shows the expected number of events from the SM background as classified according to the number of b-tagged jets and isolated leptons in the event.

Table 6.6 shows the expected number of signal events with b-tagged jets and isolated leptons for the three benchmark models. Model A, which is predominantly a four top signal, has significantly more multi-lepton and b-jet events passing selection cuts than Model B and Model C, which have fewer four top events. In Table 6.6, the signal significance achievable with $1\ fb^{-1}$ integrated luminosity is shown. By requesting at least 4 b-tagged jets it is possible to observe signal significance $S/\sqrt{B}$ $\geq$5 for events with a single lepton. The one-lepton four-b-jet channel will prove to be robust and the best channel for discovery.

6.4 Searching for Gluino Events with $\widetilde{W}^{\pm}$ Tracks

Charged tracks resulting from long lived pair produced charginos can provide an unambiguous SUSY signal in particle colliders[171, 172, 173, 174, 175, 176, 177]. Assuming the Higgsino mass parameter $\mu \gtrsim 1$ TeV as is natural in theories with heavy gravitinos[1], the charged and neutral Wino masses are essentially degenerate at tree level. The largely model independent mass splitting which results from loop corrections is $\delta m \sim 160$ MeV [171]. To a good approximation the charged Wino decay width can be given by the two body decay width for $\widetilde{W}^{\pm} \to \widetilde{W}^0 \pi^{\pm}$[175]:

$$\Gamma(\widetilde{W}^{\pm}) = \frac{2G_F^2}{\pi} \cos^2\theta_c f_\pi^2 \delta m^3 \sqrt{1 - \frac{m_\pi^2}{\delta m^2}}, \tag{6.3}$$

[1]For example, it was recently shown in [178] and [135] that $\mu \sim$ TeV arises naturally in certain M-theory compactifications.

Number of Background Events (B)

Standard Model

B	*2b*	*3b*	*4b*
1ℓ	286.2	41.4	1.04
OS	32.8	5.65	0.007
SS	0.3	0.06	0
3L	0.14	0.007	0

Number of Signal Events (S)

	Model A				**Model B**				**Model C**		
S	*2b*	*3b*	*≥4b*		*2b*	*3b*	*≥4b*		*2b*	*3b*	*≥4b*
1L	47.1	39.3	19.3	*1L*	33.5	26.9	13.8	*1L*	18.0	14.4	7.4
OS	12.4	9.9	3.9	*OS*	6.4	5.0	1.7	*OS*	2.0	0.9	0.6
SS	6.6	5.1	2.3	*SS*	2.3	1.2	0.2	*SS*	0.7	0.6	0.2
3L	3.0	2.1	0.7	*3L*	0.7	1.0	0.3	*3L*	0	0.1	0.1

Significance $\left(\mathrm{S}/\sqrt{\mathrm{B}+1}\right)$

	Model A				**Model B**				**Model C**		
	2b	*3b*	*≥4b*		*2b*	*3b*	*≥4b*		*2b*	*3b*	*≥4b*
1L	2.77	6.03	13.5	*1L*	1.97	4.13	9.66	*1L*	1.06	2.21	5.18
OS	2.13	3.83	3.88	*OS*	1.10	1.93	1.69	*OS*	0.34	0.34	0.40
SS	5.75	4.95	2.30	*SS*	2.00	1.16	0.20	*SS*	0.58	0.58	0.20
3L	2.80	2.09	0.70	*3L*	0.65	0.99	0.30	*3L*	0	0.10	0.10

Table 6.6: Number of SM events, number of signal event, and signal significance, with 2, 3, or 4 b-tagged jets and OS, SS, or 3 leptons at the early LHC-7, for $1fb^{-1}$ integrated luminosity. For the 1-lepton counts, *cut-1* was applied, while for the other lepton counts *cut-2* was applied. These numbers were found for $m_{\tilde{g}} = 500$ GeV and $m_{LSP} = 100$ GeV.

where θ_c is the Cabbibo and angle and the pion decay width $f_\pi \sim 130$ MeV. For large values of $\mu \gtrsim 1$ TeV and moderate values of $\tan\beta$ the loop contribution dominates the mass splitting, resulting in a charged Wino lifetime $c\tau \sim \mathcal{O}(5)$ cm [171][2].

A prolific source of detectable charged Wino tracks results from three body decays of pair produced gluinos, $pp \to \tilde{g}\tilde{g} \to \widetilde{W}^{\pm}, \widetilde{W}^0 +$ jets. In typical heavy squark and Wino LSP models, the gluino has a $\mathcal{O}(50\%)$ branching ratio to $\widetilde{W}^{\pm}$ final states; these events result in many hard objects, and are easily triggered on [179, 180]. The NLO gluino pair production cross section for the mass range of interest, 600 GeV $\lesssim m_{\tilde{g}} \lesssim$ 1000 GeV, is $\mathcal{O}(10 - 1000)$ fb. Increasing the LHC center of mass energy from $\sqrt{s} = 7$ TeV to $\sqrt{s} = 8$ TeV approximately doubles the gluino production cross section (as calculated by PROSPINO[181]). Thus with 10 fb^{-1} of luminosity, we should already expect numerous gluino pair production events at LHC-8; roughly half of these gluinos will produce a charged Wino as a 3-body decay product, since the SU(2) symmetry relates the branching ratio to $q\bar{q}\widetilde{W}^0$, $q'\bar{q}\widetilde{W}^-$ and $\bar{q}'q\widetilde{W}^+$.

In order to detect charged Winos resulting from gluino decays, $\widetilde{W}^{\pm}$ must live long enough to form a track in the inner detector. Specifically, we focus on the detection capabilities of the ATLAS detector. In the barrel region, the inner detector of the ATLAS detector contains three layers of pixel detector at average radii of 5 cm, 9 cm, 12 cm, then there are four layers of semiconductor tracker (SCT), located respectively at 30 cm, 37 cm, 44 cm and 51 cm away from the beam line. The transition radiation tracker (TRT) is located outside the SCT, 55.4 cm away from the beam line [182]. If the charged Wino reaches the third layer of the SCT its track can be reconstructed using the information from the pixel detector and the SCT, and its three-momentum can be determined with good resolution [183]. Perhaps it will be possible to use shorter chargino tracks. The soft pion (or lepton) resulting from the chargino decay would also be a distinctive signal if it could be observed, and would give useful information regarding the kinematics of the event. To

$m_{\widetilde{W}}$	1st SCT Layer	2nd SCT Layer	3rd SCT Layer	4th SCT Layer
100 GeV	416.3	292.6	208.2	147.9
150 GeV	232.2	150.6	98.9	69.5
200 GeV	125.3	76.5	46.4	30.8
250 GeV	85.2	42.2	24.7	14.8
300 GeV	49.7	27.6	17.0	9.4

Table 6.7: Inclusive count of the number of charginos which make it past a given detector layer. These results correspond to 10 fb^{-1} of LHC-8 data ($\sigma_{\tilde{g}\tilde{g}} \sim 235$ fb), with $m_{\tilde{g}} = 750$ GeV.

estimate the usefulness of looking for stiff charginos, we simulate decays of charged Winos resulting from gluino pair production. The pair produced gluino events are generated by the MadGraph

[2]However if $\mu \sim M_2$, there is an $\mathcal{O}(m_W{}^2/\mu^2)$ tree level mass splitting which can potentially become $\mathcal{O}(1)$ GeV, significantly decreasing the lifetime such that $c\tau \ll 1$ cm.

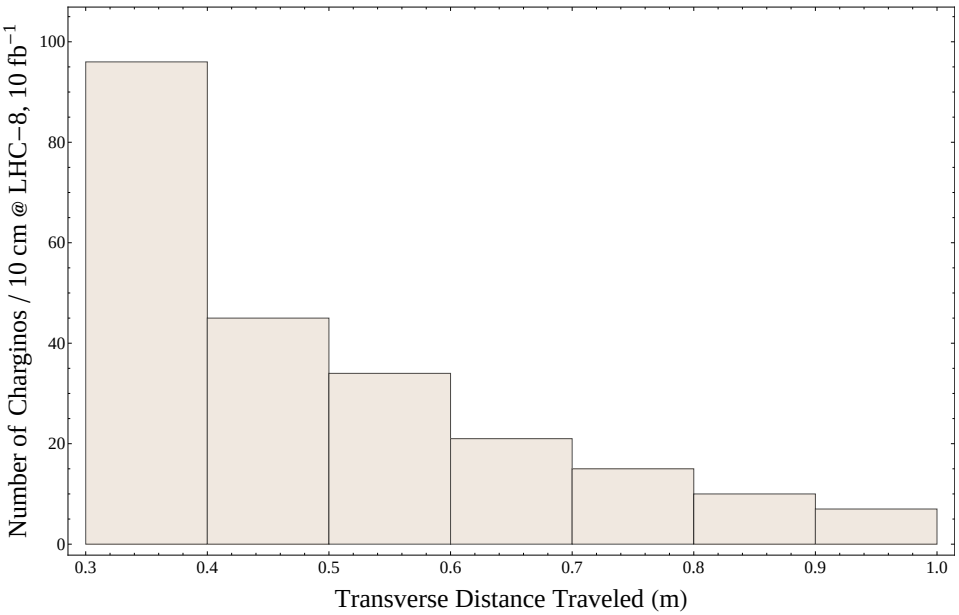

Figure 6.3: Charged Winos resulting from gluino pair production, binned as a function of transverse distance traveled from the beam line. These results correspond to 10 fb^{-1} of LHC-8 data ($\sigma_{\tilde{g}\tilde{g}} \sim 235$ fb), with $m_{\tilde{g}} = 750$ GeV, $m_{\widetilde{W}} = 150$ GeV. For graphical purposes, charginos traveling a transverse distance < 30 cm are not shown.

5/MadEvent package [184], and the gluino decays (as well as hadronization and showering) are implemented through PYTHIA6 [153]. The mass splitting δm which enters into the decay width is calculated using SOFTSUSY [185]. The results for $m_{\tilde{g}} = 750$ GeV[3] with 10 fb^{-1} of LHC-8 data (without any kinematic cuts) are shown in Figure 1 and Table 1. In Fig. 1, the charged Winos[4] are binned as a function of transverse distance traveled before decay. Table 1 shows an inclusive count of the number charginos which make it past a given detector layer. These results indicate that with the 10 fb^{-1} of LHC-8 data expected at the end of 2012, for $m_{\widetilde{W}} \lesssim 300$ GeV we expect $\gtrsim 20$ charginos will make it past the third SCT layer.

To search for gluinos, one can use the usual SUSY search channels (or even looser cuts) to isolate relatively pure events from the gluino decay, and then search for chargino tracks in those events. For a concrete example, in the G2-MSSM (resulting from M-theory compactified on a G_2 manifold [187]) the gluino has a substantial branching fraction to third generation quarks: $\tilde{g} \to t\bar{b}W^- + h.c.$. As demonstrated in [179, 180], searching for events containing a lepton and multiple b-jets is the most powerful way to discover this kind of model. With the additional signals given by chargino tracks, one can also make use of the weaker SUSY search channels such as 1

[3]We note that with heavy squarks, and the enhancement of gluino decays to heavy quarks due to a lighter stop and sbottom, 750 GeV gluinos are not excluded by any ATLAS or CMS analysis.

[4]In order for the non-thermal cosmology to give approximately correct relic density and not overclose the universe, the chargino cannot be very heavy, so we only consider charginos mass from 100 GeV to 300 GeV[186].

lepton + 1 b-jet. As an example, we consider a G2-MSSM model with a 750 GeV gluino and 150 GeV Wino LSP with 10 fb^{-1} of LHC-8 data[5]. After applying cuts similar to the 1 lepton + 1 b-jet ATLAS search channel[188]:

$$1 \text{ lepton}, \not{E}_T > 80 \text{ GeV}, \geq 4 \text{ jets}, \geq 1 \text{ b-jets}, \tag{6.4}$$

about 200 gluino pair events survive. Roughly 10 of these surviving events will contain a long chargino track which can be reconstructed. Aside from the 1 lepton + 1 b-jet channel, this chargino signal can be observed in many other SUSY channels, as illustrated in Table 2. In this table, the kinematic cuts defining the signal regions of the 1 b-jet + $\not{E}_T$ channel are defined in [188], and the cuts defining the signal regions of the jets + $\not{E}_T$ channel are defined in [189]. These results

b-jets + $\not{E}_T$ Signal Region[188]	SR0-A1 $m_{eff} >$ 500	SR0-B1 $m_{eff} >$ 700	SR0-C1 $m_{eff} >$ 900
Charginos Past 3rd SCT	28	25	17

jets + $\not{E}_T$ Signal Region[189]	4-jet, m_{eff} >500	4-jet, m_{eff} >1000	4-jet, High Mass
Charginos Past 3rd SCT	40	26	20

Table 6.8: Number of charginos which make it past the 3rd SCT layer in signal regions of various ATLAS SUSY search channels. These results are for 10 fb^{-1} of LHC-8 data. We have chosen channels expected to be sensitive to gluino pair production events. Other search channels give weaker chargino signals, which can be enhanced by loosening cuts. The m_{eff} cuts are given in units of GeV.

demonstrate that the signal of chargino tracks is robust under typical SUSY squark/gluino search cuts; in particular, increasing the m_{eff} cut from 500 GeV to 1000 GeV still maintains $\sim 60\%$ of the chargino signal. Thus chargino tracks provide an additional "free" channel for gluino discovery, which can be studied without loosening cuts and introducing additional SM background events into the SUSY signal region.

The stub track resulting from chargino decay is a distinctive SUSY signal without SM background. However, in reality the signal may be contaminated by detector noise and mis-reconstructed tracks. We did not include these possible backgrounds in our study; instead we argue they can be controlled without significantly hurting the signals. First of all, the kinematic cuts we applied to remove a large amount of the SM background should also help reduce fake chargino tracks. Requiring $p_T > 80$ GeV for the chargino track candidate keeps $\sim 80\%$ of the signal events, while eliminating detector noise resulting from soft mis-reconstructed tracks. For a fake track with high

[5]Detector effects are included by running simulated events through the PGS-4[154] detector simulation.

p_T, the fake chargino p_T will be nearly collinear with $\not{E}_T$ unless there are large contributions to $\not{E}_T$ from energetic neutrinos. Thus imposing a $\Delta\phi\left(\widetilde{W}^{\pm}, \not{E}_T\right) > 0.4$ cut will reduce the background from hard jets faking chargino tracks, while keeping $\sim 60\%$ of the signal events. In addition, the pixel detector can measure dE/dx energy loss of the particle. The charginos on average have $\beta\gamma = 2$, while the SM tracks with the same momentum have much larger $\beta\gamma$. It is possible that this energy loss can be used to separate the real chargino tracks from the backgrounds. With enough events, dE/dx spectra can even be used to estimate the mass of the chargino. However, precise determination of the background after imposing cuts can only be determined by experimental detector groups upon analyzing the data.

6.5 Reconstructing the Gluino Mass

If chargino tracks are observed, one can use this additional information to separate SUSY events from the SM background, and estimate the mass of the gluino even without precise knowledge of the chargino mass. As already mentioned in the ATLAS jets + $\not{E}_T$ search, ignoring the chargino/LSP mass only changes the reconstructed gluino mass by a small amount, $O(m^2_{LSP}/m^2_{\tilde{g}})$. To obtain sufficient statistics for the analysis, we use a set of cuts slightly looser than the cuts used in the ATLAS jets + $\not{E}_T$ search[189]:

$$\begin{aligned} &\not{E}_T > 130\,\mathrm{GeV},\ \geq 4\,\mathrm{jets},\ p_T\,(j1) > 130\,\mathrm{GeV}, \\ &p_T\,(j2, j3, j4) > 50\,\mathrm{GeV},\ \Delta R(\mathrm{chargino},\ \mathrm{jets}) > 0.3 \end{aligned} \tag{6.5}$$

For 10 fb^{-1} of LHC-8 data, there will be about 60 events containing a reconstructed chargino track which pass the cuts listed in (**??**). In order to find the pair of jets most likely to have come from the same gluino as the chargino track, we calculate the transverse momentum of the other chargino/neutralino from the missing transverse momentum, and separate the 6 objects (2 charginos and 4 jets) into 2 clusters, each containing 1 chargino and 2 jets. The optimal clustering is determined by minimizing the difference in $|p_T|$ between the two clusters. Using the cluster containing the real chargino track and assuming $m_{\widetilde{W}} = 0$, we can make a histogram of the reconstructed gluino mass. Fitting the histogram with a distribution gives a reconstructed gluino mass near the actual value, with ~ 100 GeV uncertainty. Thus chargino tracks can provide an independent kinematic measure of the gluino mass, whose accuracy will improve with improving statistics.

Simply knowing that a gluino of some approximately measured mass decays to a chargino + jets of some p_T puts a valuable upper limit on the chargino mass (and therefore the dark matter mass). With more information, it may be possible to obtain a precise measurement of the chargino

mass. For instance, measuring the p_T of the soft pion resulting from the chargino decay along with the chargino track 3-momentum might allow a kinematic reconstruction of the chargino mass. However, it is unclear whether or not measuring such a soft track would be experimentally feasible. Other experimental approaches, such as determining the dE/dx spectra of the chargino tracks, can also refine measurements of the chargino mass.

Since these analysis were done, the LHC detector groups have presented gluino searches that excluded the light gluino masses. Since none of the analysis use the realistic gluion branching ratio such as BR$(t\bar{t}) \approx 7\%$, BR$(b\bar{b}) \approx 10\%$, BR$(t\bar{b} + \bar{t}b) \approx 26\%$, it is not easy to use the reported results to give precise gluino limits; we estimate that $m_{\tilde{g}} < 950\,\mathrm{GeV}$ is probably excluded, but TeV gluinos are not.

CHAPTER 7

Conclusion

7.1 conclusion and future directions

In this thesis I studied G_2 compactification of the M theory. The moduli stabilization and SUSY breaking are achieved by hidden sector QCD like interactions. To obtain a de Sitter space with a small cosmological constant, a meson field from the quark condensation has to be included. Motivated by our knowledge about the Calabi-Yau manifold, it is plausible to have a G_2 manifold with a discrete symmetry after moduli stabilization.

Once we establish all the theoretical ingredients, we focused on the $SU(5)$ GUT model. Wilson lines are introduced to break the $SU(5)$ to the standard model gauge group $SU(3)\times SU(2)\times U(1)$. By combining them with appropriate discrete symmetries on the G_2 manifold, we can solve the doublet-triplet splitting problem. The effective theory below the unification scale, G_2-MSSM, has a MSSM spectrum with distinctive features such as heavy scalars, suppressed μ term and light gauginos. The matter/R-parity can be realized as another discrete symmetry on the stabilized G_2 manifold. Anomaly-free conditions put non-trivial constrains not only on the discrete symmetry itself, but also on the Yukawa couplings. The approximate symmetry suppressing the μ term will also suppress at least one eigenvalue of the Yukawa matrix of the down-type quarks or the leptons. Then we demonstrated the little hierarchy problem is alleviated in the G_2-MSSM because of the large trilinear couplings. The compactification predicts the gravitino mass is exponentially suppressed comparing to the Planck scale. The lower bound of the moduli/gravitino mass is obtained from cosmology. To preserve the well established BBN mechanism, it is important that the moduli and the gravitino decay well before BBN time. This in turn requires $m_{3/2}\sim O(50\,\mathrm{TeV})$.

The rest of this thesis focused on the phenomenology of G_2-MSSM. First we considered the dark matter candidates. Wino LSP and axion are both good candidates for dark matter and the relic abundances of both are of the same order according to the theoretical calculation. Wino LSP has a large annihilation cross section. It can be used to partially explain the "anomalies" in the observation of recent indirect dark matter experiments. The direct detection experiments are more

challenging for wino dark matter due to its very small cross section. The only way to increase the cross section is to increase the Higgsino component by lowering the μ term. However the μ term is determined from the top-down approach independently. Thus we can obtain a upper limit of the direct detection cross section well below the current experimental bounds.

The LHC phenomenology had two parts. First we calculated the Higgs mass in G_2-MSSM. Because of the heavy scalars, the lightest Higgs particle received large loop corrections. After resuming the major contributions, the mass of the lightest Higgs particle in G_2-MSSM is close to 125 GeV, about $\pm 1.5\,\mathrm{GeV}$ for $\tan\beta$ prefered by the theory, which is consistent with the recent results from ATLAS [10] and CMS [11]. The more exciting possibility is the direct observation of superparticles at the LHC. Because the scalars are too heavy to be produced directly, we concentrated on the light gauginos. Gluino searches using MET and multijets are always a good approach. In some cases the decay branching fractions to the 3rd generation quarks are enhanced, so targeting channels with b-jets and/or leptons with large MET can be more effective. There is also a potentially interesting search channel for the light chargino. The disappearing chargino tracks are not only useful in searching for new physics, but can also provide extra kinematic information for quantitative studies.

On the theoretical aspect, G_2-manifolds are notoriously difficult to construct, but new developments in recent years might soon evolve to produce compact G_2-manifolds with singularities suited for phenomenological purposes. It is also important to understand the top Yukawa coupling in M theory. There is a construction for the standard model gauge group, but there is still no satisfying solution for unification theories.

We will understand the phenomenology a lot better with deeper knowledge of the G_2-manifold. Meanwhile it is interesting to consider the phenomenology of more general scenarios like enlarged gauge group such as $SO(10)$, or extra matter fields.

APPENDIX A

Useful Results

A.1 Implications of Top-Down Constraints

A.1.1 Constraints on Wilson Line Parameters from Anomaly Cancellation

The $SU(3)-SU(3)-Z_N$, $SU(2)-SU(2)-Z_N$ and $U(1)_Y-U(1)_Y-Z_N$ anomaly coefficients for a non-R Z_N symmetry are given by:

$$\begin{aligned}
A_{SU(3)-SU(3)-Z_N} \equiv A_3 &= \frac{1}{2}\sum_{i=1}^{3}\left(2q_{Q^i}+q_{U^i}+q_{D^i}\right)+\frac{1}{2}\left(q_{T_u}+q_{T_d}\right)\\
A_{SU(2)-SU(2)-Z_N} \equiv A_2 &= \frac{1}{2}\sum_{i=1}^{3}\left(3q_{Q^i}+q_{L^i}\right)+\frac{1}{2}\left(q_{H_u}+q_{H_d}\right)\\
A_{U(1)-U(1)-Z_N} \equiv A_1 &= \frac{1}{2}\sum_{i=1}^{3}\left(\frac{1}{5}q_{Q^i}+\frac{8}{5}q_{U^i}+\frac{6}{5}q_{E_c^i}+\frac{2}{5}q_{D^i}+\frac{3}{5}q_{L^i}\right)\\
&\quad+\frac{1}{5}\left(q_{T_u}+q_{T_d}\right)+\frac{3}{10}\left(q_{H_u}+q_{H_d}\right)
\end{aligned} \tag{A.1}$$

where q_{Q^i} represents the Z_N charge for the i'th generation of the Q superfield, and similarly for q_{U^i}, q_{D^i}, etc. As discussed in section 3.2.5.1, anomaly cancellation requires that 3.25 is satisfied. Furthermore, consitency with the Wilson line mechanism described in Chapter 3 requires that (3.4)-(3.6) are satisfied. It is straightforward to show using (3.4) and (3.5) that the anomaly coefficients in (A.1) satisfy:

$$2A_3+3A_2=5A_1. \tag{A.2}$$

Therefore A_1 provides no additional constraint, and anomaly cancellation is achieved provided the conditions on A_3 and A_2 in (3.25) are satisfied. In other words, $A_3 = A_2$ is sufficient to

achieve anomaly cancellation regardless of whether or not a Green-Schwarz axion is present. By combining the condition $A_3 = A_2$ with (3.4)-(3.6), we obtain:

$$\sum_{i=1}^{3} 5\rho\left(\delta_{\bar{5}_i} - \delta_{10_i}\right) = 5\rho\left(\delta_{5_H} - \delta_{\bar{5}_H}\right) \;\; Mod\, N = q_{H_u} + q_{H_d}. \tag{A.3}$$

Here the δ_{10_i} and $\delta_{\bar{5}}$ parameterize the Wilson line splitting of the $SU(5)$ multiplets, and the sum over i represents a sum over all three generations. Since doublet-triplet splitting requires $5\rho \neq Mod\, N$ and recalling that by our parameterization $\delta_i = 0$ or 1, we can enumerate the possible solutions to (3.25):

1. $\sum_{i=1}^{3}\left(\delta_{\bar{5}_i} - \delta_{10_i}\right) = \left(\delta_{5_H} - \delta_{\bar{5}_H}\right)$. In this case, the anomaly constraints are trivially satisfied regardless of the value which 5ρ takes.

2. $\sum_{i=1}^{3}\left(\delta_{\bar{5}_i} - \delta_{10_i}\right) = -\left(\delta_{5_H} - \delta_{\bar{5}_H}\right)$ or $\sum_{i=1}^{3}\left(\delta_{\bar{5}_i} - \delta_{10_i}\right) = 3\left(\delta_{5_H} - \delta_{\bar{5}_H}\right)$. In this case, the anomaly constraints are satisfied if $10\rho = N$. This requires even N and results in $5\rho = N/2$, and thus $Z_M = Z_{N/2}$ assuming no other moduli charges.

3. $\sum_{i=1}^{3}\left(\delta_{\bar{5}_i} - \delta_{10_i}\right) = -2\left(\delta_{5_H} - \delta_{\bar{5}_H}\right)$. In this case, anomaly freedom requires $15\rho = N$, and thus $5\rho = N/3$.

4. $\sum_{i=1}^{3}\left(\delta_{\bar{5}_i} - \delta_{10_i}\right) = -3\left(\delta_{5_H} - \delta_{\bar{5}_H}\right)$. In this case, anomaly freedom requires $20\rho = N, 2N$ and thus $5\rho = N/2, N/4$.

A.1.2 Fermion Mass Forbidden by Z_N

For the Z_N solution to the μ problem described in this work, top-down constraints imply that at least one of the mass eigenvalues in either the down or lepton sector must be forbidden by Z_N if Z_N solves the doublet-triplet splitting problem. In what follows, we give a simple derivation of this result.

A three by three matrix A with entries $A_{i,j}$ will have a nonzero determinant if:

$$\Pi_{i=1}^{3}\left(A_{i,\sigma_i}\right) \neq 0. \tag{A.4}$$

where σ_i is some permutation of 1, 2 and 3. For example, if we are considering the diagonal components of A then $(\sigma_1, \sigma_2, \sigma_3) = (1, 2, 3)$, and (A.4) would result in $A_{11}A_{22}A_{33} \neq 0$. If A has a zero diagonal component, $\det A \neq 0$ if (A.4) is satisfied for some other permutation σ_i.

If all mass eigenvalues in the down quark sector are allowed by Z_N, then (A.4) amounts to a condition on the Z_N charges of MSSM fields:

$$q_{Q_i} + q_{H_d} + q_{D^c_{\sigma(i)}} = 0, \tag{A.5}$$

for $i = 1, 2, 3$. A similar equation with L_i and $E^c_{\sigma(i)}$ arises from the lepton Yukawa matrix.

Regardless of the permutation chosen for σ_i, we can sum (A.5) over i and obtain the conditions for all lepton and down quark mass eigenvalues to be allowed by Z_N:

$$\sum_{i=1}^{3} q_{Q_i} + q_{H_d} + q_{D^c_i} = 0 \sum_{i=1}^{3} q_{L_i} + q_{H_d} + q_{E^c_i} = 0. \tag{A.6}$$

Using (4) and (5) this can be rewritten as:

$$\sum_{i=1}^{3} 5\rho \left(\delta_{10_i} - \delta_{\overline{5}_i}\right) = \text{ Mod } N. \tag{A.7}$$

From equation (A.7), we see that this **can not** be satisfied if Z_N achieves doublet-triplet splitting. Therefore if the Z_N discussed here solves the μ problem, then at least one mass in the down/lepton sector is forbidden by Z_N and must be generated in some manner once Z_N is broken.

A.1.3 Constraints on the LSP Lifetime

The constraints on the LSP lifetime can by approximated as [190]:

$$\tau_{LSP} \lesssim 0.1 \text{ seconds or } \tau_{LSP} \gtrsim 10^{25} \text{ seconds} \tag{A.8}$$

The bound $\tau_{LSP} \lesssim 0.1$ second comes from primordial nucleosynthesis constraints on long-lived BSM [191, 192, 193, 194, 195], and the bound $\tau_{LSP} \gtrsim 10^{25}$ seconds comes from indirect detection constraints. In the case of purely trilinear RPV (i.e. no blinear RPV operator present), the LSP lifetime is given by:

$$\frac{\tau_{lsp}}{1 \text{ sec}} \approx \frac{10^{-17}}{\lambda^2} \left(\frac{m_0}{\text{TeV}}\right)^4 \left(\frac{100 \text{ GeV}}{m_{LSP}}\right)^5. \tag{A.9}$$

where λ is the dominant trilinear RPV coupling in $\lambda, \lambda', \lambda''$ following the notation of (3.27). Taking the squark mass m_0 to be 10 TeV and $m_{LSP} = 100$ GeV, the constraint (A.8) can be expressed as:

$$\lambda \gtrsim 10^{-6} \text{ or } \lambda \lesssim 10^{-19}. \tag{A.10}$$

As previously discussed, if moduli stablization regenerates the trilinear RPV coupling then $\lambda \sim \mathcal{O}\left(10^{-15}\right)$. Therefore if the only form of RPV in the theory is a trilinear RPV term forbidden by

Z_N but generated by moduli stablization, the theory will be ruled out by experimental constraints on LSP lifetime.

A.2 Largest Spin Independent Cross Sections

Following [110], the spin-independent cross section for the LSP scattering off a nucleon, is given in the decoupling limit ($M_Z \ll M_A$) by the approximation

$$\sigma_{\rm SI}\left(\chi N \to \chi N\right) \approx 5 \times 10^{-45}\text{cm}^2 \left(\frac{115\,\text{GeV}}{m_h}\right)^4 \left(\frac{Z_{H_u}\sin\beta - Z_{H_d}\cos\beta}{0.1}\right)^2 \left(Z_W - \tan\theta_W Z_B\right)^2 \tag{A.11}$$

where the Z's give the composition of the LSP

$$\chi \equiv Z_B\,\tilde{B} + Z_W\,\tilde{W} + Z_{H_d}\,\tilde{H}_d + Z_{H_u}\,\tilde{H}_u. \tag{A.12}$$

Consider the neutralino mass matrix [196]:

$$\mathcal{M} = \begin{pmatrix} M_1 & 0 & -M_Z\cos\beta\sin\theta_W & M_Z\sin\beta\sin\theta_W \\ 0 & M_2 & M_Z\cos\beta\cos\theta_W & -M_Z\sin\beta\cos\theta_W \\ -M_Z\cos\beta\sin\theta_W & M_Z\cos\beta\cos\theta_W & 0 & -\mu \\ M_Z\sin\beta\sin\theta_W & -M_Z\sin\beta\cos\theta_W & -\mu & 0 \end{pmatrix} \tag{A.13}$$

in the $\{\tilde{B}, \tilde{W}, \tilde{H}_d, \tilde{H}_u\}$ basis.The analytical expression [111, 112, 113] for the components in the LSP can be written as:

$$\begin{aligned}
\alpha Z_B &= z_B = -\sin\theta_W \\
\alpha Z_W &= z_W = \cos\theta_W \frac{M_1 - M_\chi}{M_2 - M_\chi} = \cos\theta_W \frac{\left(M_1 - M_\chi\right)^2}{\Delta} \\
\alpha Z_{H_d} &= z_{H_d} = \frac{\mu\left(M_1 - M_\chi\right)\left(M_2 - M_\chi\right) + M_Z^2\sin\beta\cos\beta\left(\left(M_1 - M_2\right)\cos^2\theta_W + M_2 - M_\chi\right)}{M_Z\left(M_2 - M_\chi\right)\left(-\mu\cos\beta + M_\chi\sin\beta\right)} \\
\alpha Z_{H_u} &= z_{H_u} = \frac{M_\chi\left(M_1 - M_\chi\right)\left(M_2 - M_\chi\right) + M_Z^2\cos^2\beta\left(\left(M_1 - M_2\right)\cos^2\theta_W + M_2 - M_\chi\right)}{M_Z\left(M_2 - M_\chi\right)\left(-\mu\cos\beta + M_\chi\sin\beta\right)}
\end{aligned} \tag{A.14}$$

where $\alpha = \sqrt{z_B^2 + z_W^2 + z_{H_d}^2 + z_{H_u}^2}$ is an overall normalization factor and $\Delta \equiv (M_\chi - M_1)(M_\chi - M_2)$.

The combination $Z_{H_u}\sin\beta - Z_{H_d}\cos\beta$, that appears in the scattering cross section takes an

especially simple form

$$Z_{H_u}\sin\beta - Z_{H_d}\cos\beta = \frac{(M_\chi\sin\beta - \mu\cos\beta)(M_1 - M_\chi)(M_2 - M_\chi)}{M_Z(M_2 - M_\chi)(-\mu\cos\beta + M_\chi\sin\beta)} = \frac{M_1 - M_\chi}{M_Z}. \quad \text{(A.15)}$$

It is clear from (A.15) that as $M_1 - M_\chi$ increases, $Z_{H_u}\sin\beta - Z_{H_d}\cos\beta$ grows slower than the Z_W component. Thus after normalization both the $\tilde{H}_u$ and the $\tilde{H}_d$ components will decrease. So the maximum of $Z_{H_u}\sin\beta - Z_{H_d}\cos\beta$ is realized when $M_1 - M_\chi$ is minimal.

The eigenvalues of the neutralino mass matrix (A.13) are given by the solutions to:

$$(x - M_1)(x - M_2)(x - \mu)(x + \mu) + \left(M_1\cos^2\theta_W + M_2\sin^2\theta\right)M_Z^2\mu\sin 2\beta = 0 \quad \text{(A.16)}$$

Then the LSP mass, corresponding to $M_\chi \equiv x$, can be found by taking the limit $M_\chi \ll \mu$, so that (A.16) is simply a quadratic equation. Then it is easy to see that the minimal value of $M_1 - M_\chi$, which maximizes $Z_{H_u}\sin\beta - Z_{H_d}\cos\beta$, corresponds to the situation when $M_1 - M_2$ is also minimized. Additionally, when $M_1 = M_2$, the term $Z_W - \tan\theta_W Z_B$ also reaches its maximum. Thus the maximum scattering cross sections will occur when $M_1 = M_2$.

To normalize the expressions in (A.14) (i.e. finding α) is tedious. Instead, a new basis is defined where $\tilde{\gamma} = \cos\theta_W\tilde{B} + \sin\theta_W\tilde{W}$ and $\tilde{Z} = -\sin\theta_W\tilde{B} + \cos\theta_W\tilde{W}$, where in the supersymmetric limit, these are the superpartners of the photon and Z-boson, respectively. The new mass matrix, in the $\{\tilde{\gamma}, \tilde{Z}, \tilde{H}_d, \tilde{H}_u\}$ is

$$\mathcal{M} = \begin{pmatrix} M_1\cos\theta_W{}^2 + M_2\sin\theta_W{}^2 & (M_2 - M_1)\sin\theta_W\cos\theta_W & 0 & 0 \\ (M_2 - M_1)\sin\theta_W\cos\theta_W & M_2\cos\theta_W{}^2 + M_1\sin\theta_W{}^2 & M_Z\cos\beta & -M_Z\sin\beta \\ 0 & M_Z\cos\beta & 0 & -\mu \\ 0 & -M_Z\sin\beta & -\mu & 0 \end{pmatrix} \quad \text{(A.17)}$$

Taking the limit $M_1 = M_2 \equiv M$, one immediately one finds that $\tilde{\gamma}$ in an eigenvector with mass eigenvalue M. The next lightest eigenvector of the remaining 3×3 sub-matrix will be mostly $\tilde{Z}$, and to leading order in M_Z/μ, the mass is

$$M_\chi \simeq M - \frac{M_Z^2}{\mu}\left(\frac{M}{M_Z} - \sin 2\beta\right) \quad \text{(A.18)}$$

Next we will assume that the phases of M and μ are such that absolute value of M_χ is smaller than $|M|$, so that it is indeed the LSP. The other scenario, in which the LSP is mostly $\tilde{\gamma}$, will have negligible scattering cross-section.

Diagonalizing the remaining 3×3 sub-matrix, the coefficients of $\tilde{H}_u$ and $\tilde{H}_d$ component to

leading order is

$$Z_{H_d} = \frac{1}{2}\left(\frac{(\sin\beta - \cos\beta)\, M_Z}{\mu + M} + \frac{(\sin\beta + \cos\beta)\, M_Z}{\mu - M}\right) = \frac{M_Z\,(\mu \sin\beta + M\cos\beta)}{\mu^2 - M^2}$$
$$Z_{H_u} = \frac{1}{2}\left(\frac{(\sin\beta - \cos\beta)\, M_Z}{\mu + M} - \frac{(\sin\beta + \cos\beta)\, M_Z}{\mu - M}\right) = -\frac{M_Z\,(\mu \cos\beta + M\sin\beta)}{\mu^2 - M^2} \quad \text{(A.19)}$$

and from the definition on $\tilde{Z}$,

$$Z_W - \tan\theta_W Z_B = \cos\theta_W{}^{-1}. \quad \text{(A.20)}$$

Finally, using (A.19) and (A.20) as inputs to (A.11) the upper limit for the cross section is

$$\sigma_{\rm SI}\left(\chi N \to \chi N\right) \approx 6 \times 10^{-45}\text{cm}^2 \left(\frac{115\,\text{GeV}}{m_h}\right)^4 \left(\frac{1\,\text{TeV}}{\mu}\right)^2 \left(\frac{\sin 2\beta + M_2/\mu}{1 - (M_2/\mu)^2}\right)^2 \quad \text{(A.21)}$$

From the discussion in the text we expect $M_2/\mu \lesssim 0.2$, $\sin 2\beta \lesssim 0.8$ and $\mu \gtrsim 1\,\text{TeV}$, giving largest scattering cross-sections around $\sigma_{\rm SI} \lesssim 6 \times 10^{-45}\text{cm}^2$. However, as discussed in Section 6.3, the constraints cannot all be satisfied simultaneously, so in practice only a cross section of about $10^{-45}\,\text{cm}^2$ could be achieved.

BIBLIOGRAPHY

[1] **PAMELA** Collaboration, O. Adriani *et al.*, "An anomalous positron abundance in cosmic rays with energies 1.5.100 GeV," *Nature* **458** (2009) 607–609, arXiv:0810.4995 [astro-ph].

[2] **AMS Collaboration** Collaboration, M. Aguilar *et al.*, "First Result from the Alpha Magnetic Spectrometer on the International Space Station: Precision Measurement of the Positron Fraction in Primary Cosmic Rays of 0.5350 GeV," *Phys.Rev.Lett.* **110** no. 14, (2013) 141102.

[3] O. Adriani *et al.*, "A new measurement of the antiproton-to-proton flux ratio up to 100 GeV in the cosmic radiation," *Phys. Rev. Lett.* **102** (2009) 051101, arXiv:0810.4994 [astro-ph].

[4] J. J. Engelmann, P. Ferrando, A. Soutoul, P. Goret, and E. Juliusson, "Charge composition and energy spectra of cosmic-ray nuclei for elements from Be to NI - Results from HEAO-3-C2," *Astronomy and Astrophysics* **233** (July, 1990) 96–111.

[5] **The Fermi LAT** Collaboration, A. A. Abdo *et al.*, "Measurement of the Cosmic Ray e+ plus e- spectrum from 20 GeV to 1 TeV with the Fermi Large Area Telescope," arXiv:0905.0025 [astro-ph.HE].

[6] D. Feldman, Z. Liu, and P. Nath, "Gluino NLSP, Dark Matter via Gluino Coannihilation, and LHC Signatures," *Phys.Rev.* **D80** (2009) 015007, arXiv:0905.1148 [hep-ph].

[7] S.-T. Yau, "On the ricci curvature of a compact Kähler manifold and the complex Monge-Ampére equation, I," *Comm. Pure Appl. Math.* **31** (1978) 339.

[8] B. S. Acharya, K. Bobkov, G. L. Kane, J. Shao, and P. Kumar, "The G_2-MSSM - An M Theory motivated model of Particle Physics," *Phys. Rev.* **D78** (2008) 065038, arXiv:0801.0478 [hep-ph].

[9] B. S. Acharya and K. Bobkov, "Kahler Independence of the G(2)-MSSM," *JHEP* **1009** (2010) 001, arXiv:0810.3285 [hep-th].

[10] "Combined coupling measurements of the higgs-like boson with the atlas detector using up to 25 fb^{-1} of proton-proton collision data," Tech. Rep. ATLAS-CONF-2013-034, CERN, Geneva, Mar, 2013.

[11] "Combination of standard model higgs boson searches and measurements of the properties of the new boson with a mass near 125 gev," Tech. Rep. CMS-PAS-HIG-13-005, CERN, Geneva, 2013.

[12] D. Joyce, "Compact Riemannian 7-manifolds with holonomy G_2. Part I," *J.Diff.Geom.* **43** (1996) 291.

[13] D. Joyce, "Compact Riemannian 7-manifolds with holonomy G_2. Part II," *J.Diff.Geom.* **43** (1996) 329.

[14] M. Atiyah and E. Witten, "M theory dynamics on a manifold of G(2) holonomy," *Adv.Theor.Math.Phys.* **6** (2003) 1–106, arXiv:hep-th/0107177 [hep-th].

[15] A. Corti, M. Haskins, J. Nordstrom, and T. Pacini, "G_2-manifolds and associative submanifolds via semi-Fano 3-folds," arXiv:1207.4470 [math.DG].

[16] B. S. Acharya, "On Realizing N=1 superYang-Mills in M theory," arXiv:hep-th/0011089 [hep-th].

[17] B. S. Acharya, "M theory, Joyce orbifolds and superYang-Mills," *Adv.Theor.Math.Phys.* **3** (1999) 227–248, arXiv:hep-th/9812205 [hep-th].

[18] E. Witten, "Anomaly cancellation on G(2) manifolds," arXiv:hep-th/0108165 [hep-th].

[19] B. S. Acharya and E. Witten, "Chiral fermions from manifolds of G(2) holonomy," arXiv:hep-th/0109152 [hep-th].

[20] B. S. Acharya and S. Gukov, "M theory and singularities of exceptional holonomy manifolds," *Phys.Rept.* **392** (2004) 121–189, arXiv:hep-th/0409191 [hep-th].

[21] T. Friedmann and E. Witten, "Unification scale, proton decay, and manifolds of G(2) holonomy," *Adv.Theor.Math.Phys.* **7** (2003) 577–617, arXiv:hep-th/0211269 [hep-th].

[22] T. Pantev and M. Wijnholt, "Hitchin's Equations and M-Theory Phenomenology," *J.Geom.Phys.* **61** (2011) 1223–1247, arXiv:0905.1968 [hep-th].

[23] M. B. Green and J. H. Schwarz, "Anomaly Cancellation in Supersymmetric D=10 Gauge Theory and Superstring Theory," *Phys.Lett.* **B149** (1984) 117–122.

[24] S. M. Barr, "A New Symmetry Breaking Pattern for SO(10) and Proton Decay," *Phys.Lett.* **B112** (1982) 219.

[25] J. Derendinger, J. E. Kim, and D. V. Nanopoulos, "Anti-SU(5)," *Phys.Lett.* **B139** (1984) 170.

[26] I. Antoniadis, J. R. Ellis, J. Hagelin, and D. V. Nanopoulos, "Supersymmetric Flipped SU(5) Revitalized," *Phys.Lett.* **B194** (1987) 231.

[27] E. Kuflik and J. Marsano, "Comments on Flipped SU(5) (and F-theory)," *JHEP* **1103** (2011) 020, arXiv:1009.2510 [hep-ph].

[28] B. S. Acharya, K. Bobkov, G. Kane, P. Kumar, and D. Vaman, "An M theory Solution to the Hierarchy Problem," *Phys.Rev.Lett.* **97** (2006) 191601, arXiv:hep-th/0606262 [hep-th].

[29] B. S. Acharya, K. Bobkov, G. L. Kane, P. Kumar, and J. Shao, "Explaining the Electroweak Scale and Stabilizing Moduli in M Theory," *Phys.Rev.* **D76** (2007) 126010, arXiv:hep-th/0701034 [hep-th].

[30] B. S. Acharya, F. Denef, and R. Valandro, "Statistics of M theory vacua," *JHEP* **0506** (2005) 056, arXiv:hep-th/0502060 [hep-th].

[31] J. M. Maldacena and C. Nunez, "Supergravity description of field theories on curved manifolds and a no go theorem," *Int.J.Mod.Phys.* **A16** (2001) 822–855, arXiv:hep-th/0007018 [hep-th].

[32] B. S. Acharya, G. Kane, and E. Kuflik, "String Theories with Moduli Stabilization Imply Non-Thermal Cosmological History, and Particular Dark Matter," arXiv:1006.3272 [hep-ph].

[33] E. Witten, "Deconstruction, G(2) holonomy, and doublet triplet splitting," arXiv:hep-ph/0201018 [hep-ph].

[34] A. Brignole, L. E. Ibanez, and C. Munoz, "Soft supersymmetry breaking terms from supergravity and superstring models," arXiv:hep-ph/9707209 [hep-ph].

[35] B. S. Acharya *et al.*, "Non-thermal Dark Matter and the Moduli Problem in String Frameworks," *JHEP* **06** (2008) 064, arXiv:0804.0863 [hep-ph].

[36] Y. Kawamura, "Triplet doublet splitting, proton stability and extra dimension," *Prog.Theor.Phys.* **105** (2001) 999–1006, arXiv:hep-ph/0012125 [hep-ph].

[37] L. J. Hall and Y. Nomura, "Gauge unification in higher dimensions," *Phys.Rev.* **D64** (2001) 055003, arXiv:hep-ph/0103125 [hep-ph].

[38] L. J. Hall, H. Murayama, and Y. Nomura, "Wilson lines and symmetry breaking on orbifolds," *Nucl.Phys.* **B645** (2002) 85–104, arXiv:hep-th/0107245 [hep-th].

[39] Y. Kawamura and T. Miura, "Classification of Standard Model Particles in E_6 Orbifold Grand Unified Theories," arXiv:1301.7469 [hep-ph].

[40] E. Witten, "Deconstruction, G(2) holonomy, and doublet triplet splitting," arXiv:hep-ph/0201018 [hep-ph].

[41] L. M. Krauss and F. Wilczek, "Discrete Gauge Symmetry in Continuum Theories," *Phys.Rev.Lett.* **62** (1989) 1221.

[42] Y. Hosotani, "Dynamical Mass Generation by Compact Extra Dimensions," *Phys.Lett.* **B126** (1983) 309.

[43] P. Candelas, G. T. Horowitz, A. Strominger, and E. Witten, "Vacuum Configurations for Superstrings," *Nucl.Phys.* **B258** (1985) 46–74.

[44] G. Giudice and A. Masiero, "A Natural Solution to the mu Problem in Supergravity Theories," *Phys.Lett.* **B206** (1988) 480–484.

[45] J. Wess and J. Bagger, "Supersymmetry and supergravity,".

[46] B. S. Acharya and M. Torabian, "Supersymmetry Breaking, Moduli Stabilization and Hidden U(1) Breaking in M-Theory," *Phys.Rev.* **D83** (2011) 126001, arXiv:1101.0108 [hep-th].

[47] K. Babu, I. Gogoladze, and K. Wang, "Natural R parity, mu term, and fermion mass hierarchy from discrete gauge symmetries," *Nucl.Phys.* **B660** (2003) 322–342, arXiv:hep-ph/0212245 [hep-ph].

[48] T. Araki, T. Kobayashi, J. Kubo, S. Ramos-Sanchez, M. Ratz, *et al.*, "(Non-)Abelian discrete anomalies," *Nucl.Phys.* **B805** (2008) 124–147, arXiv:0805.0207 [hep-th].

[49] M. Cvetic, I. Garcia Etxebarria, and J. Halverson, "Three Looks at Instantons in F-theory – New Insights from Anomaly Inflow, String Junctions and Heterotic Duality," *JHEP* **1111** (2011) 101, arXiv:1107.2388 [hep-th].

[50] H. M. Lee, S. Raby, M. Ratz, G. G. Ross, R. Schieren, *et al.*, "Discrete R symmetries for the MSSM and its singlet extensions," *Nucl.Phys.* **B850** (2011) 1–30, arXiv:1102.3595 [hep-ph].

[51] L. E. Ibanez and G. G. Ross, "Discrete gauge symmetries and the origin of baryon and lepton number conservation in supersymmetric versions of the standard model," *Nucl.Phys.* **B368** (1992) 3–37.

[52] L. E. Ibanez and G. G. Ross, "Discrete gauge symmetry anomalies," *Phys.Lett.* **B260** (1991) 291–295.

[53] J. Preskill, S. P. Trivedi, F. Wilczek, and M. B. Wise, "Cosmology and broken discrete symmetry," *Nucl.Phys.* **B363** (1991) 207–220.

[54] T. Banks and M. Dine, "Note on discrete gauge anomalies," *Phys.Rev.* **D45** (1992) 1424–1427, arXiv:hep-th/9109045 [hep-th].

[55] C. Csaki and H. Murayama, "Discrete anomaly matching," *Nucl.Phys.* **B515** (1998) 114–162, arXiv:hep-th/9710105 [hep-th].

[56] H. M. Lee, S. Raby, M. Ratz, G. G. Ross, R. Schieren, *et al.*, "Discrete R symmetries for the MSSM and its singlet extensions," *Nucl.Phys.* **B850** (2011) 1–30, arXiv:1102.3595 [hep-ph].

[57] H. K. Dreiner, C. Luhn, and M. Thormeier, "What is the discrete gauge symmetry of the MSSM?," *Phys.Rev.* **D73** (2006) 075007, arXiv:hep-ph/0512163 [hep-ph].

[58] K. Kurosawa, N. Maru, and T. Yanagida, "Nonanomalous R symmetry in supersymmetric unified theories of quarks and leptons," *Phys.Lett.* **B512** (2001) 203–210, arXiv:hep-ph/0105136 [hep-ph].

[59] H. M. Lee, S. Raby, M. Ratz, G. G. Ross, R. Schieren, *et al.*, "A unique Z_4^R symmetry for the MSSM," *Phys.Lett.* **B694** (2011) 491–495, arXiv:1009.0905 [hep-ph].

[60] J. L. Evans, M. Ibe, J. Kehayias, and T. T. Yanagida, "Non-Anomalous Discrete R-symmetry Decrees Three Generations," *Phys.Rev.Lett.* **109** (2012) 181801, arXiv:1111.2481 [hep-ph].

[61] M. Asano, T. Moroi, R. Sato, and T. T. Yanagida, "Non-anomalous Discrete R-symmetry, Extra Matters, and Enhancement of the Lightest SUSY Higgs Mass," *Phys.Lett.* **B705** (2011) 337–341, arXiv:1108.2402 [hep-ph].

[62] M. Paraskevas and K. Tamvakis, "On Discrete R-Symmetries in MSSM and its Extensions," *Phys.Rev.* **D86** (2012) 015009, arXiv:1205.1391 [hep-ph].

[63] R. Kappl, B. Petersen, S. Raby, M. Ratz, R. Schieren, *et al.*, "String-Derived MSSM Vacua with Residual R Symmetries," *Nucl.Phys.* **B847** (2011) 325–349, arXiv:1012.4574 [hep-th].

[64] B. S. Acharya, G. Kane, E. Kuflik, and R. Lu, "Theory and Phenomenology of μ in M theory," *JHEP* **1105** (2011) 033, arXiv:1102.0556 [hep-ph].

[65] H. Murayama and A. Pierce, "Not even decoupling can save minimal supersymmetric SU(5)," *Phys.Rev.* **D65** (2002) 055009, arXiv:hep-ph/0108104 [hep-ph].

[66] I. Affleck and M. Dine, "A New Mechanism for Baryogenesis," *Nucl.Phys.* **B249** (1985) 361.

[67] M. Ambroso and B. A. Ovrut, "The Mass Spectra, Hierarchy and Cosmology of B-L MSSM Heterotic Compactifications," *Int.J.Mod.Phys.* **A26** (2011) 1569–1627, arXiv:1005.5392 [hep-th].

[68] P. Langacker and J. Wang, "U(1)-prime symmetry breaking in supersymmetric E(6) models," *Phys.Rev.* **D58** (1998) 115010, arXiv:hep-ph/9804428 [hep-ph].

[69] M. Cvetic, J. Halverson, and R. Richter, "Mass Hierarchies versus proton Decay in MSSM Orientifold Compactifications," arXiv:0910.2239 [hep-th].

[70] D. M. Pierce, J. A. Bagger, K. T. Matchev, and R.-j. Zhang, "Precision corrections in the minimal supersymmetric standard model," *Nucl.Phys.* **B491** (1997) 3–67, arXiv:hep-ph/9606211 [hep-ph].

[71] C. Csaki, A. Falkowski, Y. Nomura, and T. Volansky, "New Approach to the mu-Bmu Problem of Gauge-Mediated Supersymmetry Breaking," *Phys.Rev.Lett.* **102** (2009) 111801, arXiv:0809.4492 [hep-ph].

[72] M. Dine, "Some issues in gauge mediation," *Nucl.Phys.Proc.Suppl.* **62** (1998) 276–280, arXiv:hep-ph/9707413 [hep-ph].

[73] S. P. Martin and M. T. Vaughn, "Two loop renormalization group equations for soft supersymmetry breaking couplings," *Phys.Rev.* **D50** (1994) 2282, arXiv:hep-ph/9311340 [hep-ph].

[74] B. Allanach, "SOFTSUSY: a program for calculating supersymmetric spectra," *Comput.Phys.Commun.* **143** (2002) 305–331, arXiv:hep-ph/0104145 [hep-ph].

[75] G. Degrassi, P. Slavich, and F. Zwirner, "On the neutral Higgs boson masses in the MSSM for arbitrary stop mixing," *Nucl.Phys.* **B611** (2001) 403–422, arXiv:hep-ph/0105096 [hep-ph].

[76] A. Dedes and P. Slavich, "Two loop corrections to radiative electroweak symmetry breaking in the MSSM," *Nucl.Phys.* **B657** (2003) 333–354, arXiv:hep-ph/0212132 [hep-ph].

[77] P. Nath and R. L. Arnowitt, "Nonuniversal soft SUSY breaking and dark matter," *Phys.Rev.* **D56** (1997) 2820–2832, arXiv:hep-ph/9701301 [hep-ph].

[78] K. L. Chan, U. Chattopadhyay, and P. Nath, "Naturalness, weak scale supersymmetry and the prospect for the observation of supersymmetry at the Tevatron and at the CERN LHC," *Phys.Rev.* **D58** (1998) 096004, arXiv:hep-ph/9710473 [hep-ph].

[79] J. L. Feng, K. T. Matchev, and T. Moroi, "Focus points and naturalness in supersymmetry," *Phys.Rev.* **D61** (2000) 075005, arXiv:hep-ph/9909334 [hep-ph].

[80] T. Banks, D. B. Kaplan, and A. E. Nelson, "Cosmological implications of dynamical supersymmetry breaking," *Phys.Rev.* **D49** (1994) 779–787, arXiv:hep-ph/9308292 [hep-ph].

[81] B. de Carlos, J. Casas, F. Quevedo, and E. Roulet, "Model independent properties and cosmological implications of the dilaton and moduli sectors of 4-d strings," *Phys.Lett.* **B318** (1993) 447–456, arXiv:hep-ph/9308325 [hep-ph].

[82] M. Berg, D. Marsh, L. McAllister, and E. Pajer, "Sequestering in String Compactifications," *JHEP* **1106** (2011) 134, arXiv:1012.1858 [hep-th].

[83] B. S. Acharya, P. Grajek, G. L. Kane, E. Kuflik, K. Suruliz, *et al.*, "Identifying Multi-Top Events from Gluino Decay at the LHC," arXiv:0901.3367 [hep-ph].

[84] L. Randall and R. Sundrum, "Out of this world supersymmetry breaking," *Nucl. Phys.* **B557** (1999) 79–118, arXiv:hep-th/9810155.

[85] P. Langacker, G. Paz, L.-T. Wang, and I. Yavin, "Z'-mediated Supersymmetry Breaking," *Phys. Rev. Lett.* **100** (2008) 041802, arXiv:0710.1632 [hep-ph].

[86] T. Moroi and L. Randall, "Wino cold dark matter from anomaly-mediated SUSY breaking," *Nucl. Phys.* **B570** (2000) 455–472, arXiv:hep-ph/9906527.

[87] G. Kane and S. Watson, "Dark Matter and LHC: What is the Connection?," *Mod. Phys. Lett.* **A23** (2008) 2103–2123, arXiv:0807.2244 [hep-ph].

[88] B. S. Acharya, K. Bobkov, and P. Kumar, "An M Theory Solution to the Strong CP Problem and Constraints on the Axiverse," *JHEP* **1011** (2010) 105, arXiv:1004.5138 [hep-th].

[89] K. Bobkov, V. Braun, P. Kumar, and S. Raby, "Stabilizing All Kahler Moduli in Type IIB Orientifolds," *JHEP* **1012** (2010) 056, arXiv:1003.1982 [hep-th].

[90] M. Kamionkowski and M. S. Turner, "Thermal relics: Do we know their abundances?," *Phys. Rev.* **D42** (1990) 3310–3320.

[91] D. J. H. Chung, E. W. Kolb, and A. Riotto, "Nonthermal supermassive dark matter," *Phys. Rev. Lett.* **81** (1998) 4048–4051, arXiv:hep-ph/9805473.

[92] G. F. Giudice, E. W. Kolb, and A. Riotto, "Largest temperature of the radiation era and its cosmological implications," *Phys. Rev.* **D64** (2001) 023508, arXiv:hep-ph/0005123.

[93] A. W. Strong and I. V. Moskalenko, "Propagation of cosmic-ray nucleons in the Galaxy," *Astrophys. J.* **509** (1998) 212–228, arXiv:astro-ph/9807150.

[94] P. Gondolo, J. Edsjö, P. Ullio, L. Bergström, M. Schelke, and E. A. Baltz, "DarkSUSY: Computing supersymmetric dark matter properties numerically," *JCAP* **0407** (2004) 008, arXiv:astro-ph/0406204.

[95] P. Gondolo, J. Edsjö, P. Ullio, L. Bergström, M. Schelke, E. A. Baltz, T. Bringmann, and G. Duda. http://www.physto.se/~edsjo/darksusy.

[96] F. Donato, N. Fornengo, D. Maurin, and P. Salati, "Antiprotons in cosmic rays from neutralino annihilation," *Phys. Rev.* **D69** (2004) 063501, arXiv:astro-ph/0306207.

[97] L. Bergstrom, J. Edsjo, M. Gustafsson, and P. Salati, "Is the dark matter interpretation of the EGRET gamma excess compatible with antiproton measurements?," *JCAP* **0605** (2006) 006, arXiv:astro-ph/0602632.

[98] **BESS** Collaboration, S. Orito *et al.*, "Precision measurement of cosmic-ray antiproton spectrum," *Phys. Rev. Lett.* **84** (2000) 1078–1081, arXiv:astro-ph/9906426.

[99] **BESS** Collaboration, T. Maeno *et al.*, "Successive measurements of cosmic-ray antiproton spectrum in a positive phase of the solar cycle," *Astropart. Phys.* **16** (2001) 121–128, arXiv:astro-ph/0010381.

[100] Y. Asaoka *et al.*, "Measurements of cosmic-ray low-energy antiproton and proton spectra in a transient period of the solar field reversal," *Phys. Rev. Lett.* **88** (2002) 051101, arXiv:astro-ph/0109007.

[101] J. Lavalle, J. Pochon, P. Salati, and R. Taillet, "Clumpiness of dark matter and positron annihilation signal: Computing the odds of the galactic lottery," arXiv:astro-ph/0603796.

[102] J. Lavalle, Q. Yuan, D. Maurin, and X. J. Bi, "Full Calculation of Clumpiness Boost factors for Antimatter Cosmic Rays in the light of ΛCDM N-body simulation results," arXiv:0709.3634 [astro-ph].

[103] J. M. Clem, D. P. Clements, J. Esposito, P. Evenson, D. Huber, J. L'Heureux, P. Meyer, and C. Constantin, "Solar Modulation of Cosmic Electrons," *Astrophysical Journal* **464** (June, 1996) 507–+.

[104] L. J. Gleeson and W. I. Axford, "Cosmic Rays in the Interplanetary Medium," *Astrophysical Journal* **149** (Sept., 1967) L115–L118.

[105] L. Zhang and K. S. Cheng, "Cosmic-ray positrons from mature gamma-ray pulsars," *Astronomy and Astrophysics* **368** (Mar., 2001) 1063–1070.

[106] S. Profumo, "Dissecting Pamela (and ATIC) with Occam's Razor: existing, well-known Pulsars naturally account for the 'anomalous' Cosmic-Ray Electron and Positron Data," arXiv:0812.4457 [astro-ph].

[107] J. Diemand, B. Moore, and J. Stadel, "Earth-mass dark-matter haloes as the first structures in the early universe," *Nature.* **433** (2005) 389–391, arXiv:astro-ph/0501589.

[108] E. A. Baltz and J. Edsjo, "Positron Propagation and Fluxes from Neutralino Annihilation in the Halo," *Phys. Rev.* **D59** (1998) 023511, arXiv:astro-ph/9808243.

[109] D. Maurin, R. Taillet, and C. Combet, "Approximate formulae for exotic GCR anti-p and anti-d: Fluxes and astrophysical uncertainties," arXiv:astro-ph/0609522.

[110] T. Cohen, D. J. Phalen, and A. Pierce, "On the Correlation Between the Spin-Independent and Spin-Dependent Direct Detection of Dark Matter," *Phys.Rev.* **D81** (2010) 116001, arXiv:1001.3408 [hep-ph].

[111] M. El Kheishen, A. Aboshousha, and A. Shafik, "Analytic formulas for the neutralino masses and the neutralino mixing matrix," *Phys.Rev.* **D45** (1992) 4345–4348.

[112] V. D. Barger, M. Berger, and P. Ohmann, "The Supersymmetric particle spectrum," *Phys.Rev.* **D49** (1994) 4908–4930, arXiv:hep-ph/9311269 [hep-ph].

[113] G. Bertone, D. Hooper, and J. Silk, "Particle dark matter: Evidence, candidates and constraints," *Phys.Rept.* **405** (2005) 279–390, arXiv:hep-ph/0404175 [hep-ph].

[114] S. Kachru, R. Kallosh, A. D. Linde, and S. P. Trivedi, "De Sitter vacua in string theory," *Phys.Rev.* **D68** (2003) 046005, arXiv:hep-th/0301240 [hep-th].

[115] F. Denef, M. R. Douglas, B. Florea, A. Grassi, and S. Kachru, "Fixing all moduli in a simple f-theory compactification," *Adv.Theor.Math.Phys.* **9** (2005) 861–929, arXiv:hep-th/0503124 [hep-th].

[116] O. Lebedev, H. P. Nilles, and M. Ratz, "De Sitter vacua from matter superpotentials," *Phys.Lett.* **B636** (2006) 126–131, arXiv:hep-th/0603047 [hep-th].

[117] E. Dudas, C. Papineau, and S. Pokorski, "Moduli stabilization and uplifting with dynamically generated F-terms," *JHEP* **0702** (2007) 028, arXiv:hep-th/0610297 [hep-th].

[118] H. Abe, T. Higaki, T. Kobayashi, and Y. Omura, "Moduli stabilization, F-term uplifting and soft supersymmetry breaking terms," *Phys.Rev.* **D75** (2007) 025019, arXiv:hep-th/0611024 [hep-th].

[119] R. Kallosh and A. D. Linde, "O'KKLT," *JHEP* **0702** (2007) 002, arXiv:hep-th/0611183 [hep-th].

[120] O. Lebedev, V. Lowen, Y. Mambrini, H. P. Nilles, and M. Ratz, "Metastable Vacua in Flux Compactifications and Their Phenomenology," *JHEP* **0702** (2007) 063, arXiv:hep-ph/0612035 [hep-ph].

[121] J. Fan, M. Reece, and L.-T. Wang, "Mitigating Moduli Messes in Low-Scale SUSY Breaking," *JHEP* **1109** (2011) 126, arXiv:1106.6044 [hep-ph].

[122] M. Gomez-Reino and C. A. Scrucca, "Locally stable non-supersymmetric Minkowski vacua in supergravity," *JHEP* **0605** (2006) 015, arXiv:hep-th/0602246 [hep-th].

[123] G. L. Kane, C. F. Kolda, and J. D. Wells, "Calculable upper limit on the mass of the lightest Higgs boson in any perturbatively valid supersymmetric theory," *Phys.Rev.Lett.* **70** (1993) 2686–2689, arXiv:hep-ph/9210242 [hep-ph].

[124] J. Espinosa and M. Quiros, "Upper bounds on the lightest Higgs boson mass in general supersymmetric Standard Models," *Phys.Lett.* **B302** (1993) 51–58, arXiv:hep-ph/9212305 [hep-ph].

[125] B. S. Acharya, G. Kane, E. Kuflik, and R. Lu, "Theory and Phenomenology of μ in M theory," *JHEP* **1105** (2011) 033, arXiv:1102.0556 [hep-ph].

[126] M. Cvetic, J. Halverson, and R. Richter, "Realistic Yukawa structures from orientifold compactifications," *JHEP* **0912** (2009) 063, arXiv:0905.3379 [hep-th].

[127] D. Green and T. Weigand, "Retrofitting and the mu Problem," arXiv:0906.0595 [hep-th].

[128] L. Ibanez and R. Richter, "Stringy Instantons and Yukawa Couplings in MSSM-like Orientifold Models," *JHEP* **0903** (2009) 090, arXiv:0811.1583 [hep-th].

[129] J. Casas and C. Munoz, "A Natural solution to the mu problem," *Phys.Lett.* **B306** (1993) 288–294, arXiv:hep-ph/9302227 [hep-ph].

[130] S. P. Martin, "A Supersymmetry primer," arXiv:hep-ph/9709356 [hep-ph].

[131] J. D. Wells, "PeV-scale supersymmetry," *Phys.Rev.* **D71** (2005) 015013, arXiv:hep-ph/0411041 [hep-ph].

[132] C. Brust, A. Katz, S. Lawrence, and R. Sundrum, "SUSY, the Third Generation and the LHC," *JHEP* **1203** (2012) 103, arXiv:1110.6670 [hep-ph].

[133] A. G. Cohen, D. Kaplan, and A. Nelson, "The More minimal supersymmetric standard model," *Phys.Lett.* **B388** (1996) 588–598, arXiv:hep-ph/9607394 [hep-ph].

[134] H. Baer, V. Barger, P. Huang, and A. Mustafayev, "Implications of a high mass light MSSM Higgs scalar for SUSY searches at the LHC," *Phys.Rev.* **D84** (2011) 091701, arXiv:1109.3197 [hep-ph].

[135] D. Feldman, G. Kane, E. Kuflik, and R. Lu, "A new (string motivated) approach to the little hierarchy problem," *Phys.Lett.* **B704** (2011) 56–61, arXiv:1105.3765 [hep-ph].

[136] N. Arkani-Hamed and S. Dimopoulos, "Supersymmetric unification without low energy supersymmetry and signatures for fine-tuning at the LHC," *JHEP* **0506** (2005) 073, arXiv:hep-th/0405159 [hep-th].

[137] N. Arkani-Hamed, S. Dimopoulos, G. Giudice, and A. Romanino, "Aspects of split supersymmetry," *Nucl.Phys.* **B709** (2005) 3–46, arXiv:hep-ph/0409232 [hep-ph].

[138] L. J. Hall and Y. Nomura, "A Finely-Predicted Higgs Boson Mass from A Finely-Tuned Weak Scale," *JHEP* **1003** (2010) 076, arXiv:0910.2235 [hep-ph].

[139] G. Elor, H.-S. Goh, L. J. Hall, P. Kumar, and Y. Nomura, "Environmentally Selected WIMP Dark Matter with High-Scale Supersymmetry Breaking," *Phys.Rev.* **D81** (2010) 095003, arXiv:0912.3942 [hep-ph].

[140] W. Porod, "SPheno, a program for calculating supersymmetric spectra, SUSY particle decays and SUSY particle production at e+ e- colliders," *Comput.Phys.Commun.* **153** (2003) 275–315, arXiv:hep-ph/0301101 [hep-ph].

[141] G. F. Giudice and A. Strumia, "Probing High-Scale and Split Supersymmetry with Higgs Mass Measurements," *Nucl.Phys.* **B858** (2012) 63–83, arXiv:1108.6077 [hep-ph].

[142] N. Bernal, A. Djouadi, and P. Slavich, "The MSSM with heavy scalars," *JHEP* **0707** (2007) 016, arXiv:0705.1496 [hep-ph].

[143] **Tevatron Electroweak Working Group, CDF Collaboration, D0 Collaboration** Collaboration, "Combination of CDF and D0 results on the mass of the top quark using up to 5.8 fb-1 of data," arXiv:1107.5255 [hep-ex].

[144] M. Binger, "Higgs boson mass in split supersymmetry at two-loops," *Phys.Rev.* **D73** (2006) 095001, arXiv:hep-ph/0408240 [hep-ph].

[145] S. Bethke, "The 2009 World Average of alpha(s)," *Eur.Phys.J.* **C64** (2009) 689–703, arXiv:0908.1135 [hep-ph].

[146] K. Choi, A. Falkowski, H. P. Nilles, and M. Olechowski, "Soft supersymmetry breaking in KKLT flux compactification," *Nucl.Phys.* **B718** (2005) 113–133, arXiv:hep-th/0503216 [hep-th].

[147] M. Endo, M. Yamaguchi, and K. Yoshioka, "A Bottom-up approach to moduli dynamics in heavy gravitino scenario: Superpotential, soft terms and sparticle mass spectrum," *Phys.Rev.* **D72** (2005) 015004, arXiv:hep-ph/0504036 [hep-ph].

[148] K. Choi, K. S. Jeong, and K.-i. Okumura, "Phenomenology of mixed modulus-anomaly mediation in fluxed string compactifications and brane models," *JHEP* **0509** (2005) 039, arXiv:hep-ph/0504037 [hep-ph].

[149] A. Falkowski, O. Lebedev, and Y. Mambrini, "SUSY phenomenology of KKLT flux compactifications," *JHEP* **0511** (2005) 034, arXiv:hep-ph/0507110 [hep-ph].

[150] K. Choi, "Moduli stabilization and the pattern of soft SUSY breaking terms," arXiv:hep-ph/0511162 [hep-ph].

[151] J. P. Conlon and F. Quevedo, "Gaugino and Scalar Masses in the Landscape," *JHEP* **0606** (2006) 029, arXiv:hep-th/0605141 [hep-th].

[152] A. Djouadi, M. Muhlleitner, and M. Spira, "Decays of supersymmetric particles: The Program SUSY-HIT (SUspect-SdecaY-Hdecay-InTerface)," *Acta Phys.Polon.* **B38** (2007) 635–644, arXiv:hep-ph/0609292 [hep-ph].

[153] T. Sjostrand, S. Mrenna, and P. Z. Skands, "PYTHIA 6.4 Physics and Manual," *JHEP* **0605** (2006) 026, arXiv:hep-ph/0603175 [hep-ph].

[154] J. Conway, "PGS4." http://physics.ucdavis.edu/~conway/research/software/pgs/pgs4-general.htm.

[155] **CMS Collaboration** Collaboration, G. Bayatian *et al.*, "CMS technical design report, volume II: Physics performance," *J.Phys.* **G34** (2007) 995–1579.

[156] N. Chen, D. Feldman, Z. Liu, and P. Nath, "SUSY and Higgs Signatures Implied by Cancellations in b $\to$ s gamma," *Phys.Lett.* **B685** (2010) 174–181, arXiv:0911.0217 [hep-ph].

[157] **CDF Collaboration** Collaboration, D. Acosta *et al.*, "Measurement of the $t\bar{t}$ production cross section in $p\bar{p}$ collisions at $\sqrt{s} = 1.96$ TeV using lepton + jets events with secondary vertex $b-$tagging," *Phys.Rev.* **D71** (2005) 052003, arXiv:hep-ex/0410041 [hep-ex].

[158] E. A. Baltz, J. Edsjo, K. Freese, and P. Gondolo, "The Cosmic ray positron excess and neutralino dark matter," *Phys.Rev.* **D65** (2002) 063511, arXiv:astro-ph/0109318 [astro-ph].

[159] G. L. Kane, L.-T. Wang, and J. D. Wells, "Supersymmetry and the positron excess in cosmic rays," *Phys.Rev.* **D65** (2002) 057701, arXiv:hep-ph/0108138 [hep-ph].

[160] J. Hisano, S. Matsumoto, O. Saito, and M. Senami, "Heavy wino-like neutralino dark matter annihilation into antiparticles," *Phys.Rev.* **D73** (2006) 055004, arXiv:hep-ph/0511118 [hep-ph].

[161] S. Bhattacharya, U. Chattopadhyay, D. Choudhury, D. Das, and B. Mukhopadhyaya, "Non-universal scalar mass scenario with Higgs funnel region of SUSY dark matter: A Signal-based analysis for the Large Hadron Collider," *Phys.Rev.* **D81** (2010) 075009, arXiv:0907.3428 [hep-ph].

[162] H. Baer, V. Barger, A. Lessa, and X. Tata, "Supersymmetry discovery potential of the LHC at s**(1/2) = 10-TeV and 14-TeV without and with missing E(T)," *JHEP* **0909** (2009) 063, arXiv:0907.1922 [hep-ph].

[163] J. L. Feng, T. Moroi, L. Randall, M. Strassler, and S.-f. Su, "Discovering supersymmetry at the Tevatron in Wino LSP scenarios," *Phys. Rev. Lett.* **83** (1999) 1731–1734, arXiv:hep-ph/9904250.

[164] **Atlas Collaboration** Collaboration, G. Aad *et al.*, "Measurement of the top quark-pair production cross section with ATLAS in pp collisions at $\sqrt{s} = 7$ TeV," *Eur.Phys.J.* **C71** (2011) 1577, arXiv:1012.1792 [hep-ex].

[165] J. Alwall, M. Herquet, F. Maltoni, O. Mattelaer, and T. Stelzer, "MadGraph 5 : Going Beyond," *JHEP* **1106** (2011) 128, arXiv:1106.0522 [hep-ph].

[166] J. Alwall, S. de Visscher, and F. Maltoni, "QCD radiation in the production of heavy colored particles at the LHC," *JHEP* **0902** (2009) 017, arXiv:0810.5350 [hep-ph].

[167] S. Hoeche, F. Krauss, N. Lavesson, L. Lonnblad, M. Mangano, *et al.*, "Matching parton showers and matrix elements," arXiv:hep-ph/0602031 [hep-ph].

[168] M. L. Mangano, M. Moretti, F. Piccinini, R. Pittau, and A. D. Polosa, "ALPGEN, a generator for hard multiparton processes in hadronic collisions," *JHEP* **0307** (2003) 001, arXiv:hep-ph/0206293 [hep-ph].

[169] **The ATLAS Collaboration** Collaboration, G. Aad *et al.*, "Expected Performance of the ATLAS Experiment - Detector, Trigger and Physics," arXiv:0901.0512 [hep-ex].

[170] B. Altunkaynak, M. Holmes, P. Nath, B. D. Nelson, and G. Peim, "SUSY Discovery Potential and Benchmarks for Early Runs at $\sqrt{s} = 7$ TeV at the LHC," *Phys.Rev.* **D82** (2010) 115001, arXiv:1008.3423 [hep-ph].

[171] J. L. Feng, T. Moroi, L. Randall, M. Strassler, and S.-f. Su, "Discovering supersymmetry at the Tevatron in wino LSP scenarios," *Phys.Rev.Lett.* **83** (1999) 1731–1734, arXiv:hep-ph/9904250 [hep-ph].

[172] T. Moroi and L. Randall, "Wino cold dark matter from anomaly mediated SUSY breaking," *Nucl.Phys.* **B570** (2000) 455–472, arXiv:hep-ph/9906527 [hep-ph].

[173] J. F. Gunion and S. Mrenna, "A Study of SUSY signatures at the Tevatron in models with near mass degeneracy of the lightest chargino and neutralino," *Phys.Rev.* **D62** (2000) 015002, arXiv:hep-ph/9906270 [hep-ph].

[174] S. Mrenna and J. Gunion, "The degenerate Wino-like chargino neutralino scenario at a linear collider," *Int.J.Mod.Phys.* **A16S1B** (2001) 822–824.

[175] M. Ibe, T. Moroi, and T. Yanagida, "Possible Signals of Wino LSP at the Large Hadron Collider," *Phys.Lett.* **B644** (2007) 355–360, arXiv:hep-ph/0610277 [hep-ph].

[176] S. Asai, T. Moroi, K. Nishihara, and T. Yanagida, "Testing the Anomaly Mediation at the LHC," *Phys.Lett.* **B653** (2007) 81–87, arXiv:0705.3086 [hep-ph].

[177] S. Asai, T. Moroi, and T. Yanagida, "Test of Anomaly Mediation at the LHC," *Phys.Lett.* **B664** (2008) 185–189, arXiv:0802.3725 [hep-ph].

[178] B. S. Acharya, G. Kane, E. Kuflik, and R. Lu, "Theory and Phenomenology of μ in M theory," *JHEP* **1105** (2011) 033, arXiv:1102.0556 [hep-ph].

[179] B. S. Acharya, P. Grajek, G. L. Kane, E. Kuflik, K. Suruliz, *et al.*, "Identifying Multi-Top Events from Gluino Decay at the LHC," arXiv:0901.3367 [hep-ph].

[180] G. L. Kane, E. Kuflik, R. Lu, and L.-T. Wang, "Top Channel for Early SUSY Discovery at the LHC," *Phys.Rev.* **D84** (2011) 095004, arXiv:1101.1963 [hep-ph].

[181] W. Beenakker, R. Hopker, and M. Spira, "PROSPINO: A Program for the production of supersymmetric particles in next-to-leading order QCD," arXiv:hep-ph/9611232 [hep-ph].

[182] **ATLAS Collaboration** Collaboration, G. Aad *et al.*, "The ATLAS Experiment at the CERN Large Hadron Collider," *JINST* **3** (2008) S08003.

[183] S. Asai, Y. Azuma, O. Jinnouchi, T. Moroi, S. Shirai, *et al.*, "Mass Measurement of the Decaying Bino at the LHC," *Phys.Lett.* **B672** (2009) 339–343, arXiv:0807.4987 [hep-ph].

[184] J. Alwall, M. Herquet, F. Maltoni, O. Mattelaer, and T. Stelzer, "MadGraph 5 : Going Beyond," *JHEP* **1106** (2011) 128, arXiv:1106.0522 [hep-ph].

[185] B. Allanach, "SOFTSUSY: a program for calculating supersymmetric spectra," *Comput.Phys.Commun.* **143** (2002) 305–331, arXiv:hep-ph/0104145 [hep-ph].

[186] B. S. Acharya, P. Kumar, K. Bobkov, G. Kane, J. Shao, *et al.*, "Non-thermal Dark Matter and the Moduli Problem in String Frameworks," *JHEP* **0806** (2008) 064, arXiv:0804.0863 [hep-ph].

[187] B. S. Acharya, K. Bobkov, G. L. Kane, J. Shao, and P. Kumar, "The G(2)-MSSM: An M Theory motivated model of Particle Physics," *Phys.Rev.* **D78** (2008) 065038, arXiv:0801.0478 [hep-ph].

[188] "Search for supersymmetry in pp collisions at sqr(s)=7 tev in final states with missing transverse momentum and b-jets with the atlas detector," Tech. Rep. ATLAS-CONF-2012-003, CERN, Geneva, Feb, 2012.

[189] **ATLAS Collaboration** Collaboration, G. Aad *et al.*, "Search for squarks and gluinos using final states with jets and missing transverse momentum with the ATLAS detector in sqrt(s) = 7 TeV proton-proton collisions," arXiv:1109.6572 [hep-ex].

[190] H. K. Dreiner, "An Introduction to explicit R-parity violation," arXiv:hep-ph/9707435 [hep-ph].

[191] M. Reno and D. Seckel, "Primordial Nucleosynthesis: The Effects of Injecting Hadrons," *Phys.Rev.* **D37** (1988) 3441.

[192] J. R. Ellis, G. Gelmini, J. L. Lopez, D. V. Nanopoulos, and S. Sarkar, "Astrophysical constraints on massive unstable neutral relic particles," *Nucl.Phys.* **B373** (1992) 399–437.

[193] M. Kawasaki, K. Kohri, and T. Moroi, "Big-Bang nucleosynthesis and hadronic decay of long-lived massive particles," *Phys.Rev.* **D71** (2005) 083502, arXiv:astro-ph/0408426 [astro-ph].

[194] M. Kawasaki, K. Kohri, and T. Moroi, "Hadronic decay of late - decaying particles and Big-Bang Nucleosynthesis," *Phys.Lett.* **B625** (2005) 7–12, arXiv:astro-ph/0402490 [astro-ph].

[195] K. Jedamzik, "Big bang nucleosynthesis constraints on hadronically and electromagnetically decaying relic neutral particles," *Phys.Rev.* **D74** (2006) 103509, arXiv:hep-ph/0604251 [hep-ph].

[196] J. Frere and G. L. Kane, "ON THE POSSIBILITY OF FINDING LIGHT UNCOLORED SUPERSYMMETRIC PARTNERS AT PRESENT AND FUTURE MACHINES," *Nucl.Phys.* **B223** (1983) 331.